SEASONALITY OF THE MARINE CARBONATE SYSTEM IN THE SOUTHERN BENGUELA: NUTRIENT STOICHIOMETRY, ALKALINITY PRODUCTION, AND CO_2 FLUX

Luke Gregor

A thesis presented for the degree of
Master of Science

in the Department of Oceanography
Faculty of Science
University of Cape Town
South Africa

February 2012

UNIVERSITY OF CAPE TOWN
IYUNIVESITHI YASEKAPA • UNIVERSITEIT VAN KAAPSTAD

Abstract

An observational study was undertaken to determine the seasonality of the marine carbonate system of the southern Benguela focusing on three key points: the processes driving bulk stoichiometry, alkalinity production on the continental shelf, and the air-sea flux of CO_2. Monthly samples were taken along the St. Helena Bay Monitoring Line in the southern Benguela for ten of the months in 2010. Samples were analysed for dissolved inorganic carbon (DIC) and total alkalinity (TA). Temperature, salinity, oxygen and nutrients were also measured. The formation of a seasonal oxygen minimum zone due to stratification and retention of organic matter in the lee of Cape Columbine supported anaerobic remineralisation (Monteiro and Van der Plas, 2006). Denitrification was found to be the key modifier of stoichiometry from Redfield ratios, attributing up to 17% of total changes to DIC throughout the year. The C:N ratio was closest to the Redfield ratio during summer and winter (6.8:1 and 6.3:1 respectively). Autumn C:N ratios were higher due to denitrification and sulphate reduction (8.0:1). The southern Benguela was a net heterotrophic system in autumn due to this additional anaerobic remineralisation contribution. Summer and winter were autotrophic on average as the large photosynthetic contribution was able to off-set the DIC enriched upwelled waters. Gross TA production, which is driven by denitrification and sulphate reduction (Wolf-Gladrow et al., 2007), was largest in autumn. Calcification played an important role in decreasing net TA production during autumn. Deep mixing after winter, allowed by a lack of stratification, resulted in stirring of the sediments and pore water where anaerobic remineralisation is strongest. This resulted in September being the month of greatest TA production. It was estimated that the southern Benguela produced 8.96 Gmol yr^{-1} of TA, which is insignificant on a global scale equating to 0.1% global shelf production (Hu and Cai, 2011). However, increased TA was important on a local scale, buffering pH by up to 0.4 units in bottom waters. Air-sea CO_2 flux was found to be -8.31, 4.13 and -5.15mmol m^{-2} day^{-1} for summer, autumn and winter respectively. High productivity in summer and reduced upwelling in winter resulted the system to be a CO_2 sink. Calcification by coccolithophores increased pCO_2 in surface waters in autumn, resulting in the system being a net source. Annual air-sea CO_2 flux was -1.59 mol m^{-2} yr^{-1}, which compared well with two other estimates of -1.36 and -1.62 mol m^{-2} yr^{-1} (Monteiro, 1996; Santana-Casiano et al., 2009). This equated to 0.1% of global CO_2 fluxes. This relatively small contribution for such a productive region was due to the large opposing contributions of photosynthesis and remineralisation.

Declaration

I know the meaning of Plagarism and declare that all of the work in the document, save for that which is properly acknowledged, is my own.

Supervisors

Dr. Pedro M. S. Monteiro:
Coasts and Oceans, Natural Resource & the Environment,
Council for Scientific and Industrial Research, South Africa

Dr. Howard Waldron:
Department of Oceanography,
University of Cape Town, South Africa

Acknowledgements

I would like to thank several people who were involved in making this thesis possible, from collection all the way through to the final draft.

I would like to thank my supervisors the opportunity of doing this MSc. Pedro Monteiro for all the travel opportunities, which broadened my horizons, and ideas and guidance throughout my dissertation. Howard Waldron for the humor, logical rigour and critique during discussions. I am thankful to the National Research Fund for a studentship and the Council for Scientific and Industrial Research Parliamentary Grant, both which allowed me to do this degree.

Thanks to the DEA and DAF for allowing me this valuable opportunity on board their vessels. The crew and captains of the Ellen Kuzwayo and Africana. Marco Worship and Dr. Larry Hutchings for their support in organising berths.

For all their hours spent in the CO_2 labs at CSIR, I would like to thank Tanya Tarrassova, Leletu Nohayi, and Warren Joubert. And for advice, ideas, endless cups of tea, and nonsense, office 118: Brett, Sarah, Carl, Raïssa and Miriam and the occasional Ceinwen.

Last, but not least I would also like to thank my parents for all their prayer, support and advice.

Contents

1 Introduction **1**

2 Literature Review **4**

2.1 History of the Problem 4
2.2 Carbon Cycle 5
2.3 Carbon flux in the oceans 8
2.3.1 Global Ocean 8
2.3.2 Calculating Flux 8
2.4 Marine Carbonate Chemistry 11
2.4.1 Temperature Effect 15
2.4.2 Photosynthesis 16
2.4.3 Calcification 18
2.5 "The Other CO_2 Problem" 20
2.5.1 Chemistry of Ocean Acidification 20
2.5.2 Biological impacts 21
2.6 Carbon in the Continental Margins 22
2.6.1 Carbon Flux 23
2.6.2 Coastal Hypoxia 23
2.6.3 Anaerobic remineralisation 24
2.6.4 Alkalinity Production on continental shelves . 27
2.7 Eastern Boundary Currents 27
2.7.1 CO_2 Flux 29
2.8 Benguela Upwelling System 30
2.8.1 Physical Features and Processes 30
2.8.2 Low Oxygen Water 33
2.8.3 Southern Benguela 34
2.9 Questions and Aims 38
2.9.1 What controls stoichiometry? 38
2.9.2 What is the alkalinity production on the southern Benguela shelf? 39
2.9.3 What is the air-sea CO_2 flux of the southern Benguela? 40

3 Methods **41**
3.1 Cruises and data collection 41
3.2 Sample Analysis 43
3.2.1 Dissolved Inorganic Carbon 44
3.2.2 Alkalinity 45
3.2.3 Quality Control 47
3.2.4 Normalisation 48
3.2.5 Other Marine Carbonate Parameters 49
3.2.6 Other Biogeochemical Parameters 50
3.3 Physics 51
3.3.1 Wind Data 51
3.3.2 Ekman Transport 51
3.4 Flux calculations 52
3.5 Ancillary Data 52
3.6 Data Processing 53

4 Results **55**
4.1 Physical characterisation 55
4.1.1 Winds and upwelling 55
4.1.2 Temperature-Salinity Plots 58
4.2 Marine Carbonate System 62
4.2.1 Nutrients and Stoichiometry 65
4.2.2 Alkalinity 68
4.2.3 pH 69
4.3 CO_2 Flux 72

5 Discussion **75**
5.1 Physics 75
5.2 What controls stoichiometry? 77
5.2.1 Remineralisation 78
5.2.2 Anaerobic remineralisation 80
5.2.3 Photosynthesis 82
5.2.4 Air-sea CO_2 Flux 84
5.2.5 Calcification 85
5.2.6 Contributions to the Marine Carbonate System 86

5.2.7 Oxygen Ventilation in the OMZ 90
5.3 Coastal Alkalinity Production 92
5.3.1 Biogeochemistry of shelf alkalinity 93
5.3.2 Alkalinity Production 95
5.3.3 Global Relevance 96
5.3.4 Contribution to pH 98
5.3.5 High CO_2 World 100
5.4 CO_2 Flux 102
5.4.1 Revelle Factor 102
5.4.2 Wind and ΔpCO_2: Components of flux 103
5.4.3 Flux quantified 105

6 Conclusion **109**
6.1 Seasonality of the stoichiometry 109
6.2 Alkalinity: Sink or Source 111
6.3 Seasonal air-sea pCO_2 Flux 112

References **114**

A Appendix: Supplementary Data **I**
A.1 Active upwelling divergence zone I
A.2 Biogechemical Data III
A.3 Satellite Data V

B Appendix: Box and Whisker Plots **VII**

C Appendix: Recalculation Scripts **XII**
C.1 Script Downloads XII
C.2 Code Listing XII

List of Figures

2.1 A diagram shown a box-model of the carbon cycle, where the size and residence time (τ) of each reservoir are given. Image was taken from Sigman and Boyle (2000). 6
2.2 Schematic showing the processes affecting carbon carbon flux between the atmosphere, surface ocean and deep ocean. 7

2.3 A plot showing the parametrization of k_w for different studies at different wind speeds. A temperature of 20°C was assumed. . . . 9
2.4 A *Bjerrum plot* showing the relationship between the marine carbonate species as shown in equation 2.3. A DIC concentration of 2300 µmol kg^{-1} was used. (Zeebe and Wolf-Gladrow, 2001) . . . 12
2.5 The Revelle factor for the upper 50 m of the ocean. Where the factor is high, changes in pH or pCO_2 are large for a given change in DIC. Image taken from Sabine et al. (2004) 20
2.6 Diagram showing various processes affecting nitrogen (blue text). Values in brackets show the change in alkalinity per unit of nitrogen. 26
2.7 Map of continental shelves. Eastern boundary regions are highlighted in yellow. The Benguela region is shown in red. Image adapted from Kudela et al. (2005) 28
2.8 Features and processes of the Benguela Current Large Marine Ecosystem (BCLME) after Hutchings et al. (2009). Low Oxygen Water (LOW) 30
2.9 T-S diagrams showing watermasses found in the Cape and Angola Basins (after Shillington et al., 2006). Key: Antarctic Intermediate Water (AAIW); High (HSAIW) and Low (LSAIW) Salinity Antarctic Intermediate Waters South Atlantic Central Waters (SACW); High Salinity Central Water (HSCW); Low Salinity Central Water (LSCW). 32
2.10 An ideal conceptual model of phytoplankton succession throughout the year in an upwelling system. Where "R" represents ruderal, "C" for colonist, and "S" for stress-tolerant species. Image taken from Smayda and Reynolds (2001). 34
2.11 Circulation during the summer months in the greater St. Helena Bay region. After Pitcher and Nelson (2006) 36
3.1 Southern Benguela topography and station locations. ETOPO1 topography data used Amante and Eakins (2009) 41
3.2 A diagram representation of the VINDTA 3C. Objects are shown in blue (and green labels) and black (and yellow labels) to distinguish between DIC and TA apparatus respectively. 43
3.3 Confidence interval for CRMs (before recalculation) for each month. Mean value is not shown as confidence interval applies to CRMs as well as samples after recalculation. 48
3.4 Plots showing the contrast between the two salinity correction methods for TA. On the left is the result of the standard correction. On the right is the correction procedure as suggested by Friis et al. (2003). 49

3.5 An example of a monthly sampling section showing the zonation along the vertical and horizontal. Numbers at the top of the section show the station number. The labels on the y-axis and the top x-axis are the names used to describe the zones. On the horizontal, stations were defined by longitude. And in the vertical: surface samples were defined by thermocline depth. Bottom samples were within 50 m from the bottom, unless 3/4 of the bottom depth was deeper than 50 m. Remaining samples were classified as intermediate. 53

4.1 Wind rose plots for CCMP winds (m s^{-1}) for the domain 32.0 to 33.0°S and 17.0 to 18.0°E. Data is divided into three seasons, where *(a), (b)* and *(c)* are summer, autumn and winter respectively. Note that the radius of each plot varies as selected seasons are different lengths. 55

4.2 Bakun Upwelling Index (BUI) for 33.0 to 32.0 ˚S, and 17.0 to 18.0 ˚E with a one day moving average. Winds were rotated by 15˚ to compensate for coastal rotation. Data units are in transport (m^3 s^{-1}) per 100 m of coastline, where positive values denote upwelling and negative values downwelling. Vertical black lines represent the days on which samples were taken. Gray bars indicate a fourteen day period prior to sampling (discussed further in figure 4.3). 56

4.3 Cumulative upwelling for each month fourteen days prior to sampling, as indicated in figure 4.2. Note that the y-axis is in 10^8 m^3 per month for 100 m of coastline. Positive values are upwelling and negative values represent downwelling. 57

4.4 TS-diagrams for summer *(a)*, autumn *(b)* and winter *(c)*. Blocks denote the following water masses: AAIW = Antarctic Intermediate Water; SACW = South Atlantic Central Water; MUW = Modified Upwelled Water; OSW = Oceanic Surface Water. . . . 59

4.5 A plot showing the depths of the thermocline (m) for sampled months along the y-axis and longitude along the x-axis. 60

4.6 Plots of salinity vs. nitrate *(a-c)* for each season: summer, autumn, winter respectively. The dashed line marks the upwelled waters' salinity (34.80).
Plots of temperature vs. nitrate *(d-f)* for each season. The dashed line at 10°C represents the temperature of newly upwelled water. RMSE shows the root mean squared error.
In reference to key: SS = shelf-slope, SO = outer-shelf, SI = inner-shelf and NS = near-shore 61

4.7 nDIC (a-c) and nTA (d-f) averages and standard deviations for each zone for summer (top), autumn (middle) and winter (bottom). Concentrations are in µmol kg^{-1}. SS = shelf-slope, SO = outer-shelf, SI = inner-shelf and NS = near-shore, S = Shallow, I = Intermediate and B = Bottom 63

4.8 Three plots for summer *(a)*, autumn *(b)* and winter *(c)* comparing nDIC and normalised total alkalinity nTA*. January, February, March and December were omitted due to unreliable data. A reference line of 2345 µmol kg^{-1} was drawn to highlight the source water concentration of nTA*. Colour vectors, in figure *(d)* show the various mechanisms of change to the marine carbonate system. SS = shelf-slope, SO = outer-shelf, SI = inner-shelf and NS = near-shore 64

4.9 Scatter plots of nitrate vs. phosphate *(a-c)* for summer, autumn and winter respectively. The red line represents the expected Redfield ratio of 16:1.
Scatter plots of nDIC vs. nitrate *(d-f)* throughout the year for summer, autumn and winter respectively. Note that January and February were excluded due to failing quality control. The red line represents the Redfield ratio of 6.6:1.
SS = shelf-slope, SO = outer-shelf, SI = inner-shelf and NS = near-shore. RMSE shows the root-mean-squared error of the best fit line. P shows the P-value for an independant t-test comparing the expected Redfield values to the observed values, where the null hypothesis is that the data fits the best-fit line. 66

4.10 Normalised DIC (34.8) plotted against apparent oxygen utilisation (AOU). January and February were omitted due to bad quality data. The red line is the expected ratio according to Redfield stoichiometery (C:O = 0.77). RMSE shows the root-mean-squared error of the best fit line. P shows the P-value for an independant t-test comparing the expected Redfield values to the observed values, where the null hypothesis is that the data fits the best-fit line. SS = shelf-slope, SO = outer-shelf, SI = inner-shelf and NS = near-shore 67

4.11 Plot of normalised alkalinity and dissolved oxygen (DO) for all months excluding February, March and December. The dashed lines are one standard deviation from the mean (2348.21±25.92). SS = shelf-slope, SO = outer-shelf, SI = inner-shelf and NS = near-shore 68

4.12 Temperature plotted against pH. The dotted lines are average pH for each season, summer *(a)*, autumn *(b)* and winter *(c)*. Two plots of nDIC vs. pH *(d)* and nDIC vs. pH normalised to a TA value of 2345 µmol kg^{-1} *(e)*. SS = shelf-slope, SO = outer-shelf, SI = inner-shelf and NS = near-shore 70

4.13 Hovmöller diagrams of ΔpCO_2 *(a)* and wind speed *(b)* for January to December 2010. ΔpCO_2 (µatm) in the upper plot is calculated by $pCO_{2\ (sea)}$- $pCO_{2\ (air)}$. A positive value (red) is a carbon source. The lower plot, wind speed (m s^{-1}), is plotted from the CCMP product by Atlas et al. (2011). 72

4.14 On the right, a plot of CO_2 flux (mmol $m^{-2}d^{-1}$) for all months with valid CO_2 data. The dashed line is where flux is zero. On the left is a plot of the flux averaged for the section. 74

5.1 The nutrient trapping mechanism as described by Tyrrell and Lucas (2002). Water is circulated up onto the shelf along the bottom and off the shelf at the surface. This drives recycling of particulate organic matter on the shelf. 76

5.2 Trajectory plots of average nDIC and nTA* for summer, autumn and winter (*a, b* and *c* respectively). Black circle (•) represents SACW; ■ is bottom inner-shelf water; ◊ shows near-shore surface water; and □ is inner-shelf surface water. Contours show pCO_2 at 10°C and salinity of 34.8. Plotted points represent SACW, followed by inner-shelf bottom, nearshore surface and inner-shelf surface. Coloured arrows show several of the dominant processes that are discussed throughout this chapter. 78

5.3 Plot of the contributions by various processes to the marine carbonate system. Note that positive black bars represent aerobic oxidation (or remineralisation) and negative black bars are the photosynthetic contribution to carbon. 'Other' represents the difference between the actual and the calculated nDIC. Age of the water using warming rates (Guastella, 1992) for the nearshore is 1.9 and 4.3 days for summer, autumn. For the inner-shelf the water age is 5.5 and 5.4 days old respectively. For more information see table A.1. 88

5.4 Bar graph showing the interpolated area for dissolved oxygen throughout 2010. Note that months on the x-axis are not plotted chronologically, but rather by season. 89

5.5 A map showing the positions of stations 4 and 5 relative to stoichiometry *(a)*. Two line plots showing the dissolved oxygen *(b)* and salinity *(c)* of bottom samples of stations four and five. Correlation between the two parameters for stations four and five was -0.86 and -0.93 respectively. 91

5.6 A scatter plot showing nTA and nDIC plotted against each other. Note that nTA is not corrected for nitrate. The vectors indicate the various processes that alter nTA. 92

5.7 Diagram showing the uptake of nitrate (NO_3^-) as explained by Wolf-Gladrow et al. (2007). In order to maintain ionic charge, a cell has to co-transport a NO_3^- ion with a sodium ion (Na^+) via a sodium-dependant symport. To avoid a buildup of Na^+, it is exchanged with a H^+ ion via an antiport. A decrease in H^+ leads to an increase in alkalinity. 93

5.8 Bar chart showing the loss or gain of TA during 2010 where positive (gray) is net gain, negative (black) is loss. Where there is a simultaneous loss and gain of TA, a white bar represents the total gain for that month. February, March and December were omitted due to bad data. See table A.2 for more info. 95

5.9 Sections of interpolated TA ($\mu mol.kg^{-1}$) on top and potential density ($\sigma = kg.L^{-1}$ - 1000) on the bottom. Notice how the strong density gradient coincides with the top of the TA tongue. 97

5.10 Scatter plot showing the Revelle factor vs. pH *(a)*. There is a clear distinction between the surface and bottom waters due to differences in the Revelle factor.
Plot of Ω_{Ca} against ΔpH_{2345} *(b)*. The latter is the difference between pH and pH normalised to a TA of 2345 $\mu mol\ kg^{-1}$, *i.e.* the contribution of nTA* to pH. 99

5.11 A Hovmöller plot of the Revelle factor for the southern Benguela throughout 2010. 102

5.12 Three plots showing the influence of the state parameters on the Revelle factor *(c)*. pCO_2 is plotted against DIC *(a)* and TA *(b)*. The vertical dashed lines represent the surface ranges of DIC and TA in the southern Benguela. The coloured areas demarcate the corresponding pCO_2 and Revelle factor ranges expected in the southern Benguela. The Revelle factor is plotted with DIC and TA on the same x-axis. In each data-set, non-changing parameters were set to SACW values. 103

5.13 Scatter plot of wind speed (m s^{-1}) against $|\Delta pCO_{2\ (sea\text{-}air)}|$ (µatm). Contours represent the CO_2 flux (mmol $m^{-2}d^{-1}$), where black and gray lines have 20 and 5 mmol intervals respectively. However, the first gray line is plotted at 1 mmol $m^{-2}d^{-1}$. The color axis is absolute flux (mmol $m^{-2}d^{-1}$). The red arrow shows a hypothetical increase of wind speed and consequent out-gassing. 104

5.14 A plot showing the FCO_2 (mmol m^{-2} d^{-1}) for the SHBML. The Hovmöller diagram on the right shows daily CO_2 flux using daily winds and ΔpCO_2 calculated from interpolated parameters. The solid black line is where flux is zero and black dots are actual samples. The dotted line is the end of the shelf, and samples beyond this line were not included in flux calculations. On the left is the integrated CO_2 flux (mmol m^{-2} d^{-1}) for each day of the year. 107

5.15 FCO_2 data from the QUIMA-VOS line for 2005 and 2006 (after Santana-Casiano et al., 2009). The markers show pCO_2 (summer, autumn and winter) for where the SHBML intersects the QUIMA line. Data accessed via the SOCAT library Pfeil et al. (2011). A constant atmospheric CO_2 concentration of 390 µatm was assumed. 107

6.1 Bar graph summarising each mechanism responsible for DIC changes. The last column, 'NET', shows the sum of all the other processes. This indicates that there is a net export flux of carbon, *i.e.* the sum of photosynthesis calcification and flux is greater than the remineralisation processes. 110

A.1 Dissolved oxygen vs. nitrate for summer (a), autumn (b) and winter (c). III

A.2 Scatter plots for nDIC vs. phosphate for summer (a), autumn (b) and winter (c). The red line shows the ideal Redfieldian ratio. The thin black line is the best fit line with equation. IV

A.3 An array of MODIS aqua chl-a (mg m^{-3}) images from ftp://podaac-ftp.jpl.nasa.gov. Nine of the ten sampled months are shown (July omitted). Images are a composite of four days prior to the sampling date. The white markers show the stations of the SHBML. V

B.1 Box and whisker plot of salinity data before quality control. . . VIII

B.2 Box and whisker plot of temperature data before quality control. VIII

B.3 Box and whisker plot of oxygen data before quality control. . . . IX

B.4 Box and whisker plot of nitrate data before quality control. . . . IX

B.5 Box and whisker plot of phosphate data before quality control. . X

B.6 Box and whisker plot of silicate data before quality control. . . . X

B.7 Box and whisker plot of dissolved inorganic carbon data before quality control. XI
B.8 Box and whisker plot of alkalinity data before quality control. . . XI

List of Tables

2.1 Summary of the gas transfer velocities by various authors. 11
3.1 Sampling information from monthly cruises. The Storage column shows the maximum number of days that a batch of samples was stored. 42
3.2 A comparison of the standard errors of dissociation constants found by different authors (adapted from Mojica-Prieto and Millero (2002)) 46
5.1 Table showing the stoichiometric ratios for the SHBML. Surface stoichiometry are split from the intermediate and bottom samples. The ideal Redfield ratios are shown in the furthest right column. 77
5.2 Stoichiometric ratios for processes discussed in chapter5.2. 80
5.3 The conceptual methodology to arrive at the contributions of each process discussed in section 5.2. Note that the contribution by some processes cannot be found due to insufficient data. These were grouped together as "other" in figure 5.3. 86
5.4 Table summarising the results from the CO_2 flux calculations. Note that season fluxes are given in mmol m^{-2} d^{-1} and that yearly is given in mol m^{-2} yr^{-1}. Yearly estimates given in this study are those from different wind configurations. Ingassing is negative and outgassing is positive. See text for more details. 105
A.1 This table shows the contribution of various processes for three zones for all seasons. Three zones used were: inshore-bottom, bay-surface and inshore surface. The average of each zone was used for the measured variables (nTA, nDIC, NO_3^-, PO_4^-). Age of surface water was calculated using the warming rate calculated by Guastella (1992). Contributions were calculated using stoichiometery from data trends (figures 4.9 a-f). See table 5.3 for derivation of marine carbonate system processes. The first line of each season (SRC) shows source water (SACW) concentrations. VI
A.2 Table showing the percentage area of good and bad linearly interpolated alkalinity data for a section from the coast to 17.5 °E. Percentage area of TA loss and gain are also shown. Section has a total area of ~89.29 km^2. VII

1 Introduction

Over the last 200 years, the marine carbonate system has played a vital role in regulating Earth's climate, by taking up 48% anthropogenic carbon dioxide (CO_2) (Sabine et al., 2004). The rate at which atmospheric CO_2 concentrations are increasing creates much uncertainty, making understanding the Earth's feedbacks and changes a difficult task. One such example in the ocean is acidification due to increasing atmospheric CO_2. Falkowski et al. (2000) call for a systems approach, where not only the carbon cycle is considered, but also other biogeochemical and climatological cycles. Key to understanding these cycles on a global scale, is to first understand them on a regional scale. The southern Benguela upwelling system may offer such a laboratory, due to its locality and unique biogeochemistry.

The southern Benguela is one of three sectors along the southern African west coast, spanning the coastlines of Angola, Namibia and South Africa (Shillington et al., 2006). The southern sector is marked by a strong seasonality of upwelling, due to seasonal changes in equatorward winds. Upwelling results in nutrient rich waters to be brought into the euphotic zone, where phytoplankton can consequently thrive. From a carbon cycle perspective, this system is interesting, as the uptake of CO_2, by highly productive phytoplankton, is juxtaposed by out-gassing, as CO_2 enriched water is upwelled and exposed to the atmosphere.

The carbon enrichment of this upwelling source water, occurs predominantly on the shelf of the southern Benguela. As water advects over the shelf, it is enriched by remineralising organic matter from previous productivity. Given the correct stratification and circulation, oxygen depletion may occur in the bottom waters over the shelf due to lack of ventilation. Remineralisation in these conditions can lead to various biogeochemical pathways, such as denitrification and sulfate reduction. These processes alter the original nutrient and carbon stoichiometry of the system (Tyrrell and Lucas, 2002).

This also leads to changes in the marine carbonate system parameters, importantly alkalinity, which acts as a buffer against ocean acidification.

In this thesis, I will investigate the seasonal changes to the marine carbonate system in the southern Benguela in 2010, with a focus on: the stoichiometric ratios of carbon and nutrients; production of alkalinity on the southern Benguela shelf; and the carbon flux throughout the year. This multifaceted approach to the marine carbonate cycle, may help to understand mechanisms that drive CO_2 fluxes on a larger scale. This study also addresses the lack of seasonal CO_2 observations for the southern Benguela, allowing for an unbiased investigation of the marine carbonate system.

In order to see how the southern Benguela fits into the global carbonate cycle, a literature review follows this introduction. The literature review briefly looks at the history of the anthropogenic climate change problem. The global carbon cycle is then discussed. The literature review gradually narrows in from the global scope down to the local scale that is the Benguela, all the while describing the marine carbonate system chemistry. The key questions for this thesis are posed at the end of the literature review.

In the methodology section, the sampling and analytical procedures are explained. This is followed by the results section in which basic data is presented under physics, marine carbonate system and air-sea CO_2 flux sections. Data which required additional analysis is shown in the discussion.

The discussion is sectioned into four parts. The first investigates the physical characteristics of the system throughout 2010 and sets the scene for the biogeochemical sections. Thereafter, the nutrient stoichiometric ratios are addressed. The stoichiometric ratios are then used to calculate the contribution of photosynthesis and remineralisation processes to the carbonate system. The third section investigates the southern Benguela's contribution to shelf production of alkalinity based on changes to alkalinity. The role of pH in the southern Benguela is also investigated with regard to ocean

acidification. Lastly, the air-sea CO_2 flux of the southern Benguela is presented and compared to the previous estimates. The contribution of the wind *vs.* ΔpCO_2 to the flux is also discussed in this section.

This thesis concludes by summarising the findings and implications. Suggestions for future studies are also made in this section. Three appendixes are listed at the end of the thesis containing:

A) supplementary data, plots and equations follows;

B) box and whisker plots for quality control purposes;

C) and source code listing for the program used to process alkalinity.

2 Literature Review

2.1 History of the Problem

Since the start of the Industrial Revolution, man has been burning fossil fuels and increasing the rate of land use change. Over two centuries later, atmospheric carbon dioxide (CO_2) levels have risen from a pre-industrial estimate of 280 ppmv (parts per million per volume) to *ca.* 392 ppmv (Tans and Keeling, 2011). The rate of this increase surpasses anything seen in the last 420k years (Falkowski et al., 2000). This is reason for great concern as CO_2 is a greenhouse gas, meaning that with increased atmospheric concentrations, our planet should theoretically warm, hence "global warming". The effects of CO_2 have also been felt in the surface oceans, with global pH decreasing by 0.1. Moreover, the ever rising need for energy means that the rate of CO_2 release is all but decreasing (Solomon et al., 2007).

While this has become a 20^{th} and 21^{st} century problem, knowledge of the issue goes back to the mid 19^{th} century when CO_2 was first identified as having "greenhouse gas" properties (Tyndall, 1861), though the term had not yet been coined. This came about 50 years later when, Swedish Nobel laureate, Svante Arrhenius created the *greenhouse law*. Arrhenius (1896) was the first to propose that Earth's climate could be changed by anthropogenic forcing, though his insight may have been somewhat limiting:

> *"By the influence of the increasing percentage of carbonic acid in the atmosphere, we may hope to enjoy ages with more equable and better climates"Svante Arrhenius, 1908*

It was Callendar (1938) who first raised the alarm on global warming as a threat. However, his publication was ill timed as the 1940s to 1960s was marked by a period of fluctuation and uncertainty in global temperatures (Le Treut et al., 2007). By the 1970s these uncertainties were attributed to atmospheric aerosol shading, which were on the decrease with the use of cleaner energy sources

(Peterson et al., 2008). Conversely, temperatures were again on the rise and so was the evidence for global warming (Peterson et al., 2008). In 1988 the Intergovernmental Panel on Climate Change (IPCC) was created to "provide the governments of the world with a clear scientific view of what is happening to the world's climate" (IPCC, 2011).

Though the advent of the IPCC was only in the 1980s, numerous studies had already started investigating the broad topic of global warming. Keeling (1960) published what is now the first two years of the *Keeling curve*. His data showed that atmospheric CO_2 was increasing at an appreciable rate and naively stated that the oceans had not played a role in taking up CO_2. This was in the wake of a groundbreaking publication by Revelle and Suess (1957) who suggested that, while oceanic uptake of CO_2 may not be 100% efficient, the oceans were the long term regulator of global atmospheric CO_2. This set the tone for the years to come: the ocean was recognised as being important however, there was a great deal of uncertainty in the short term role of the ocean.

2.2 Carbon Cycle

As stated earlier, the Earth's atmospheric CO_2 concentrations are regulated by the oceans over long periods. To understand this we need to look at the big picture - the global carbon cycle (figure 2.1). The carbon cycle consists of different reservoirs that operate on different residence times or flux rates, which determines the balance in each pool. The terrestrial reservoir operates on the shortest time scale of less than ten years. The ocean has been divided into two separate reservoirs, namely the surface ($<$ 1 km) and deep ocean. This distinction is made due to the vastly different residence times between the two systems. The surface ocean operates on a time scale in the order of tens of years, compared to the deep ocean's residence time of 100s of years. This pales in comparisson to the geological reservoir's residence time, which is longer than 100k years.

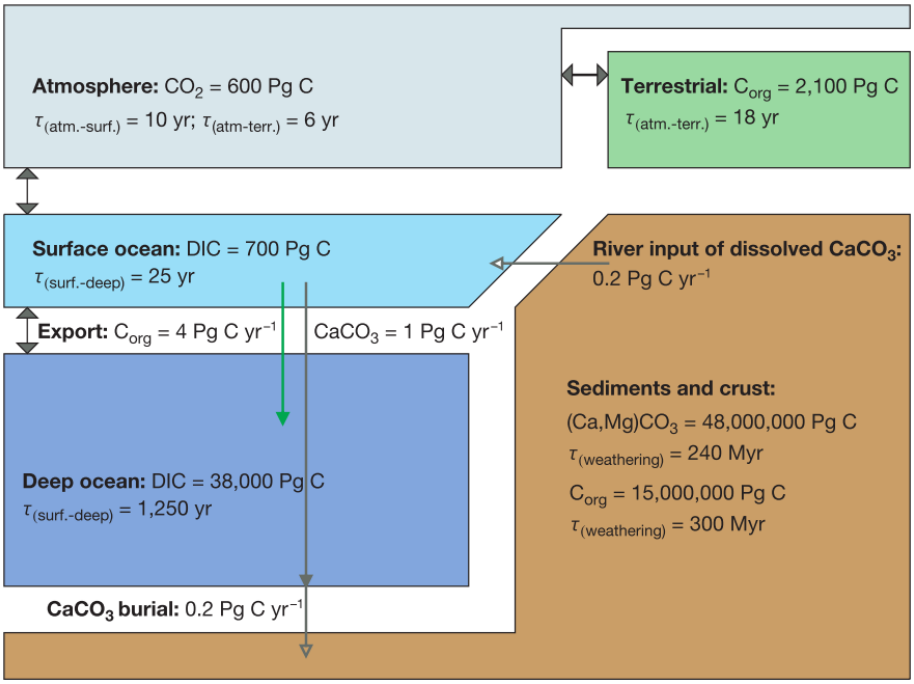

Figure 2.1: A diagram shown a box-model of the carbon cycle, where the size and residence time (τ) of each reservoir are given. Image was taken from Sigman and Boyle (2000).

The pre-industrial carbon cycle was considered to be at equilibrium, despite large natural annual terrestrial fluxes. However, the input of anthropogenic CO_2 has created an imbalance, leading to a build-up of carbon in the reservoirs with shorter time scales, predominantly the atmosphere, and secondly the surface ocean.

The carbon cycle has not always conformed to the pre-industrial configuration (figure 2.1). Over the last two million years, Earth's climate has been dominated by glacial-interglacial cycles (Sigman and Boyle, 2000). Unlike our current climate change situation, the primary driver of switches between glacials and interglacials is thought to have been kick-started by variations in the Earth's orbital eccentricity, which translates to changes in solar radiation. Note however, that ice-core records from the last 420k years do show that temperature and atmospheric CO_2 were closely correlated (Jouzel et al., 1987). Paillard and Parrenin (2004) found a controversial explanation for this close relationship using a model driven by solar

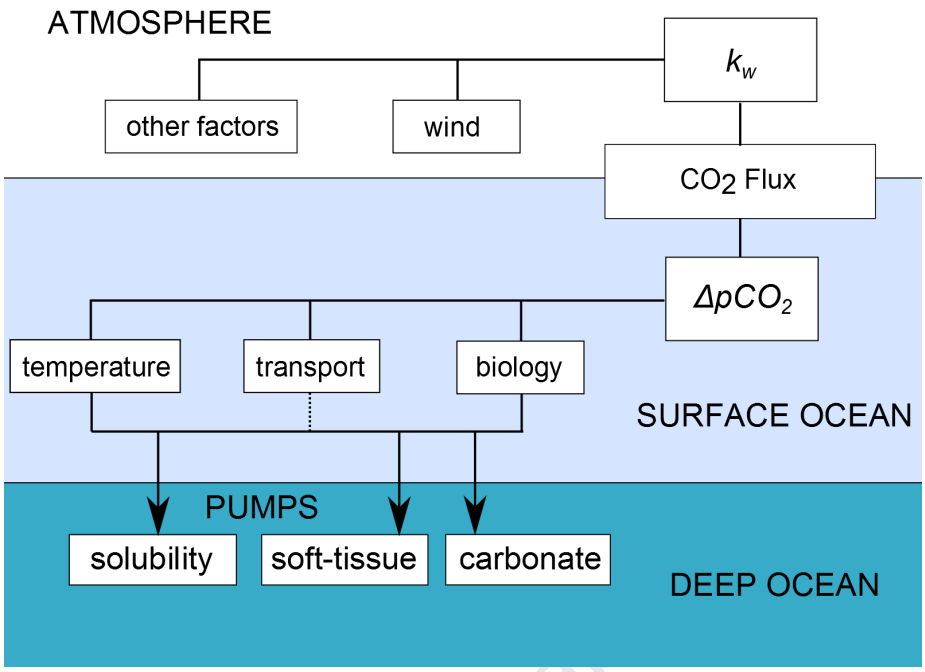

Figure 2.2: Schematic showing the processes affecting carbon carbon flux between the atmosphere, surface ocean and deep ocean.

insolation. Their model showed that Antarctic sea-ice extent could alter CO_2 air-sea fluxes enough to switch from one phase to another. This is due to the important role that deep water formation in high latitudes plays in transporting CO_2 from the atmosphere into the deep ocean. This reinforces the role of the deep ocean as a long term regulator of atmospheric CO_2. It also introduces one of the mechanisms by which the surface ocean is linked to the deep ocean.

Vertical distribution of CO_2 in the ocean reveals that the deep ocean is 12% richer in inorganic carbon than the surface (Sarmiento and Bender, 1994). Sequestration into the deep ocean thus requires a mechanism that can transport carbon against this concentration gradient. This inspired the term "pump" in Volk and Hoffert (1985) who recognise three carbon pumps, namely the solubility, soft-tissue and carbonate pumps. However, the interface between the atmosphere and the ocean will be considered.

2.3 Carbon flux in the oceans

2.3.1 Global Ocean

While the Keeling curve showed that global atmospheric CO_2 had been increasing, it was far more difficult proving the same in the oceans due to high frequency, seasonal and interanual variability. Up to the 1990s, ship based pCO_2 (partial pressure of CO_2) measurements were scarce. But, the increasing recognition of the ocean as an important role player in climate change, resulted in large scale action through the formation of the Joint Global Ocean Flux Study (JGOFS, 1990). The main focus of JGOFS was to quantify the air-sea exchanges of CO_2 for the open ocean, the number of *in-situ* pCO_2 measurements increased drastically from the '90s onward.

In 1997, Takahashi et al. produced the first global estimate of air-sea exchange based on *in-situ* data. This estimation was based on 250k data points and was a seaward flux ranging from 0.60 to 1.34 Pg C yr^{-1}. However, this data was sparse through all seasons ranging from 1960 to 1995. Publications followed in 1999, 2002 and 2009, with 550k, 980k and 3.0 million measurements respectively. Increased measurements did not result in different results; it did however, improve our understanding of the seasonality of CO_2 flux. The latest two publications found that global flux was 2.0±0.6 and 2.0±1.0 Pg.C.yr^{-1} respectively. The increase in uncertainty was largely due to closer inspection of the sources of error in their calculation.

2.3.2 Calculating Flux

Quantifying the magnitude of the decadal climatological flux of the oceans has now, to some extent, been achieved. The latest study by Sweeney et al. (2009) shows, there is a great deal of error in the estimates. To understand this large error we will look at how these flux estimates are derived. Direct determination of CO_2 flux is not possible at sea, but the equation below forms the basis of how CO_2

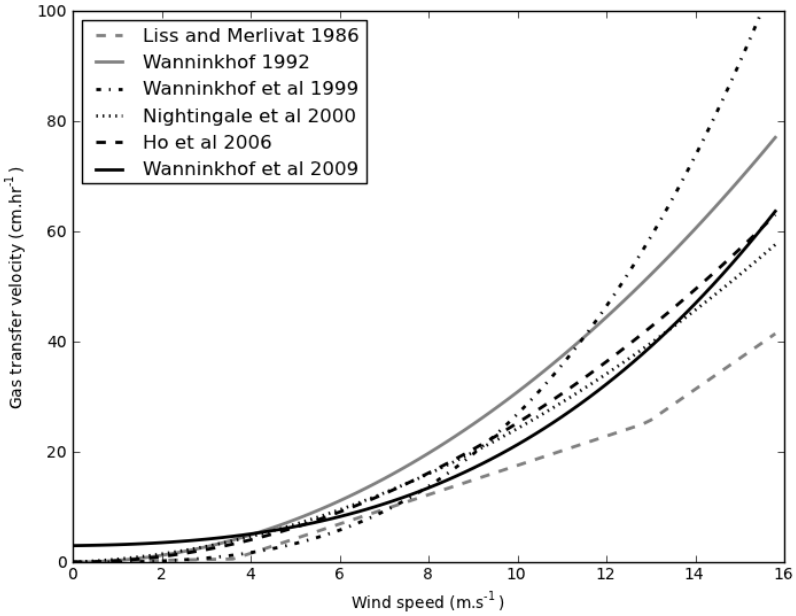

Figure 2.3: A plot showing the parametrization of k_w *for different studies at different wind speeds. A temperature of 20°C was assumed.*

flux (F) is calculated:

$$F = k_w \cdot K_0 \cdot (pCO_2^{sea} - pCO_2^{air}) \tag{2.1}$$

Where k_w is the gas transfer velocity (also called the *piston velocity*), K_0 the *solubility parameter* and the equation in the brackets is the difference between the pCO_2 of the sea and the atmosphere (ΔpCO_2).

The gas transfer velocity is an empirically determined parameter, but our understanding thereof derives from several theoretical models. The simplest of these is the stagnant-film model (Liss and Slater 1974; Broecker and Peng 1974). This model assumes a thin layer of water in which diffusion with the atmosphere and the mixed surface water occurs. However, this model fails to incorporate mixing between the surface layer and the stagnant film. The replacement film (Danckwerts, 1951) and the eddy impingement models (McCready

and Hanratty, 1984) address this problem by defining a dynamic interface or film. In each of these models the concept is fairly similar:

- The transfer velocity is dependent on the turbulence at the interface and and the thickness of the film.
- Turbulence at the interface is affected primarily by wind stress.

Other factors such as wave breaking, bubble formation, humidity and temperature gradients and surfactants may also alter the gas exchange velocity (Nightingale, 2009). The thickness of the film is determined by turbulence and is mathematically represented by the Schmidt number (Sc). The Sc can be broken into two components: the ratio of the kinematic viscosity of water (v), and molecular diffusivity of a particular gas (ϵ) as shown below:

$$Sc = {}^{v}/_{\varepsilon} \tag{2.2}$$

The Sc allows a gas transfer velocity to be determined for different temperatures and gasses. In practice, Sc is defined empirically (Wanninkhof, 1992). Additionally the Sc is normalised to account for different physical conditions (see Table 2.1), where values for CO_2 in freshwater are normalised to 600 and saltwater is normalised to 660. A Schmidt dependence number (n in Sc^{n}) is applied to account for the behaviour of the different theoretical boundary layer models. An n of $-2/3$, as used by Liss and Merlivat (1986), assumes a smooth interface surface, whereas an n of $-1/2$ is better at representing a fluid interface.

Because of the complexity of such micro-scale processes, none of the models can accurately represent k_w. In practice k_w is thus also determined empirically (figure 2.3). Lab and field studies have identified different relationships based on wind speed to parameterise k_w. Several techniques are typically used to investigate this relationship between CO_2 flux and wind speed. One of the earlier studies by Liss and Merlivat (1986) used SF_6 as a deliberate tracer of CO_2 flux to arrive at a parameterisation of three linear functions of k_w, depending on the wind speed (see table 2.1). Wanninkhof (1992) simplified

Table 2.1: Summary of the gas transfer velocities by various authors.

Author	Gas Transfer Velocity
Liss and Merlivat, 1986	$0.17 \cdot U \cdot (Sc/600)^{-2/3} for\, U \leqslant 3.6\, m.s^{-1}$ $(U - 3.4) \cdot 2.8 \cdot (Sc/600)^{-2/3} for\, 3.6 < U \leqslant 13\, m.s^{-1}$ $(U - 2.8) \cdot 5.9 \cdot (Sc/600)^{-2/3} for\, U > 13\, m.s^{-1}$
Wanninkhof, 1992	$0.31 \cdot U^2 \cdot (Sc/660)^{-1/2}$
Wanninkhof and McGillis, 1999	$0.0283 \cdot U^3 \cdot (Sc/660)^{-1/2}$
Nightingale et al., 2000	$(0.333 \cdot U + 0.222 \cdot U^2) \cdot (Sc/600)^{-1/2}$
Ho et al., 2006	$(0.266 \cdot U^2) \cdot (Sc/600)^{-1/2}$
Wanninkhof et al., 2009	$\left(3 + 0.1 \cdot U + 0.064 \cdot U^2 + 0.011 \cdot U^3\right) (Sc/660)^{-1/2}$

Liss and Merlivat's three part approximation by using the bomb-derived radiocarbon abundance (^{14}C), producing relationship where flux is determined as the quadratic function of wind speed. The simplicity of this parameterisation has made this estimation very popular in the literature. Sweeney et al. (2009) estimated the error on this estimation of k_w to be 30% of their total error. A cubic relationship between wind speed and CO_2 flux was found by Wanninkhof and McGillis (1999) who directly measured covariance flux of CO_2. But this estimate is considered an overestimation (Takahashi et al., 2002). Wanninkhof et al. (2009) produced a polynomial parametrization of k_w which reportedly reduces the error from 30% to 15% if used in calculating global flux as done in Sweeney et al. (2009).

Because wind speed's dominant role in determining k_w, the wind product used accounts for a great deal of the uncertainty in the flux calculations. Sweeney et al. (2009) attribute 20% of the total error was due to winds (where NCEP-DOE AMIP-II Reanalysis winds were used). Atlas et al. (2011) released a new cross-calibrated wind product, which reduces the wind derived error.

2.4 Marine Carbonate Chemistry

Once CO_2 has entered the ocean, it is influenced by several factors, namely biology, temperature and transport (figure 2.2). The interaction between these three factors determines whether the ocean is a sink or source. In this section temperature and biology effects

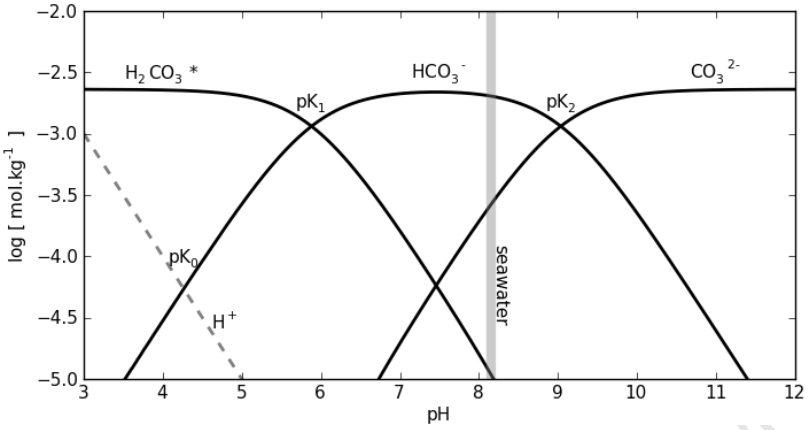

Figure 2.4: A Bjerrum plot *showing the relationship between the marine carbonate species as shown in equation 2.3. A DIC concentration of 2300 µmol kg^{-1} was used. (Zeebe and Wolf-Gladrow, 2001)*

will be investigated. The latter can be divided into two mechanisms: photosynthesis and calcification. Transport acts in conjunction with these two processes and will not be discussed. But before biology and temperature can be assessed, the carbonate chemistry of the marine carbonate system has to be understood.

The equations below describe the reactions which govern the CO_2 equilibrium in seawater:

$$\begin{aligned} CO_{2\,(aq)} + H_2O &\overset{K_0}{\longleftrightarrow} H_2CO_3^* \\ H_2CO_3^* &\overset{K_1}{\longleftrightarrow} H^+ + HCO_3^- \\ HCO_3^- &\overset{K_2}{\longleftrightarrow} H^+ + CO_3^{2-} \end{aligned} \tag{2.3}$$

Most CO_2 in the ocean is stored as bicarbonate (HCO_3^-), one of the species of dissolved inorganic carbon (DIC). The other constituents of DIC are carbonate (CO_3^{2-}) and carbonic acid (H_2CO_3). Carbonic acid is often shown as $H_2CO_3^*$, which includes $CO_{2\,(aq)}$ as these two species are synonymous and difficult to distinguish (see figure 2.4 for graphical representation). In a system closed to changes in DIC and TA, the chemical speciation of the marine carbonate system depends solely on the dissociation constants, which are af-

fected by temperature, salinity and pressure. DIC is one of three forms of carbon found in the ocean, where dissolved organic carbon (DOC) and particulate organic carbon (POC) are the other two. The definition of DIC is shown below:

$$\begin{array}{rcccc} DIC & = & [H_2CO_3^*] + & [HCO_3^-] + & [CO_3^{2-}] \\ & = & (0.5\%) & (88.9\%) & (10.6\%) \end{array} \tag{2.4}$$

Note that the speciation percentage shown in equation 2.4 are sensitive to changes in salinity, temperature and pressure and TA (where the values for the aforementioned variables are 35.0, 20 º C, 0 dBar and 2300 µmol kg^{-1} respectively). DIC is one of the four measurable parameters of the marine carbonate system. The other three are pH, pCO_2 and alkalinity. With any two of these parameters the speciation of the marine carbonate system can be determined. However, DIC and alkalinity are the only parameters that are conservative with respect to temperature and pressure. Hence, these state variables are used in carbon cycle models rather than pH and pCO_2(Wolf-Gladrow et al., 2007).

The definition of total alkalinity (TA) defined by Dickson (1981) is: "the number of moles of hydrogen ion equivalent to the excess of proton acceptors (bases formed from weak acids with a dissociation constant K $\leq 10^{-4.5}$ at 25°C and zero ionic strength) over proton donors (acids with K $> 10^{-4.5}$) in 1 kg of sample." This is more explicitly shown by the equation below:

$$\begin{array}{rcl} TA & = & [HCO_3^-] + 2[CO_3^{2-}] + [B(OH)_4^-] + [OH^-] + [HPO_4^{2-}] + \\ & & 2[PO_4^{3-}] + [SiO(OH)_3^-] + [NH_3] + [HS^-] + ... \\ & & -[H^+]_F - [HSO_4^-] - [HF] - [H_3PO_4] - .. \end{array} \tag{2.5}$$

The bulk of alkalinity is made up by the first three ions in equation 2.5. Respectively, these make up roughly 76.8%, 18.8%, 4.2% of alkalinity for a seawater solution and the sum of these is often used as a rough approximation for alkalinity. Borate is proportionally constant to salinity throughout the ocean and is thus a conserva-

tive parameter (Sarmiento and Gruber, 2006; Wolf-Gladrow et al., 2007).

According to *Henry's Law* pCO_2, which has been discussed in section 2.3, determines the amount of CO_2 that can dissolve into water proportional to the pressure exerted by the gas. However, pCO_2 can also be calculated by the solving the marine carbonate system as shown in the following equation:

$$pCO_2 = \frac{K_2}{K_0 K_1} \frac{[HCO_3^-]^2}{[CO_3^{2-}]} \tag{2.6}$$

where the dissociation constants, K_n, are from equation 2.3. The above equation shows that pCO_2 clearly depends on the DIC and TA of seawater, emphasising the importance of the two state variables. The relationship between increased DIC and the concomitant increase of pCO_2 is described by the Revelle factor, to be described in section 2.5. Note for an increase in TA, pCO_2 is reduced. It also points out that pCO_2 is affected by changes to the dissociation constants.

The pH of seawater, -$\log_{10}$ [H^+], is a partial product of the speciation of the marine carbonate system. This operational definition of pH in seawater is an oversimplification and thus measured pH is not representative of true pH. In practice, pH is measured with reference to buffer solutions, of which the standard falls on the NBS scale. The problem with this scale is that the buffer solutions have a low ionic strength in comparison to seawater (Zeebe and Wolf-Gladrow, 2001). This led to the creation of the total scale (pH_T) by Hansson (1973). This scale uses buffers made up of artificial seawater, which includes sulphate ions to account for their presence in seawater. A slight improvement was made to pH_T by the addition of fluoride ions in the buffer solution (Goyet and Poisson, 1989), giving rise to the seawater scale (pH_{SWS}). However, the small contribution of fluoride ions to seawater means that pH_T and pH_{SWS} differ very little. It is thus that the pH_T is and should be used where possible.

The definition of the pH_{SWS} is shown below:

$$pH_{SWS} = -log_{10}\left([H^+] + [HSO_4^-] + [HF]\right) \tag{2.7}$$

With regard to the marine carbonate system, an decrease in DIC leads to the decrease in pH (equation 2.3). And an increase in TA, $[CO_3^{2-}]$, results in the increase in pH. The repercussions hereof will be discussed in full in section 2.5.

2.4.1 Temperature Effect

From the previous section, it is clear that the state variables, DIC and TA, do not change with changes in temperature, but importantly, pH and pCO_2 are not conservative to changes in temperature. Changes in water temperature result in shifting the equilibrium coefficients (equation 2.4 and 2.5), but sum of the constituents does not change. Takahashi et al. (1993) quantified the relationship between temperature and pCO_2 with the equation shown below:

$$\frac{\delta ln\, pCO_2}{\delta T} \approx 0.0423 C^{-1} \tag{2.8}$$

Where $\delta ln\, pCO_2$ is the change in pCO_2 and δT is the change in temperature. This equation applies to a closed carbonate system (where DIC and alkalinity do not change). The outcome of this relationship is that for a temperature increase of 16°C, pCO_2 doubles. The converse is true for cooling water.

Equation 2.8 considers only a closed system. What then happens to a parcel of water which is allowed to exchange CO_2 with the atmosphere? If we consider a parcel of water initially at equilibrium with the atmosphere and cooling, pCO_2 would decrease, allowing CO_2 to transfer into the ocean. But how does this affect the conservative parameters, DIC and alkalinity? For every unit of CO_2 that enters the ocean we'd expect DIC to increase by one (equations 2.3 and 2.4). Total alkalinity does not change as there is no charge imbalance for a unit of CO_2 entering the ocean.

This mechanism is what drives the solubility pump in high latitudes where deep water forms. As water at the surface cools, CO_2 is taken up, but the density also increases, causing the water to sink to the deep ocean. Surprisingly, the solubility pump accounts for only a quarter of the 12% DIC gradient observed between the shallow and deep sea. This means that the biological pumps play a more important role in drawing carbon into the deep ocean.

2.4.2 Photosynthesis

Photosynthesis in the oceans is limited to the euphotic zone due to its dependence on light. Using solar radiation as an energy source, phytoplankton convert DIC to organic carbon. Other nutrients such as nitrate (NO_3^-) and phosphate (PO_4^{3-}) are used during photosynthesis. These are known as macro-nutrients as they are required in relatively large quantities compared to micro-nutrients such as iron. The equation below shows the average uptake rates of phytoplankton for the global ocean:

$$106CO_2 + 16NO_3^- + PO_4^{3-} + 78H_2O + 18H^+ \Leftrightarrow C_{106}H_{175}O_{42}N_{16}P + 138O_2 \tag{2.9}$$

these ratios at which nutrients are taken up are referred to as *Redfield ratios* after Redfield et al. (1963). According to the Redfield ratio, for a given amount of phosphate taken up, 106 units of carbon are taken up, thus resulting in a decrease in DIC. While not immediately apparent, photosynthesis also results in an increase in TA. Alkalinity increases for the reduction of one unit of nitrate, thus for every increase in DIC, TA increases by 6.6 ($^{106}/_{16}$). This will be discussed in full in the discussion (section 5.3.2).

The ratio at which these are taken up are not fixed, as has often been assumed in the past with the Redfield ratio. The original ratios were determined empirically and the authors understood that these uptake ratios may change under various circumstances. Arrigo et al. (1999) discussed the physiological driving of these different ratios, in particular the N:P ratios. Based on a physiological model by

Klausmeier et al. (2004), Arrigo et al. (1999) identified three survival strategies, which he termed *survivalist*, *bloomer* and *generalist*. The survivalists are phytoplankton that are adapted for low resources - light and nutrients - such that they have a N:P ratio greater than 30. The bloomers, on the other hand, are adapted for rapid reproduction and growth, thus they have greater phosphorus requirements. Their N:P ratio was reportedly less than ten. The generalist group is thought to have a near Redfield ratio nutrient requirement, with a balance between growth and survival. Klausmeier et al. (2004) stated that the Redfield ratio is not an optimum, but rather a average of all species. With this knowledge, Anderson and Sarmiento (1994) revisited the inter-cellular stoichiometery of the deep ocean to arrive at a slightly different average uptake (C:N:P = 117:16:1).

Initially the Redfield ratio did not include oxygen stoichiometry, however Richards (1965) extrapolated the equation to include oxygen by stoichiometric balancing. Later studies by Takahashi et al. (1985) and Peng and Broecker (1987) found that O:P in the thermocline was 172 and 175 respectively. Hedges et al. (2002) pointed out that the oxygen ratio represented in equation 2.9 is the minimum produced in photosynthesis and thus, required in remineralisation. In regions where oxygen is limited, anaerobic remineralisation may occur.

One macro-nutrient that has not yet been considered is silicate ($Si(OH)_4$). The taxon diatoms use silicate to produce protective glass-like frustules. The uptake ratio of silicate by these phytoplankton is typically on a 1:1 ratio with nitrate (Brzezinski, 1985). While this has no major effect on DIC directly (can influence TA at high concentrations), diatoms are thought to play a vital role in exporting DIC into the deep ocean, as their frustules act as ballast. This leads to greater sinking rates, which result in remineralisation of organic carbon in the deep rather than the surface ocean.

Oceanic photosynthesis may contribute 46.2% of the global net primary production (Field et al., 1998), but how much of this is exported into the deep ocean? Eppley and Peterson (1979) used Dug-

dale and Goering's (1967) concept of *new* and *regenerated production* to arrive at an estimation of carbon export . New production is that which is fueled by nitrate rather than regenerated nitrogen from the euphotic zone. This means that if there is an uptake of nitrate, there is an equivalent export and by using the Redfield ratio they could arrive at a production estimate. The authors estimated that new production accounted for only 10-20% of production. However, Yool et al. (2007) found that nitrification in the euphotic zone may be more significant that previously thought. The authors suggest that this may skew the global f-ratio by Eppley and Peterson, leading to a lower estimate. A more accurate approximation of carbon export into the deep may be *export production*, which expresses the net carbon that fluxes to the deep ocean. According to Schlitzer (2002) export production, *i.e.* the soft tissue pump, accounts for 11 Pg C yr^{-1}, which according to Field et al.'s estimate, is 22.6% of oceanic net primary production.

2.4.3 Calcification

Similarly to diatoms, there are a number of marine taxa (foraminifera, corals and pteropods and coccolithophores) that produce protective *tests* from calcium carbonate ($CaCO_3$). Of these, coccolithophores are the most abundant calcifiers in the surface ocean (Zondervan et al., 2001). These taxa produce their tests by mineralising calcium (Ca^{2+}), which is abundant in the surface ocean, and CO_3^{2-} by the reaction shown below:

$$Ca^{2+} + 2HCO_3^- \Longleftrightarrow CaCO_3 + CO_2 + H_2O \tag{2.10}$$

The reduction in two units of HCO_3^- results in a decrease of DIC and TA by the same amount. However, CO_2 is produced as a byproduct of the mineralisation. Thus, while resulting in a net reduction of DIC, pCO_2 increases due to a decrease in TA. This distinguishes the carbonate pump from the soft-tissue and the solubility pumps as it results in a net increase in surface pCO_2 rather than a decrease.

Zondervan et al. (2001) point out that calcification occurs alongside photosynthesis, thus CO_2 produced by calcification may be taken up by the soft-tissue pump. In order for a phytoplankton community to be a carbon sink, the calcification to photosynthesis ratio must be less than 1.5 (Iglesias-Rodriguez et al., 2008), where this ratio is dependent on DIC, TA salinity and temperature.

Carbon export into the deep ocean, by sinking organic matter, is comcomitant with TA export. The increase in TA and DIC is only realised in the deep ocean if the $CaCO_3$ tests dissolve. This depends on the saturation state (Ω) of the surrounding watermass, which in turn depends on the concentration of Ca^{2+} and CO_3^{2-}, along with temperature, salinity, pressure and pCO_2. If Ω is greater than one, the water is oversaturated with respect to $CaCO_3$ and conversely if Ω is less than one, Ca^{2+} and CO_3^{2-} are under-saturated. Additionally Ω varies slightly between the two mineral species, calcite and aragonite. The level at which $\Omega = 1$ is known as the lysocline. However Milliman et al. (1999) used a Ω of 0.8 as it has been found that this is the point at which $CaCO_3$dissolves.

Global $CaCO_3$ production and export is estimated to be 0.7 Pg C yr^{-1}(Milliman and Droxler, 1996). Milliman et al. (1999) looked at calcite dissolution in the Pacific and reported that 60% of $CaCO_3$ produced in the surface ocean dissolved within the upper 1000m, a depth well above the lysocline. The authors suggest that this dissolution may be due to grazing related processes. This suggests that 40% of $CaCO_3$ is exported into the deep ocean. Half of this makes it to the sediment layer but is dissolved and the other half (0.13 Pg C yr^{-1}) is buried in the sediments. The rate of alkalinity loss from the ocean is thus double the carbon burial rate. Milliman et al. (1999) argued that the alkalinity cycle is a stable system, therefore there must be a compensating production or import of alkalinity. Deep ocean vents may contribute to balance this loss of alkalinity, but their input is marginal. Chen (2002) strongly advocated the continental margins as sources of alkalinity for the global ocean.

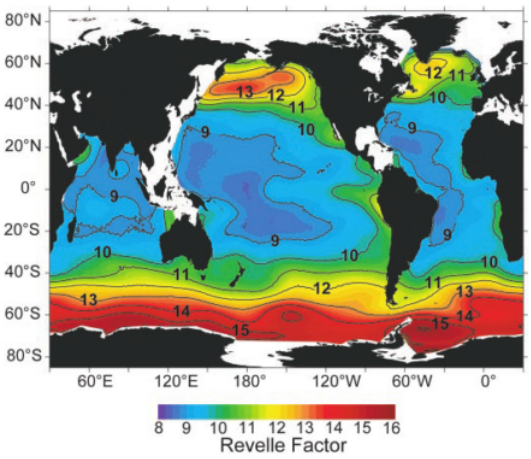

Figure 2.5: The Revelle factor for the upper 50 m of the ocean. Where the factor is high, changes in pH or pCO_2 are large for a given change in DIC. Image taken from Sabine et al. (2004)

2.5 "The Other CO_2 Problem"

2.5.1 Chemistry of Ocean Acidification

Often referred to as "the other CO_2 problem" (Doney et al., 2009), ocean acidification only in recent years became a topical issue. As expressed earlier, increasing atmospheric CO_2 concentration leads to increased CO_2 concentration in the surface ocean. This has already seen a decrease in global surface pH, which has fallen from 8.2 to 8.1 (Royal-Society, 2005). This may not seem like a large margin, but equates to a ~30% increase in $[H^+]$. Though, if we consider pure water, this is far less of an increase than expected. This is due to the "buffering capacity" of seawater, also known as the *Revelle factor*.

The Revelle factor is representative of the amount by which pCO_2 increases, and thus pH decreases, for a given addition of DIC. This is dependent on the absolute concentrations of DIC and TA (Sarmiento and Gruber, 2006):

$$Revelle\ factor \approx \frac{\Delta pCO_2 \cdot DIC}{pCO_2 \cdot \Delta DIC} \tag{2.11}$$

Thus where regions have a high Revelle factor, the influx of CO_2 results in a large change in pH. This is true for the polar oceans (figure 2.5), where the Revelle factor is up to 15. This is due to the cold surface temperatures, which allow for high DIC, coupled with low TA. The addition of anthropogenic CO_2 has already led to shoaling of the calcite and aragonite saturation horizons in the Weddel Gyre (Hauck et al., 2010). With ever increasing anthropogenic CO_2, Mcneil and Matear (2008) reported that under-saturation of aragonite could occur as soon as 2030 in the Southern Ocean. There is also evidence for shoaling of the lysocline off the Californian coast due to anthropogenic CO_2 (Feely et al., 2008a).

2.5.2 Biological impacts

Responses to ocean acidification (synonymous to decreasing Ω) have been found to vary between different marine organisms. Orr et al. (2005) found that Antarctic pteropods (pelagic molluscs) may not be able to precipitate $CaCO_3$ for shell production with increased pCO_2. Coccolithophores may also be at risk in a "high CO_2 world" with reports of two species, *Emiliania huxleyi* and *Gephyrocapsa oceanica*, showing decreased calcification and malformation of their coccoliths (Riebesell et al., 2000). Coral reefs, the poster-child of ocean acidification, have shown negative responses to increased pCO_2 (Doney et al., 2009). There is an all round negative effect on calcifying in organisms and it is difficult to quantify the global ecological effect that this could have. However, not all effects are negative. Riebesell et al. (2007) found that net community production increased by 39%, while nutrient levels remained constant. Iglesias-Rodriguez et al. (2008) reported similar increases in productivity with larger cell sizes at higher CO_2 concentrations.

Riebesell et al. (2000) suggested that reduced calcification may be a natural mitigation mechanism. Because calcification is a net source of CO_2, a reduction thereof would increase the surface ocean's capacity to store CO_2. Over longer time scales, decreases in oceanic pH would result in shoaling of the carbonate compensation depth

(CCD). Zachos et al. (2005) showed sudden reduction of $CaCO_3$ in marine sediments due to shoaling of the CCD during the Paleocene-Eocene thermal maximum resulting in the extinction of many benthic foraminifera. They found that with a ∼2000 Pg C input in less than 10 kyrs, the lysocline shoaled by two kilometres. Restoration of the CCD to its original depth (prior to the PETM) is thought to have taken ∼110 kyrs.

Zachos et al. (2008) performed a simulation of mass carbon emission (similar to the PETM) in a pre-industrial environment. They explained that when the CCD shoaled, accumulated $CaCO_3$ on mid-oceanic ridges and the sea floor dissolved. This resulted in an increase in TA and DIC as carbonate ions were released. While this lowered pH and pCO_2 it did not restore these parameters to pre-industrial levels, where pCO_2 was 50% higher than initial pCO_2 after 20 kyrs. This mechanism implies a longer time scale natural mitigation mechanism.

2.6 Carbon in the Continental Margins

While the continental margins occupy only 7% of the seafloor and 0.5% of total oceanic volume (Chen and Borges, 2009), they account for 14-30% of net oceanic primary production and support 90% of the world fish catch (Gattuso et al., 1998). Additionally the continental margins play an important role in global biogeochemical cycles, accounting for 90% of sedimentary mineralization, and about 50% of the deposition of calcium carbonate (Gattuso et al., 1998). Continental margins are thus host to various processes that are comparatively uncommon in the open ocean.

In 1993 the Land–Ocean Interactions in the Coastal Zone (LOICZ) project was initiated to investigate, amongst other things, these biogeochemical processes, in order to understand and predict possible future changes with regard to increasing pressures from society (LOICZ, 2005). In this section, the key biogeochemical carbon related processes in the continental margins will be looked at.

2.6.1 Carbon Flux

Quantifying atmospheric carbon flux in the continental margins has been a difficult task and even up until recently, there was still dispute as to whether these regions were a sink or source. In attempting to address these uncertainties, Chen and Borges (2009) provided an overview of the fluxes in the continental margins. The authors trace the source of uncertainty down to the semantics of the continental margin, where one school included near-shore ecosystems (inner estuaries, salt marshes and mangroves) in flux calculations. The other school based their calculations on only the conventional continental shelf. Using the latter approach Chen and Borges (2009) found that CO_2 air-sea flux in the continental margins was 0.33 - 0.36 PgC yr^{-1}, thus a sink. Near-shore ecosystems were found to be a net source of -0.50 Pg C yr^{-1}, resulting in the continental margins being net heterotrophic (0.14 Pg C yr^{-1}) as was also found by Smith and Hollibaugh (1993). Laruelle et al. (2010) also reported continental margins to be heterotrophic, but with lower estimates, where near-shore systems emitted -0.27 $\pm$ 0.23 PgC yr^{-1} and continental margins took up an estimated 0.21 $\pm$ 0.36 PgC yr^{-1}. An earlier study by Borges et al. (2005), which found the continental margin to be a net sink, shows the uncertainty surrounding the issue of CO_2 fluxes in the continental margin. A comprehensive overview of fluxes is given in Borges (2011).

Cai et al. (2006) looked at the CO_2 exchange of continental margins, where they classified the shelves into various provinces. Their general finding was that high latitudes are sinks and low latitudes are sources with respective fluxes of 0.33 and -0.11 Pg C yr^{-1}. This highlights the heterogeneity of continental margins, that some are sources and others sinks (Liu et al., 2000; Chen and Borges, 2009).

2.6.2 Coastal Hypoxia

Zhang et al. (2010) define hypoxia as regions where dissolved oxygen (DO) is less than 62.5 µmol kg^{-1}. Such regions of low DO occur

when organic matter is mineralised in regions where circulation is not adequate to replace the hypoxic water (reverse of equation 2.9). The study of coastal hypoxia is becoming increasingly important as human impact on the environment is growing. Two such impacts are:

- Increasing CO_2 with the concomitant decline in O_2 could result in changes in systems that already experience natural hypoxia
- Eutrophication by increased nutrient input via rivers is another one of the mechanisms by which humans are impacting coastal hypoxia

Hypoxia is not always due to human impacts. Coastal upwelling systems are a known example of a natural hypoxia. Low rainfall on the adjacent coasts, means that eastern boundary systems are seldom affected by riverine inputs. But nutrients in these regions are from upwelling of nutrient rich deep waters. This leads to high productivity and eventually to oxygen consumption by remineralisation (equation 2.9).

The Humboldt current system is one of the largest hypoxic zones, commonly called oxygen minimum zones (OMZ). The Benguela is the other eastern boundary upwelling system that is known for hypoxia (Monteiro et al., 2006, 2008). Hypoxia in eastern boundary upwelling systems is unique, since poleward undercurrents are often a source of already low oxygen water from equatorial OMZs. This exacerbates the severity of hypoxia in these regions.

Seasonal or periodic anoxia is also a fairly common occurrence in coastal regions where high productivity is seasonally driven. Seitzinger et al. (2006) reported that seasonal hypoxia is often strongly related to stratification as well as the underlying sediments.

2.6.3 Anaerobic remineralisation

Anaerobic remineralisation occurs when oxygen is absent. This is common in continental shelf sediments and oxygen minimum zones in intermediate depths (Seitzinger et al., 2006). Seitzinger et al.

(2006) also considered periodic or seasonal anoxic systems to be important regions of anaerobic remineralisation.

Anaerobic remineralisation results in the reduction of oxidized nutrients, such as nitrate and sulphate. The oxygen from these donors is used in the remineralisation process and nitrogen or sulfur are electron donors. Typically two types of anaerobic remineralisation occur in anoxic conditions, namely denitrification and sulphate reduction. The occurrence of anaerobic remineralisation typically occurs in a set sequence: aerobic oxidation, denitrification and then sulphate reduction. This is due to the energy yields achieved from each reaction: 475, 448 and 77 KJ mol^{-1} respectively(Tyrrell and Lucas, 2002). A higher energy yield allows that particular remineralising bacteria to be dominant. However, the abundance of each mineral also plays a role in determining the pathway of remineralisation. This is illustrated in the Benguela system, where sulphate reduction is a more common process due to the abundance of sulphate minerals in the surface sediments (Tyrrell and Lucas, 2002).

In recent years, the development of genomics has led to the identification of a third anaerobic remineralisation path by the anaerobic oxidation of ammonium (*anammox*). The abundance and relevance of anammox is still largely unknown, but Kuypers et al. (2005) suggested it may play an important role in anaerobic remineralisation.

Denitrification

Denitrification occurs when oxygen concentrations are lower than ~9 μmol kg^{-1} (Seitzinger et al., 2006). Seitzinger et al. (2006) finds this process to be ubiquitous on continental shelves, accounting for 44% of denitrification globally. The denitrification reaction is shown below:

$$5CH_2O + 4H^+ + 4NO_3^- \Rightarrow 2N_2 + 5CO_2 + 7H_2O \tag{2.12}$$

The result of denitrification is an increase of 1 unit of TA per unit of NO_3^- due to a loss of protons (see equation 2.5), along with a similar increase in DIC (5/4). Often, the so-called canonical denitrification (equation 2.12) occurs alongside nitrification (Hu and Cai,

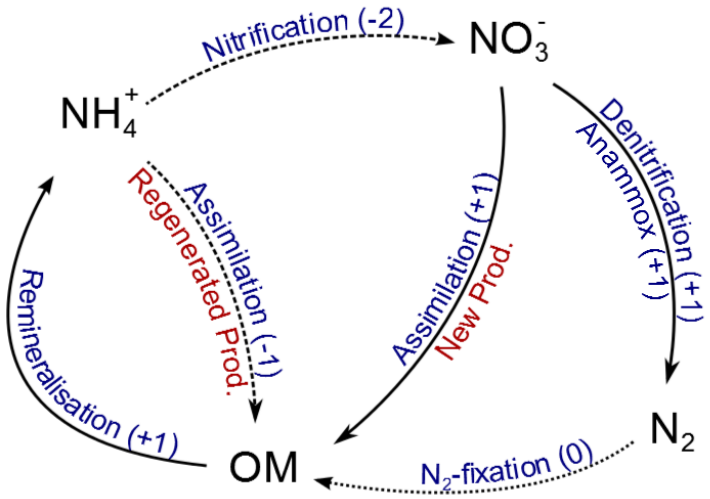

Figure 2.6: Diagram showing various processes affecting nitrogen (blue text). Values in brackets show the change in alkalinity per unit of nitrogen.

2011). This coupled nitrification-denitrification occurs when nitrified NO_3^- or NO_2^- is transported from oxic water into anoxic water and used as an electron donor. The net result is that alkalinity remains unchanged due to the loss of two units of alkalinity during nitrification (figure 2.6). If we consider canonical denitrification, where the electron donor is not nitrified, then there is a net gain in alkalinity.

Wolf-Gladrow et al. (2007) point out that, on a global scale, denitrification is canceled out by nitrogen fixation. However, this is only if we assume that the nitrogen cycle in the ocean is a homeostatic system where N_2 production is equaled by fixation.

Anammox

A recent study by Kuypers et al. (2005) found that anaerobic oxidation of ammonium (***anammox***) may play an important role in the Northern Benguela upwelling system. Denitrification in these waters is only responsible for converting NO_3^- to NO_2^-, while the anammox bacteria reduce NO_2^- to N_2. The authors infer that denitrification, as it is known today, may in fact be a coupling of denitrification and anammox. Hu and Cai (2011) reason that anammox is no different to denitrification in terms of alkalinity production still

resulting in a gain in alkalinity (depending on the source of nitrate). In this study, anammox will be considered

Sulphate Reduction

In extreme cases of anaerobic remineralisation, nitrate may be depleted. In this case methane is oxidised and sulphate (SO_4^{2-}) is reduced to form bicarbonate:

$$CH_4 + SO_4^{2+} \Rightarrow HCO_3^- + HS^- + H_2O \tag{2.13}$$

This results in a two part increase in total alkalinity and a one part increase in DIC.

2.6.4 Alkalinity Production on continental shelves

As mentioned previously, the open ocean carbonate pump is not in equilibrium due to the burial of calcium carbonate. Chen (2002) advocated that the deficit is made up by alkalinity production on continental shelves. The production of TA on continental shelves is typically due to anaerobic processes. This means that OMZs play an important role in the global alkalinity cycle. The processes mentioned in section 2.6.3 all contribute to alkalinity production or removal (figure 2.6).

Chen (2002) found that 16-31 Tmol yr^{-1} of TA is produced on the continental shelves. Hu and Cai (2011) provided a more conservative estimate of 4-5 Tmol yr^{-1}. Of this they estimated that 1.5 Tmol yr^{-1} was due to denitrification and the remainder was due to pyrite burial. These figures are dwarfed by global estimates of annual alkalinity production by Berelson et al. (2007) (42-133 Tmol yr^{-1}). If the latter estimate by Hu and Cai (2011) is the more correct, then continental shelves play little role in global alkalinity production as supported by Chen (2002).

2.7 Eastern Boundary Currents

There are four eastern boundary current (EBC) systems in the world (California, Humboldt, Canary and Benguela Current sys-

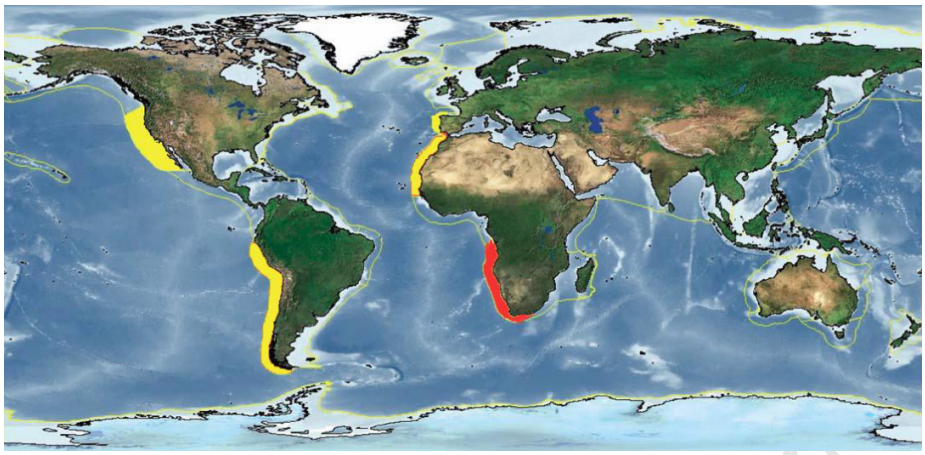

Figure 2.7: Map of continental shelves. Eastern boundary regions are highlighted in yellow. The Benguela region is shown in red. Image adapted from Kudela et al. (2005)

tems), though the Iberian system is sometimes included as a fifth. The lack of an EBC in the Indian Ocean is due to the poleward Leeuwin current off the Australian coast.

These regions are productivity hotspots, occupying 0.3% of the ocean's area, yet accounting for 2% of marine primary production (Carr, 2002). This high productivity is driven by upwelling of nutrient rich intermediate waters. Alongshore equatorward winds result in Ekman pumping, where surface water is blown offshore and replaced by the cold intermediate water. The high productivity of these regions results in uptake of CO_2, but this is juxtaposed by out-gassing of CO_2 due to warming of the upwelled water (equation 2.8). These opposing processes make EBC systems difficult to predict as carbon sinks our sources.

Based on Sea WiFS data, Carr (2002) found primary productivity was highest in a nearshore strip for all EBCs. The study also showed that the Benguela system was the most productive of the regions (0.37 Pg C yr^{-1}) followed by the Canary, Humboldt and California currents respectively (0.33, 0.20 and 0.04 Pg C yr^{-1}). However, there has been a great deal of critisism of Carr (2002) due to the study's reliance on Sea WiFS.

2.7.1 CO_2 Flux

The majority of studies investigating carbon flux in EBC systems have focused on the North American West Coast.

Friederich et al. (2002) investigated CO_2 flux in the Monterey Bay region from 1998 to 1999, where 1998 was an El Niño. The authors found that, during El Niño CO_2 flux was from the atmosphere into the ocean (-0.3 to -0.7 mol m^{-2} yr^{-1}) due to capping of warm water, which prevented upwelling. During 1999, winds favoured upwelling, resulting in a sea to air flux of 1.5-2.2 mol m^{-2} yr^{-1}. The authors did recognize that, because their study was focused on a near shore region where upwelling is intense, there may have been a bias to higher pCO_2. A similar study by Hales et al. (2005) off the Oregon coast, found that respiration of organic matter played an important role in increasing pCO_2 in subsurface waters. The authors suggested that this subsurface DIC maximum could be transported into the interior ocean by downwelling. This theory was later confirmed by Ianson et al. (2009) who found, by model analysis, that narrow shelves allowed downwelling of high pCO_2 waters into the ocean interior. The study also found that strong upwelling on wide continental shelves decreases the out-gassing of CO_2. Furthermore, Feely et al. (2008b) found that the aragonite lysocline had shoaled to the surface along regions of the Californian coast, due to the added effect of anthropogenic CO_2.

Borges and Frankignoulle (2001) reported CO_2 fluxes in the Iberian upwelling system of 0.15 - 3.29 mol m^{-2} yr^{-1} during only August. A more recent and comprehensive study in the Iberian upwelling system by Ribas-Ribas et al. (2011) found that the Gulf of Cadiz had a weak seaward flux of -0.07 mol m^{-2} yr^{-1}. This is half of what a previous study by Huertas et al. (2006) found, but is still within the range of variability.

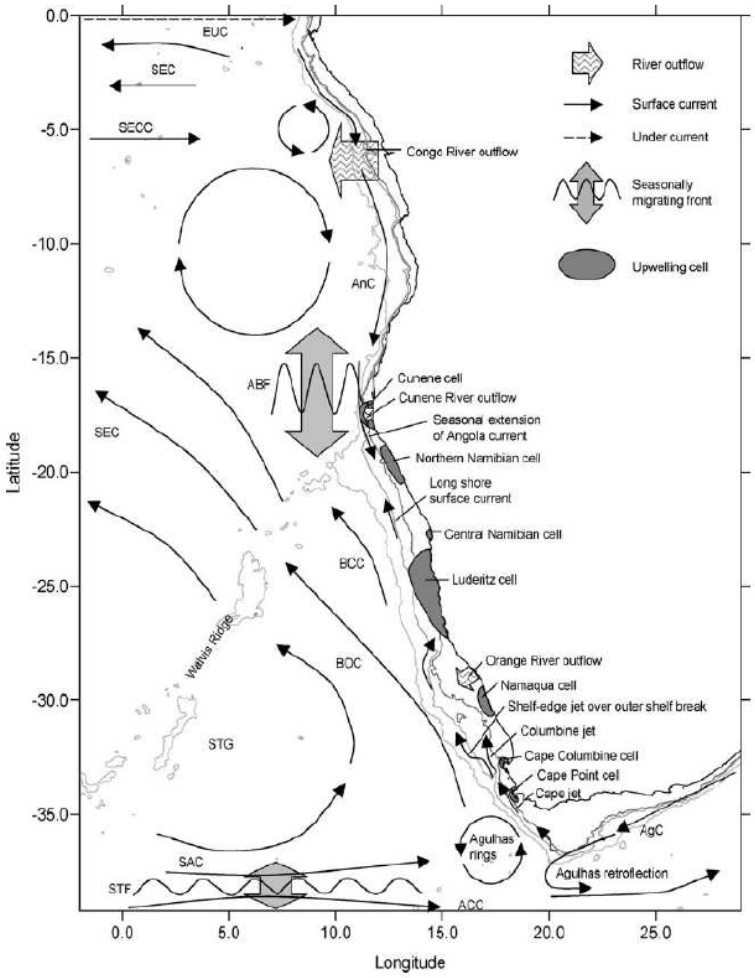

Figure 2.8: Features and processes of the Benguela Current Large Marine Ecosystem (BCLME) after Hutchings et al. (2009). Low Oxygen Water (LOW)

2.8 Benguela Upwelling System

2.8.1 Physical Features and Processes

The Benguela EBC system is situated in the south east Atlantic off the coast of Africa. Shillington et al. (2006) describes this system as the Benguela Current Large Marine Ecosystem (*BCLME*), which extends from 5-37°S. The northern sector (∼15-5°S) is characterised by the polarward flow of the Angola current. The southern and central sectors of the BCLME (∼15-37°S) are characterised by the equatorward flow of the Benguela current and extend from the

western Agulhas Bank in the south (37°S) to the confluence of the Benguela and Angola currents (∼15°S). The confluence of these two currents between 15°S and 17°S is known as the Angola-Benguela Front (ABF) (Shillington et al., 2006). This is different to the previous definition of this system by Shannon and Nelson (1996) who recognised only a northern and southern sector, which are synonymous with Shillington et al.'s central and southern sectors. A different definition of the southern Benguela was used by Andrews and Hutchings (1980), where the southern extent is at 34°S. This latter definition was used in this study. These two southern and northern sectors are defined by the upwelling regimes of the respective sectors.

Coastal upwelling is driven by alongshore winds. Seasonal north-south migration of the South Atlantic Anticyclone (SAAC) results in two different upwelling regimes. Upwelling in the central Benguela (∼15-30°S) is persistent throughout the year. In the southern Benguela (30-34°S), upwelling is dominant in the summer months, coinciding with the most southerly extent of the SAAC (Field and Shillington, 2006).

Rather than being continuous, upwelling occurs in six discrete centers (Shannon and Nelson, 1996): Cape Frio (18°S), Walvis Bay (23°S), Luderitz (27°S), Namaqua (30°S), Cape Columbine (33°S) and Cape Peninsula (34°S). Of these, the Luderitz cell is the strongest (Hutchings et al., 2009). The reason for discrete rather than continuous upwelling is the combination of intensification in windstress curl and divergence (Chelton et al., 2004; Shillington et al., 2006) and variation in shelf width (Monteiro et al., 2006). According to Hutchings et al. (2009), periodicity of upwelling events ranges between 3-10 days. This is due to meteorological variations in the position and strength of the SAAC (Tyson and Preston-Whyte, 2000).

Upwelled water is derived from central and intermediate water in either: the Angola basin in the north (∼20° and north); or the Cape Basin in the south. The Walvis Ridge forms a boundary between the two regions. Water masses in the Angola and Cape Basin are

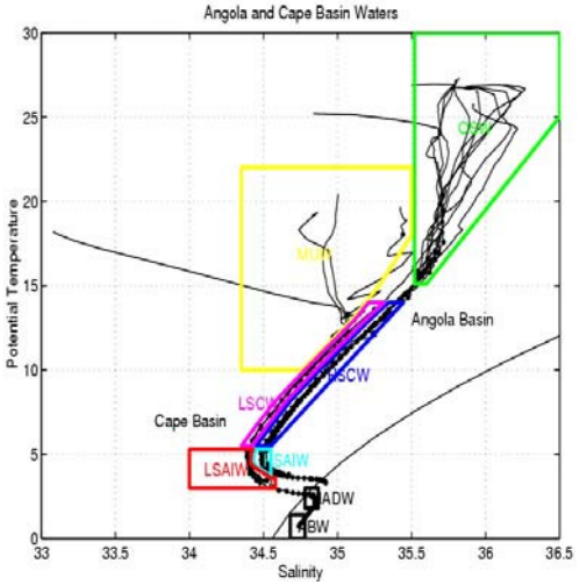

Figure 2.9: T-S diagrams showing watermasses found in the Cape and Angola Basins (after Shillington et al., 2006). Key: Antarctic Intermediate Water (AAIW); High (HSAIW) and Low (LSAIW) Salinity Antarctic Intermediate Waters South Atlantic Central Waters (SACW); High Salinity Central Water (HSCW); Low Salinity Central Water (LSCW).

fairly similar, with the latter being slightly fresher. Shillington et al. (2006) distinguish intermediate waters derived from Antarctic Intermediate Water (AAIW) as High (HSAIW) and Low (LSAIW) Salinity Antarctic Intermediate Waters respectively. This is mirrored in the shallower South Atlantic Central Waters (SACW). Where high salinity water in the Angola basin is called High Salinity Central Water (HSCW) and relatively lower salinity water (LSCW) in the Cape Basin. Monteiro (1996) suggested waters originating from the Angola basin origin are transported southward by an undercurrent, but are diverted offshore at the Lüderitz cell. The southern Benguela is thus isolated from influences from the northern Benguela.

This forms the central idea behind Monteiro's (1996) *Gate Hypothesis*. This hypothesis stems from the notion that poleward undercurrents are deflected offshore by regions where upwelled water moves onto the shelf – the so-called gates. Monteiro (1996) supports his hypothesis with the different biogeochemical signatures of

upwelled water in the different upwelling cells. He identifies three sectors, each containing two upwelling cells, namely: Cape Frio and Walvis Bay upwelling cells in the northern sector; Lüderitz and Namaqua cells in the central sector; and lastly the Cape Columbine and Cape Peninsula upwelling cells in the southern sector (Monteiro, 2009).

2.8.2 Low Oxygen Water

Low oxygen water (LOW) in the Benguela system plays an important part in defining the characteristics of the system. The production and variability of LOW in the three subsystems is driven by different processes, as outlined by Monteiro and Van der Plas (2006). LOW in the northern Benguela is controlled by upwelling of LOW from the Angola Gyre. The Angola current forms the eastern poleward leg of the gyre. At the ABF confluence, the Angola current splits into an offshore current, which completes the Angola Gyre, and a poleward undercurrent along the shelf. The undercurrent, carrying LOW, flows toward the Lüderitz cell where strong upwelling and a narrow shelf results in offshore divergence of this current. This transport mechanism, along with the persistent upwelling of the Lüderitz Cell results in persistence of suboxic conditions.

As mentioned previously, the southern Benguela is isolated from influences of the northern subsystems. LOW is thus produced by a combination of local scale, physical and biogeochemical processes (Monteiro and Van der Plas, 2006). Upwelling in the Cape Columbine and Cape Peninsula cells is fed by the oxygenated LSCW (~180 µmol kg^{-1}). Despite this, LOW is common in the upwelling cells, in particular the Cape Columbine cell, where intense hypoxic events due to stratification lead to rock lobster strandings (Cockcroft et al., 2008).

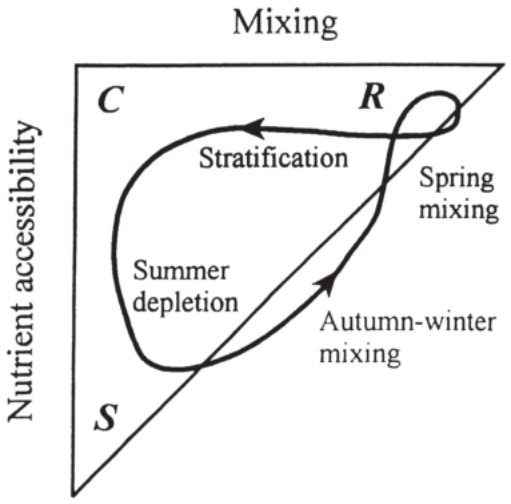

Figure 2.10: An ideal conceptual model of phytoplankton succession throughout the year in an upwelling system. Where "R" represents ruderal, "C" for colonist, and "S" for stress-tolerant species. Image taken from Smayda and Reynolds (2001).

2.8.3 Southern Benguela

The southern Benguela, as mentioned previously, extends from 30 to 37°S, however in this study we will use the end of the Cape Peninsula (34°S) *sensu* Monteiro (1996). More studies have been undertaken in the southern Benguela than the central and northern sectors. One of the recurring themes of study in the southern Benguela, is the succession of phytoplankton and harmful algal blooms (HABs).

Phytoplankton Succession

Much of the work on succession is based on the initial work by Margalef (1978). The central theme of his work was to identify the relationship between nutrient availability, turbulence, light availability and phytoplankton community assemblages. This implied that certain taxa are adapted to a particular environments. This was improved by Reynolds' (1987) concept of three distinct phytoplankton classes (Figure 2.10):

- "Invasive, r-selected, small, fast-growing, high surface-to-volume colonist (C) species"

- "Acquisitive, large, slow-growing but biomass-conserving, K-selected, nutrient stress-tolerant (S) species"
- "Attuning, light-harvesting, attenuated, disturbance-tolerant ruderal (R) species"

In accordance with this, Pitcher et al. (1991) found that diatoms (R species) dominated the upwelling phase and flagellates (S species) the the quiescent phase. This was expanded by Hutchings et al. (1994), who wrote that succession of phytoplankton assemblages in the Benguela typically follows the order of: small diatoms, large diatoms, dinoflagellates, microflagellates.

This conceptual model can also be useful in defining phytoplankton assemblages, not only temporally in the upwelling zone, but also spatially across the shelf. Physical features across the continental shelf thus also play an important role in determining the phytoplankton assemblage along a cross-shelf section. Pitcher et al. (1992) and Giraudeau and Bailey (1995) identified two upwelling features across the shelf namely the *upwelling front* and the *shelf-break front* (defined as the *offshore divergence* by the latter authors). The latter is a quasi-permanent feature that distinguishes oceanic seawater (OSW) from modified shelf water - also called modified upwelled water (MUW) by Shillington et al. (2006). The authors alluded to the fact that this feature may not be a permanent surface feature, but may be a permanent subsurface feature. According to Estrade et al. (2008) the upwelling front's position can be determined by the combination of the wind stress and the slope of the shelf (equation A.1).

Armstrong et al. (1987) looked at the distribution of phytoplankton distribution across a shelf section off Cape Columbine. They found that chlorophyll concentrations were greater inshore of the upwelling front. Smaller particles, nanoplankton, (< 20 µm) were the most abundant in the larger offshore region, where nutrients were low. This was in contrast to the net-plankton (>20 µm), mostly diatoms, that dominated the narrow, turbulent inshore region. While smaller phytoplankton may occupy a larger region

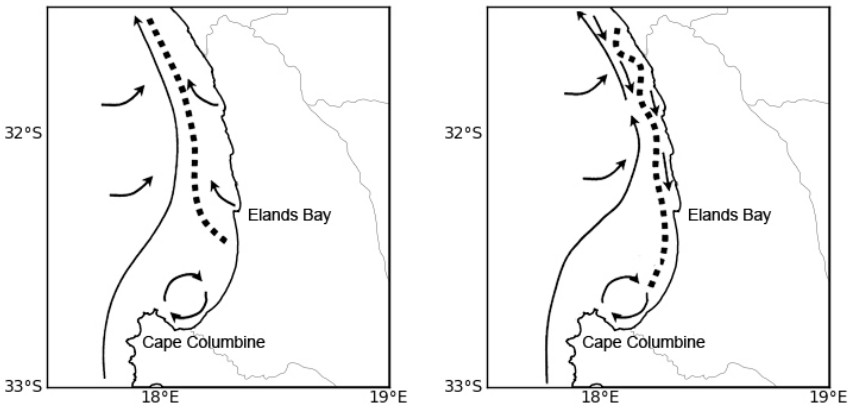

Figure 2.11: Circulation during the summer months in the greater St. Helena Bay region. After Pitcher and Nelson (2006)

across the shelf, Pitcher et al. (1991) found that diatoms dominated the carbon biomass by a significant margin during turbulent periods. Even when flagellates were the dominant taxa, their biomass was far less than the diatom biomass. Dinoflagellates were never dominant during their study, owing to the specific conditions required for a dinoflagellate bloom to occur (Smayda and Trainer, 2010).

An important factor contributing to the occurrence of HABs is quiescent stratification. The circulation of the region intensifies the HABs in the St. Helena Bay region by retention during relaxation after an upwelling event. Several studies have mentioned the unique circulation in the larger St. Helena Bay region that promotes phytoplankton blooms. Pitcher and Nelson (2006) found that the upwelling front creates a physical boundary, isolating phytoplankton inshore of this front. The result is a retention zone, where phytoplankton accumulate during upwelling conditions. Upon relaxation this phytoplankton sloshes southward, concentrating biomass in St. Helena Bay (figure 2.11).

CO_2 Exchange in the Southern Benguela

Because the southern Benguela is a highly productive upwelling system, it has long been thought of as a carbon sink, despite the previous notion that eastern boundary systems are sources (Chen and Borges, 2009). Waldron and Probyn (1992) produced an upper esti-

mate of carbon export based on new production, *i.e.* nitrate fluxes. An initial carbon uptake estimate of 8.87 µmol kg^{-1} was made. However, re-adjustment of the *f*-ratio in a later study by Waldron et al. (1998), found that carbon flux in the southern Benguela should be 7.36 mol m^{-2} yr^{-1}. Importantly, one of the assumptions of this study is that the Redfield ratios of the southern Benguela are as defined by Redfield et al. (1963).

The idea of a fixed C:N ratio has long been criticised in the literature (Arrigo, 2005). Monteiro (1996) further challenged this notion in his study of CO_2 fluxes of the Benguela. He found that using the C:N ratios would result in an underestimation of CO_2 flux due to anaerobic remineralisation and adsorption of organic nitrate. Using a box model approach, based on DIC measurements, he found that CO_2 flux in the southern Benguela was 1.36 mol m^{-2} yr^{-1}.

The most recent carbon flux estimate was based on direct pCO_2 measurements by Santana-Casiano et al. (2009). Using volunteer operated ships (VOS), they gathered a large enough data-set to calculate the carbon flux for the Benguela. They found flux rates for spring and winter to be 11 and 5.5 mmol m^{-2} day^{-1} respectively. The annual seaward flux in the southern Benguela was on the order of 1.62 mol m^{-2} yr^{-1}. A study by Santana-Casiano and González-Dávila (2008), based on the same data, found that biology, over temperature, was the dominant driver of ΔpCO_2 values.

Calcification

There is strong evidence that coccolithophores occasionally play an important role in the Benguela (Weeks et al., 2011). Coccolithophore blooms occur typically in autumn and early winter. Giraudeau (1992) found that this taxa has contributed significantly to biogenic sediments ($CaCO_3$) in the central Benguela. While there are no studies of sediments in the southern Benguela, Giraudeau and Bailey (1995) investigated coccolithophore distribution along a transect in Hondeklip Bay (30.42°S) during a June bloom. The largest abundance of coccolithophores (278×10^3 cells L^{-1}) was found in the surface waters offshore of the upwelling front, as was also found by

Mitchell-Innes and Winter (1987) in the lee of the Cape Peninsula upwelling cell (2340×10^3 cells L^{-1}). Giraudeau and Bailey (1995) noted that the lower concentrations measured in their study may be due to upwelling rather than stratified conditions (Mitchell-Innes and Winter, 1987). A much later study by Weeks et al. (2011) found the same to be true in the St. Helena Bay region. The retentive circulation of the bay seemingly had a large impact on the distribution of the coccolithophores. Interestingly, all of the southern Benguela studies, mentioned above were performed between March and June.

2.9 Questions and Aims

Based on the last section 2.8.3, gaps and uncertainties in the knowledge base of the southern Benguela have been identified. In this section, I have highlighted those shortcomings and have formulated key questions.

2.9.1 What controls stoichiometry?

The southern Benguela is a seasonal wind driven upwelling system. In the summer months strong equatorward winds drive deep, nutrient rich waters to the surface. Warming of these waters results in out-gassing of CO_2, enriched by shelf remineralisation of organic carbon. This is counteracted by the high productivity, leading to a draw-down of CO_2. It has long been recognised that the region's sink status is due to a strong biological component. However, bottom remineralisation has also been identified as an influential biogeochemical process. Tyrrell and Lucas (2002) found that loss of nitrate from the system indicated that, denitrification may result in water being "supercharged" by DIC as it moves over the shelf prior to upwelling. Monteiro (1996) stated that the C:N stoichiometry of the Benguela had been altered by such processes. And using extracellular nutrient concentrations for export calculations only is not a viable method, as Redfield ratios may underestimate the carbon export estimates. This sets the background for the first question which is:

- Does the seasonal nature of upwelling in the southern Benguela express itself on the bulk C:N stoichiometery?
  - Is C:N stoichiometry driven predominantly by remineralisation?
  - How do these processes contribute to changes in DIC?

In answering this question we will look at the stoichiometric nutrient ratios and the processes that govern the seasonal changes, if any. An attempt at quantifying the contribution of each process to the carbon cycle will be made.

2.9.2 What is the alkalinity production on the southern Benguela shelf?

Another point which both the aforementioned studies (Tyrrell and Lucas, 2002; Monteiro, 1996) also inadvertently allude to, is the shelf production of alkalinity by anoxic remineralisation. The study by Tyrrell and Lucas, found that the central and southern sectors of the Benguela had a nitrate deficit of 40 µmol kg^{-1}. This would imply an equivalent gain in alkalinity. Monteiro found that calcification was not an important mechanism. He states that the Benguela's high calcite saturation state, is the reason for the high contribution of biogenic $CaCO_3$ in the sediments. This translates into a permanent loss of alkalinity from the system. This brings us to our second question:

- Is the southern Benguela an alkalinity sink or source?
  - does calcification play an important role?
  - do the seasons leave a fingerprint on the marine carbonate system?
  - is the buffering effect of alkalinity important to the southern Benguela?

2.9.3 What is the air-sea CO_2 flux of the southern Benguela?

Carbon export in the southern Benguela has been a contentious issue over the last 20 years. Waldron et al. (1998) and Monteiro (1996) produced two estimates of carbon export. While initially considered conflicting, the two estimates were eventually considered upper and lower estimates respectively (Waldron et al., 2009). The later study by Santana-Casiano et al. (2009) confirmed Monteiro's estimate. However, their study did not include the nearshore upwelling region, nor did it present flux estimates for autumn. Santana-Casiano and González-Dávila (2008) found that biology was the key determinant in ΔpCO_2 however, the authors do not present an idea of the importance to the wind over ΔpCO_2. This may be especially important in summer months when persistent winds are present. The third question is thus:

- What is the seasonal air-sea CO_2 flux in the southern Benguela?
  - what are the key constituents in determining air-sea fluxes?

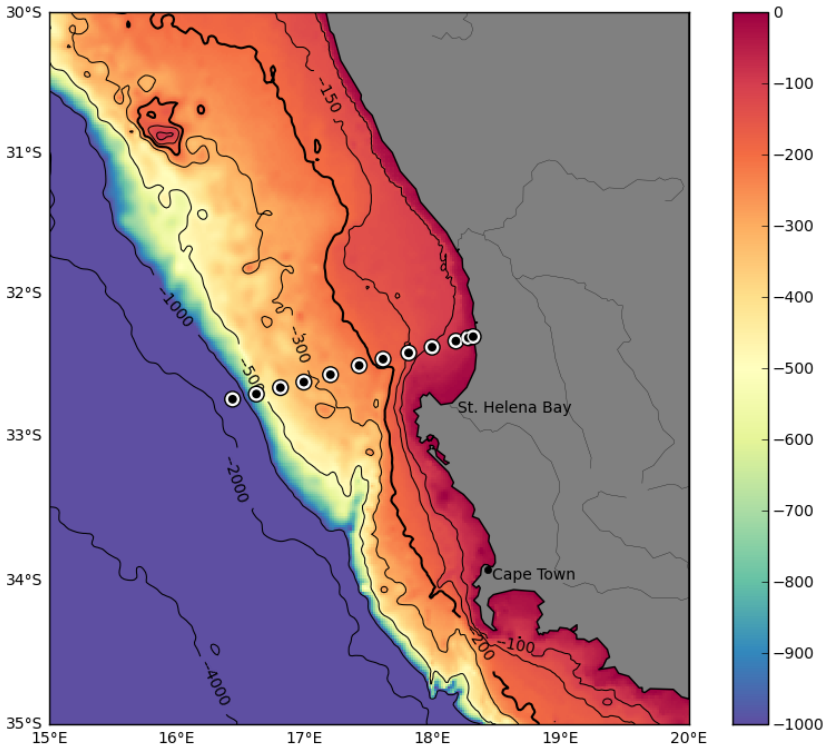

Figure 3.1: Southern Benguela topography and station locations. ETOPO1 topography data used Amante and Eakins (2009)

3 Methods

3.1 Cruises and data collection

Data was collected along the St. Helena Bay Monitoring Line (SHBML), a monthly monitoring transect run by the South African Department of Environmental Affairs (DEA) and Department of Agriculture, Forestry and Fisheries (DAFF). The transect runs offshore from the South African West Coast (32.30°S, 18.31°E), near Elands Bay, to the shelf break ∼100nm offshore (32.75°S, 16.43°E), with twelve stations at regular distances (figure 3.1). During 2010, the period of data collection, three different vessels were used, namely the RV Ellen Kuzwayo, RS Africana and RV Algoa (table 3.1) .

Table 3.1: Sampling information from monthly cruises. The Storage column shows the maximum number of days that a batch of samples was stored.

Year	Month	Day	Vessel	Storage (days)
2010	Jan	16	Africana	19
	Feb	19	Africana	35
	Mar	24	Ellen K.	42
	Apr	14	Ellen K.	93
	May	25	Ellen K.	79
	Jun	30	Ellen K.	62
	Jul	28	Ellen K.	79
	Aug	25	Africana	83
	Sep	30	Africana	53
	Dec	7	Africana	110

Each vessel was equipped with a twelve bottle rosette mounted with a Sea-Bird 911plus CTD. The CTDs on each vessel recorded temperature, conductivity, pressure, oxygen concentration and fluorescence. The rosette was lowered within ten metres of the bottom at each station and bottles were triggered on ascent. Samples were taken at standard depths in deeper waters (bottom, 1000, 600, 400, 300, 200 and 100 m). In the upper layer, samples were taken according to the fluorescence-maximum depth (f-max, below f-max, f-max, above f-max and within 3 m of the surface). Daytime quenching of fluorescence was not considered to be an important issue, as data was later organised by thermocline depth. Nutrients were collected at every sampled depth and frozen for later analysis by the DEA. Two dissolved oxygen samples were taken at each station and determined by Winkler titration to calibrate CTD optode readings. TCO_2 could only be sampled at selected depths due to limitation by the number of sample bottles. Between 74 to 95 bottles were sampled each month.

TCO_2 samples were collected as specified by DOE (2004) in the standard operating procedures. Samples were tapped from the rosette with a plastic tube into 250 mL glass bottles, similar to those used for dissolved oxygen. It was not considered necessary to use a stopper during sampling due to the diameter of the bottle neck and the relatively low gas transfer velocity of CO_2. Bottles were rinsed

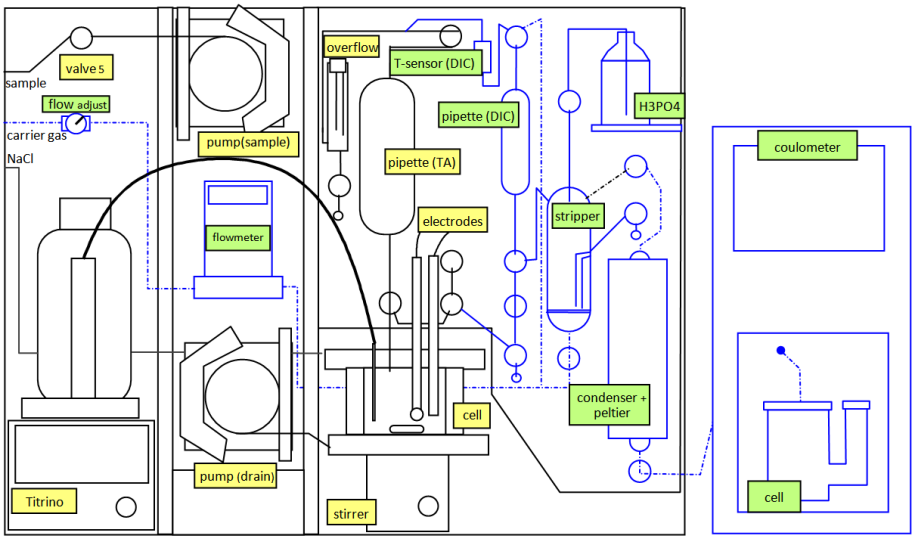

Figure 3.2: A diagram representation of the VINDTA 3C. Objects are shown in blue (and green labels) and black (and yellow labels) to distinguish between DIC and TA apparatus respectively.

three times with a small volume of sample water before filling the bottle and letting it flush by at least one bottle volume. A headspace of ∼5 mL was left to allow for the expansion of the deep water warming from 4 °C to 25 °C. Finally, each sample was preserved with 100 µL of mercuric chloride. Samples were stored at room temperature for up to three months before analysis (table 3.1). A later lab study found that samples stored for prolonged periods may suffer alkalinity enrichment due to silicate leaching. Alkalinity results from samples with a longer storage time should thus be treated with caution. A different set of bottles were used for the month of March and December - TA results from these batches were irratic despite good results from reference materials.

3.2 Sample Analysis

Samples were analysed for DIC and TA using a VINDTA 3C (**V**ersatile **I**nstrument for the **D**etermination of **T**otal dissolved inorganic carbon and **A**lkalinity) by Marianda (figure 3.2). The VINDTA 3C automates an open cell alkalinity titration and a coulometric CO_2

titration as described in the DOE (2004) manual. Details of each titration are discussed below.

3.2.1 Dissolved Inorganic Carbon

A seawater sample is pipetted into a CO_2 stripper unit where small volume of 10% orthophosphoric acid (H_3PO_4) is added to the sample to liberate the DIC as CO_2. Nitrogen is used as a carrier gas, with the flow rate set to 135mL per minute. CO_2 is then measured coulometrically using a UICinc coulometer (two models used: CM5014 and CM5015). CO_2 is bubbled through a carbon cathode solution with a platinum spiral cathode (both supplied by UICinc). A silver rod anode is suspended in a potassium iodide (KI) saturated anode solution (supplied by UIC). Potassium iodide crystals are added to the "anode arm" to ensure that the anode solution remains saturated DOE (2004). Cells were used for a maximum of 20 samples to ensure that degradation of the cell solutions did not affect the results.

The coulometer returns output in raw electron counts, which is converted by the VINDTA LabView program to μmol.kg^{-1}. The conversion equation is the same as that described in the DOE (2004) handbook:

$$C'_T = \frac{N_s - b.t - a}{c} . \frac{1}{V_s . \rho} \tag{3.1}$$

Where the terms are described by the following:

C_T	=	total dissolved inorganic carbon in the sample (μmol.kg^{-1})
N_S	=	the coulometer reading for the sample (counts)
b	=	background level of the system (counts.min^{-1})
t	=	time taken to measure sample
a	=	acid blank (counts)
c	=	coulometer calibration factor (counts.mol^{-1})
V_S	=	volume of sample
ρ	=	density of the sample

Samples were not run if a consistent background level (b), or blank, of ~70 counts per minute was not achieved. This problem was encountered often and it is suspected that the cause of the high

blanks was due to blockage of the cells' glass frits by a carbon build-up. An unorthodox solution to this problem, discovered by chance, was to leave the cathode solution in the cells overnight. Hereafter cells were rinsed using the standard procedure – once with methanol, twice with de-ionised water and then left to dry in a drying oven at 50 °C.

It was also observed that when sampling a duplicate low DIC sample after a high DIC sample, the initial low DIC sample was higher than the second. It was assumed that there was a carry-over of DIC in the system despite the rinsing cycle already in place. The problem was solved by adjusting the DIC rinsing cycle to rinse twice.

3.2.2 Alkalinity

The VINDTA 3C performs a potentiometric open cell titration to find alkalinity. About 100mL of sample is pipetted into a temperature regulated (25 °C) open cell configuration. The titrant (0.1 M HCl in a 0.7 M NaCl solution) is added in twenty-eight 0.150 mL steps by a Metrohm Titrino (719S), which also takes potential difference readings. Enough time is allowed between each addition of acid to allow for mixing and the evolution CO_2. The titration is measured by a glass and a double junction reference electrode (filled with a 0.7 M NaCl outer solution and 3.0 M KCl). Measurements are made against an auxiliary grounded, stainless steel electrode to avoid a drifting signal Mintrop (2010). The outer solution to the reference electrode was filled daily and the inner solution weekly, as recommended by Mintrop (2010). Between measurements, the titration cell is rinsed with a 0.7 M NaCl solution, which removes any alkalinity traces but is at a ionic strength similar to that of seawater. A sudden change in ionic strength will result in poor values.

Recalculation

Titration output was saved to file by the VINDTA software for recalculation. To get an alkalinity approximation that is accurate, the second inflection point on the titration curve is calculated mathematically. Mathematical recalculation can be done either by a gran

Table 3.2: A comparison of the standard errors of dissociation constants found by different authors (adapted from Mojica-Prieto and Millero (2002))

Author	Temp (°C)	Salinity	σ (pK_1)	σ (pK_2)	Media
Hansson (1973)	5 - 30	20 - 40	0.007	0.009	ASW
Mehrbach et al. (1973)	2 - 35	26 - 43	0.006	0.010	SW
Roy et al. (1993)	0 - 45	5 - 45	0.002	0.003	ASW
Lee et al. (1996)	5 - 35	35	0.004	0.005	SW
Mojica-Prieto and Millero (2002)	15 - 45	10 - 40	0.006	0.010	SW
Millero et al. (2006)	0 - 50	0 - 50	0.005	0.011	SW

calculation or by non linear optimization. Two non-linear optimization methods are currently used in the field. The first is an iterative chi-squared method implemented by the VINDTA 3C software (also available in MATLAB). The other is based on the Levenberg-Marquardt algorithm. This method was originally written by Andrew Dickson and is given in the D.O.E handbook (2004). A python translation of the Levenberg-Marquardt method was used to calculate alkalinity from raw VINDTA data (see appendix C.1 for code listing and download links).

In 2009 the new Thermodynamic Equation of State (TEOS-10) was instated. However, this study still used the old EOS-80 definition. The EOS-80 uses practical salinity, a measure of the conductivity, whereas the TEOS-10 uses absolute salinity (IOC, 2010).

Dissociation Constants

Since the early 1970s researchers have been improving on the dissociation constants of the marine carbonate system (K_1 and K_2). These constants have been measured and tested in either, artificial seawater (Hansson, 1973; Roy et al., 1993), real seawater (Mehrbach et al., 1973; Lee et al., 1996; Millero et al., 2006), or both (Mojica-Prieto and Millero, 2002) (table 3.2). Though their study is one of the earliest, constants by Mehrbach et al. (1973) are considered a yardstick for new constants. Dissociation constants by Mojica-Prieto and Millero (2002) were used to calculate TA and other parameters such as pH and pCO_2.

3.2.3 Quality Control

The accuracy and precision of the VINDTA was determined by calibrating the VINDTA with certified reference materials (CRMs). CRMs were obtained from the CO_2 laboratory (run by A.G. Dickson) at Scripps Institution of Oceanography. Three CRM batches were used during this study: 96, 101 and 105 (information for these constants can be fetched at andrew.ucsd.edu/co2qc).

To ensure that the system reproducibility was within acceptable limits ($\pm 5 \mu mol.kg^{-1}$), a duplicate CRM was run prior to sampling. Another duplicate CRM was run after sampling had been completed to ensure that the system accuracy had not drifted beyond acceptable limits ($\pm 5 \mu mol.kg^{-1}$) during the sampling. The accuracy of the measured value to the certified result was not vital as it could be corrected after analysis is complete. In the case of alkalinity, a deviation from the true value may have been caused by a change in the concentration of the titrant, HCl. These changes may be due to evaporation and "topping-up" of acid. This is corrected by adjusting the acid concentration during alkalinity calculation to achieve the CRMs actual value. A linear correction factor was applied to DIC results. Applying these corrections to sample data was done by using the daily average of CRM corrections.

Statistical Methods

Establishing the short term and long term accuracy and precision of results was done using methods suggested by DOE (2004). Because samples were analyzed in batches according to month, there were often not enough CRM samples to create control plots as suggested. However, CRM samples were used to calculate a 95% confidence interval for the mean of the CRM (before recalculation):

$$\bar{x} \pm \frac{t.s}{\sqrt{n}} \tag{3.2}$$

where $\bar{x}$ is the mean, t the Student's t value for 95% confidence interval (based on degrees of freedom), s is the standard deviation, and n the number of measurements.

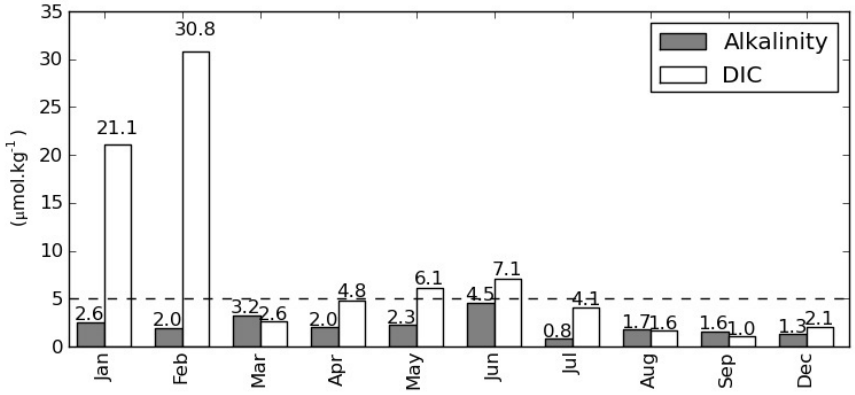

Figure 3.3: Confidence interval for CRMs (before recalculation) for each month. Mean value is not shown as confidence interval applies to CRMs as well as samples after recalculation.

3.2.4 Normalisation

In order to find the biological contribution to TA in two different water masses we have to correct for these salinity changes. A simple correction ($TA = {}^{TA}/_{S} \cdot S_{ref}$) is often used on both TA and DIC. The problem with this method of correction is that there is often over-correction leading to artificial trends in the data. This is especially true if the salinity range in the data-set is large. Friis et al. (2003) presented a new correction method in which the natural slope of the data is used to find a x intercept ($AT_{S=0}$). $AT_{S=0}$ is then subtracted from alkalinity before the correction is applied and added again after, as shown below:

$$nAT = \frac{AT_{obs} - AT_{S=0}}{S} \cdot S_{ref} + AT_{S=0} \tag{3.3}$$

This is similarly applied to DIC. The resulting difference in the two methods is marked, as is seen in figure 3.4. $AT_{S=0}$ was calculated for the entire data-set (1994 µmol.kg^{-1}) and then applied to each month.

Nitrate correction is the second factor to correct if one wants to assess the carbon pump contributions. Unlike the salinity normalisation, the nitrate correction is only applied to TA. The

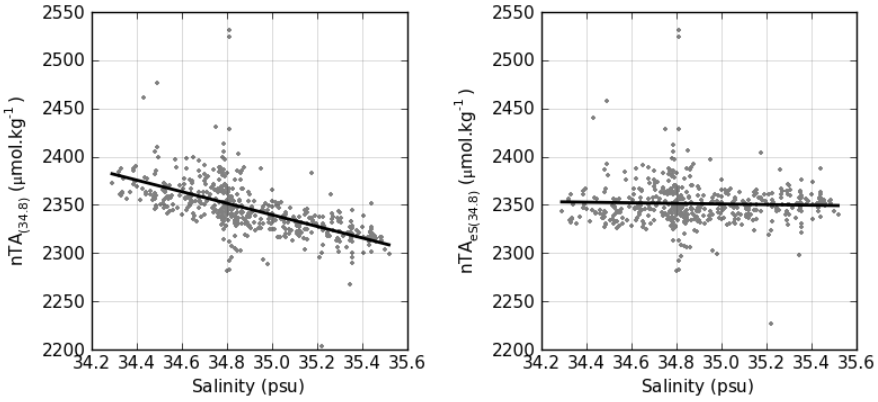

Figure 3.4: Plots showing the contrast between the two salinity correction methods for TA. On the left is the result of the standard correction. On the right is the correction procedure as suggested by Friis et al. (2003).

reason for this correction is that the assimilation and remineralisation of nitrate results in an increase and decrease of alkalinity respectively. This is not obvious if one considers Dickson's definition of TA (equation 2.5). To understand this, one has to consider the chemistry of ion uptake in the cell. This will be discussed in full in section 5.3.2. To correct for this, nitrate is typically added to alkalinity to produce *potential alkalinity* (TA*). In this study an adjusted version of potential alkalinity was used, where a reference nitrate value of 15 µmol.kg^{-1} subtracted from the traditional TA*:

$$nTA* = nTA - (NO^-_{3\,ref} - NO^-_3) \tag{3.4}$$

3.2.5 Other Marine Carbonate Parameters

Calculation of the other marine carbonate system parameters was done using the MATLAB version of the "program developed for CO_2 system calculations" by Lewis and Wallace (1998). pH was calculated on the total scale and $pK_{1\ \&\ 2}$ constants by Mojica-Prieto and Millero (2002) were used. The Revelle factor, pCO_2 and Ω_{Ca} were calculated using the same script.

3.2.6 Other Biogeochemical Parameters

Dissolved Oxygen

As mentioned, dissolved oxygen (DO) was determined by Winkler titration to calibrate the CTD optode measurements (Sea-bird SBE 43 DO sensor). DO cannot be determined directly by chemical analysis. An indirect stoichiometric titration is thus used to find the DO concentration. *Manganese chloride* ($MnCl_2$) and *alkaline iodide* (KI / KOH) are added to the water sample, to produce a manganese precipitate. Once all the oxygen has reacted, the sample is acidified with *sulfuric acid*. This results in the oxidation of the KI, to produce iodine (I_2). The I_2 is then titrated against a solution of thiosulphate. DO is calculated stoichiometrically by the volume of thiosulphate needed to reach the endpoint of the titration.

Nutrients

Nitrate, phosphate and silicate were analysed using a flow injection analysis autoanalyser, using methods described in Grasshoff et al. (1999). Each method will briefly be described below.

For the determination of *nitrate* concentration, $[NO_3^-]$, the sample is divided into two portions. This is done as $[NO_3^-]$ cannot be determined directly by chemical analysis, but $[NO_2^-]$ can. Thus to determine $[NO_3^-]$, a base $[NO_2^-]$ must be measured. Reagents, *sulphanilamide* and *N(-1-naphtyl)-ethylenediamine dihydrochloride* (NEDI), are added to one portion of sample. This induces the development of a dye, which is proportional to$[NO_2^-]$. The concentration of the azo dye is measured spectrophotometrically. The second portion passed through a cadmium column, to reduce NO_3^- to NO_2^-. The same reagents are added to the reduced quantity to find $[NO_3^- + NO_2^-]$, from which $[NO_3^-]$ is derived.

Phosphate concentration is determined by reacting a seawater sample with a *mixed reagent* (ammonium molybdate, sulfuric acid, ascorbic acid and potassium antimonyl-tartrate), which forms a blue complex. The concentration of this complex is measured spectrophotometrically.

The determination of *silicate* is similar to that of phosphate. *Acid molybdate* is added to the sample, which produces *sillicomolybdate*. This compound is reduced by adding oxalic acid, immediately followed by *ascorbic acid*. This results in the formation of a blue complex, which is measured spectrophotometrically.

3.3 Physics

3.3.1 Wind Data

Cross-Calibrated Multi-Platform Winds (Atlas et al., 2011) were used to calculate an upwelling index and the gas transfer velocity for air-sea flux of CO_2. The CCMP Winds product offers six hourly scatterometer winds at a $\frac{1}{4}$ degree resolution. Data was downloaded from the PoDaac website (ftp://podaac-ftp.jpl.nasa.gov). Atlas et al. (2011) mention in their study that some upwelling regions may suffer from underestimation, however the southern Benguela does not seem to be affected. Another shortcoming of satellite derived winds is that wind speeds in near coastal regions are often overestimated. This was briefly investigated, but correcting this data effectively merits its own study.

3.3.2 Ekman Transport

An upwelling index, after Bakun (1973) and Schwing et al. (1996), was calculated from CCMP Winds:

$$\vec{M} = \frac{1}{f} \cdot \left(\rho_a \, C_d \, U_{10}^2\right) \tag{3.5}$$

Where M is Ekman transport and f is the Coriolis parameter. The function in brackets represents winds stress (τ), where ρ_a is the density of air, C_d is a drag coefficient and U_{10} is a surface wind vector. U_{10} is given by the rotated meridional component of the wind vector. Bakun (1973) defines C_d as a constant, however, Trenberth et al. (1990) define, what they call, the neutral drag coefficient (C_N) on the wind speed. The latter was used in this study, as the authors

reported that C_{d} is dependant on "wind speed and atmospheric stability". Below is their definition of C_{N}:

$$\begin{aligned} 10^3 C_N &= 0.49 + 0.065U \quad \text{for} \quad U > 10\mathrm{m}.s^{-1} && (3.6a) \\ &= 1.14 \quad \text{for} \quad 3 \leqslant U \leqslant 10\mathrm{m}.s^{-1} && (3.6b) \\ &= 0.62 + 1.56U^{-1} \quad \text{for} \quad U \leqslant 3\mathrm{m}.s^{-1} && (3.6c) \end{aligned}$$

3.4 Flux calculations

CO_2 flux was calculated using equation 2.6, where a K_0 by Weiss and Price (1980) for moist air was used. The saturation water vapor pressure used in the definition for CO_2 solubility was also given by the aforementioned authors. Several studies have investigated the relationship between wind speed and gas transfer velocity (figure 2.3). The gas transfer velocity by Wanninkhof et al. (2009) was used in this study:

$$k_{660} = \left(3 + 0.1(U_{10}) + 0.064(U_{10}^2) + 0.011(U_{10}^3)\right) \times \left(\frac{Sc}{660}\right)^{-1/2} \tag{3.7}$$

Where Sc is the Schmidt number (equation 2.2), as defined by Wanninkhof (1992):

$$Sc = A - Bt + Ct^2 - Dt^3 \tag{3.8}$$

where t is temperature, and A, B, C and D are constants 2073.1, 125.62, 3.6276 and 0.043219 respectively.

3.5 Ancillary Data

Ocean Data View (Schlitzer, 2009) was used to view WOCE and CARINA data-sets. Data was further processed using Enthought Python Distribution (Educational License) and Microsoft Excel 2010 was used for basic data processing.

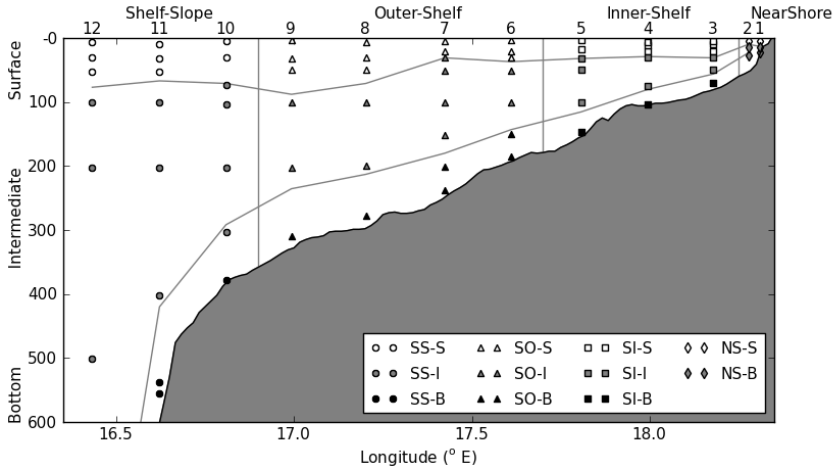

Figure 3.5: An example of a monthly sampling section showing the zonation along the vertical and horizontal. Numbers at the top of the section show the station number. The labels on the y-axis and the top x-axis are the names used to describe the zones. On the horizontal, stations were defined by longitude. And in the vertical: surface samples were defined by thermocline depth. Bottom samples were within 50 m from the bottom, unless 3/4 of the bottom depth was deeper than 50 m. Remaining samples were classified as intermediate.

3.6 Data Processing

In order to assess the seasonal cycle of the southern Benguela data was divided into three seasons: summer, autumn and winter. Spring was not included as a season as there were no samples collected for October and November. The table below shows the months that were included in each season. Values marked with * are months where no samples were taken.

Summer	Autumn			Winter				Summer			
Jan	Feb	Mar	Apr	May	Jun	Jul	Aug	Sept	Oct*	Nov*	Dec

During collection, samples were not taken at the same station and depth from month to month. In order to make make sections comparable, data was divided along the vertical and horizontal into ten different zones (figure 3.5). Cross-shelf, four boundaries were defined by longitude creating shelf-slope (SS), outer-shelf (SO), inner shelf (SI) and near-shore (NS) stations. The concept of boundaries has always been an issue for consideration in oceanography

due to the dynamic nature of natural systems. Geographic boundaries are fixed in space, such as the horizontal boundaries selected in this study. While these boundaries are easy to define, they present a problem when dynamic oceanographic features transgress across boundaries. In other words, geographic boundaries alias data due to spatial averaging.

This was partially addressed in the vertical by defining dynamic boundaries. Three zones were created for all but the NS stations, where only two were defined. The surface stations (S) were defined by the thermocline depth (maximum slope by difference as defined in Fiedler, 2010). Bottom samples (B) were defined as such if the were within 50 m of the bottom, unless [0.75 $\times$ bottom depth] was deeper than the aforementioned criteria. Samples which met neither the surface or bottom criteria were classed as intermediate stations (I). In the near-shore stations, samples were divided into "near-shore surface" (NS-S) and "near-shore bottom" (NS-B) according to the thermocline. The same key (shown in figure 3.5) is used to distinguish different zones throughout the paper.

4 Results

4.1 Physical characterisation

4.1.1 Winds and upwelling

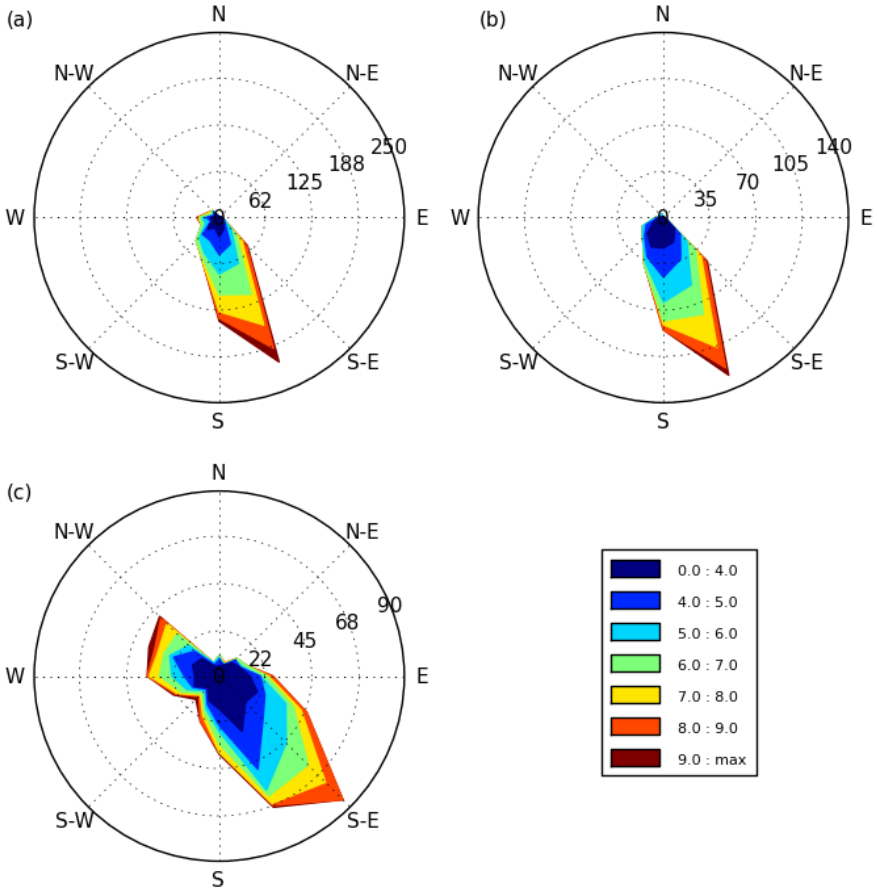

Figure 4.1: Wind rose plots for CCMP winds (m s^{-1}) for the domain 32.0 to 33.0°S and 17.0 to 18.0°E. Data is divided into three seasons, where (a), (b) *and* (c) *are summer, autumn and winter respectively. Note that the radius of each plot varies as selected seasons are different lengths.*

Strong seasonality was present in the winds during 2010 (figure 4.1). During the summer and autumn months, winds in the southern Benguela were strongly unipolar, with the dominant wind direction being SSE. However, in winter there was a definite bipolarity in the wind field where 23% of winds had a northerly component compared to 7% and 3% for summer and autumn respectively. Quiescence is

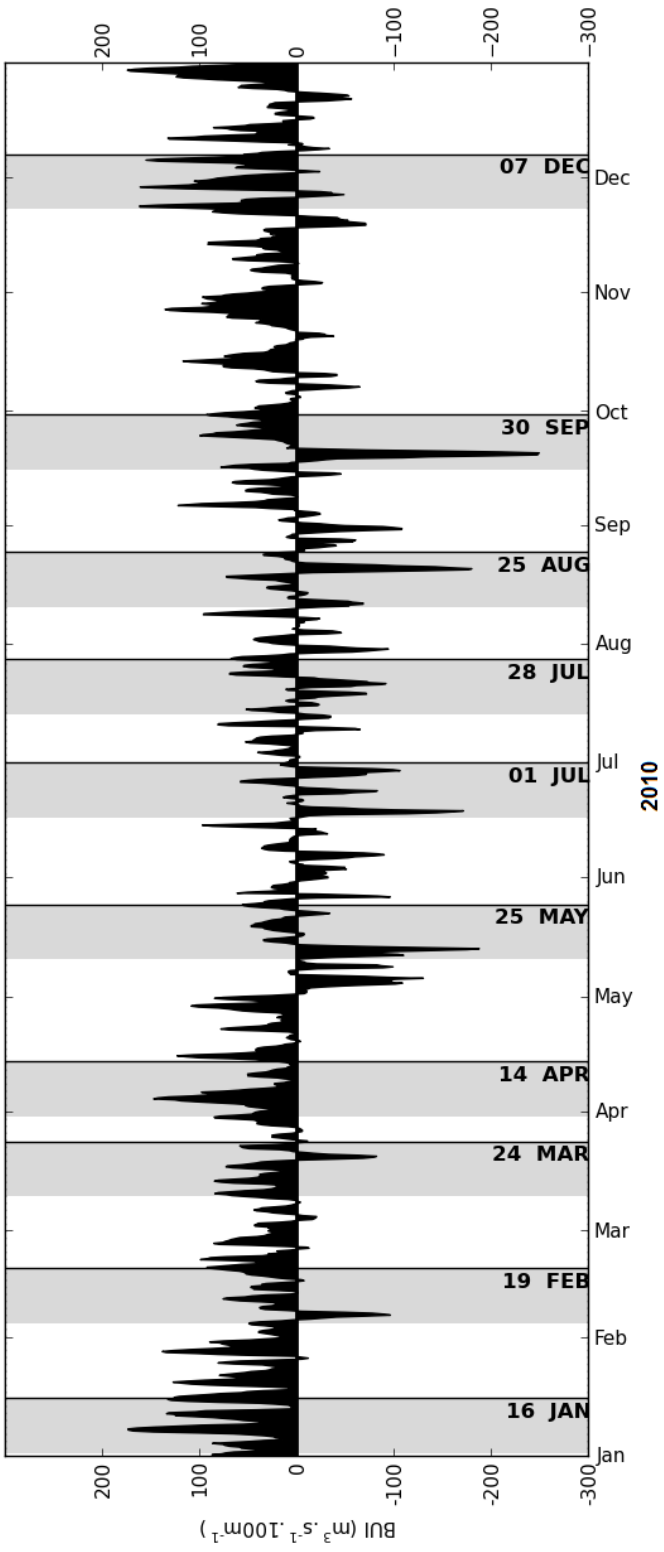

Figure 4.2: Bakun Upwelling Index (BUI) for 33.0 to 32.0 °S, and 17.0 to 18.0 °E with a one day moving average. Winds were rotated by 15° to compensate for coastal rotation. Data units are in transport ($m^3\ s^{-1}$) per 100 m of coastline, where positive values denote upwelling and negative values downwelling. Vertical black lines represent the days on which samples were taken. Gray bars indicate a fourteen day period prior to sampling (discussed further in figure 4.3).

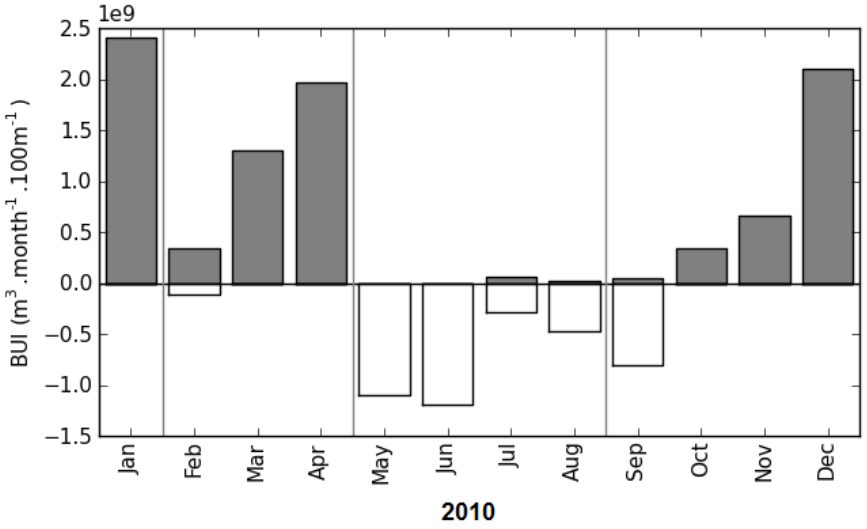

Figure 4.3: Cumulative upwelling for each month fourteen days prior to sampling, as indicated in figure 4.2. Note that the y-axis is in 10^8 m^3 per month for 100 m of coastline. Positive values are upwelling and negative values represent downwelling.

far more prevalent in winter, with 21, 31 and 42% of recoded measurements being less than 4 m.s^{-1} for summer, autumn and winter respectively. In accordance with this, winds exceeding 8 m s^{-1} accounted for 13%, 10%, and 8% for the seasons - the same order as above. However, the maximum wind speed measured was during winter at 11.28 m s^{-1}, compared to 10.97 and 10.27 m s^{-1} for summer and autumn respectively.

The rotated meridional wind component was used to derive the Ekman transport or Bakun Upwelling Index (BUI, after Bakun, 1973). Figure 4.2 shows the BUI for the sampling region. Data ranges between 285 and -330 m^3 s^{-1} 100 m^{-1}, which is similar to the ranges reported by Bakun (1973) and Schwing et al. (1996) for the North American West Coast. The total annual Ekman flux from this study was 2.68 Gm^3 yr^{-1} 100 m^{-1}. This is greater than values found by Monteiro (1996) for 1992 and 1994, when Ekman flux was 1.30 and 2.15 Gm^3 yr^{-1} 100 m^{-1} respectively. These differences may be due to different wind products, where Monteiro used *in-situ* winds.

The data shows a pulsating upwelling pattern in summer, due to strengthening and weakening of the pressure gradient between the SAAC and the continental low pressure over southern Africa. In winter, the BUI shows greater north-south intraseaonal variation due to mid-latitude cyclones being further north.

A positive BUI may not directly translate into the upwelling state of the system. In order to gain a better understanding of the upwelling state, certain criteria were applied to the data: the data had to exceed that limit for longer than the inertial oscillation for the site latitude (∼24 hrs at 32 °S). Figure 4.3 shows the cumulative divergence, where the aforementioned criteria are met and additionally fall within a fourteen day period prior to sampling. The 15th of October and November were chosen as arbitrary dates as no sampling took place. January, April and December are the three sampling periods with the strongest preceding upwelling. The moderate upwelling in the early summer months (September through November) is due to the fact that the sampling date and the upwelling pulses were out of sync. In contrast to summer and autumn, the BUI in winter is erratic and winds favoured upwelling infrequently, but intense, sporadic downwelling events occurred. This is due to increased mid-latitude cyclone activity at this latitude during winter.

4.1.2 Temperature-Salinity Plots

TS-diagrams from CTD data for each season are shown in figure 4.4. Temperature ranges from 3 to 18°C and salinity from 34.34 to 35.50. The lower limb of the TS diagrams are accounted for by deep waters (> 600 m) originating from Antarctic Intermediate Water (∼34.45). The upper limb can be ascribed to South East Atlantic Water (SEAW) with a salinity range of 34.60 to 35.50 (Monteiro, 1996).

Upwelled water along the SHBML typically has a salinity of ∼34.8. This water is consequently modified by surface processes such as solar heating, evaporation, precipitation or riverine input.

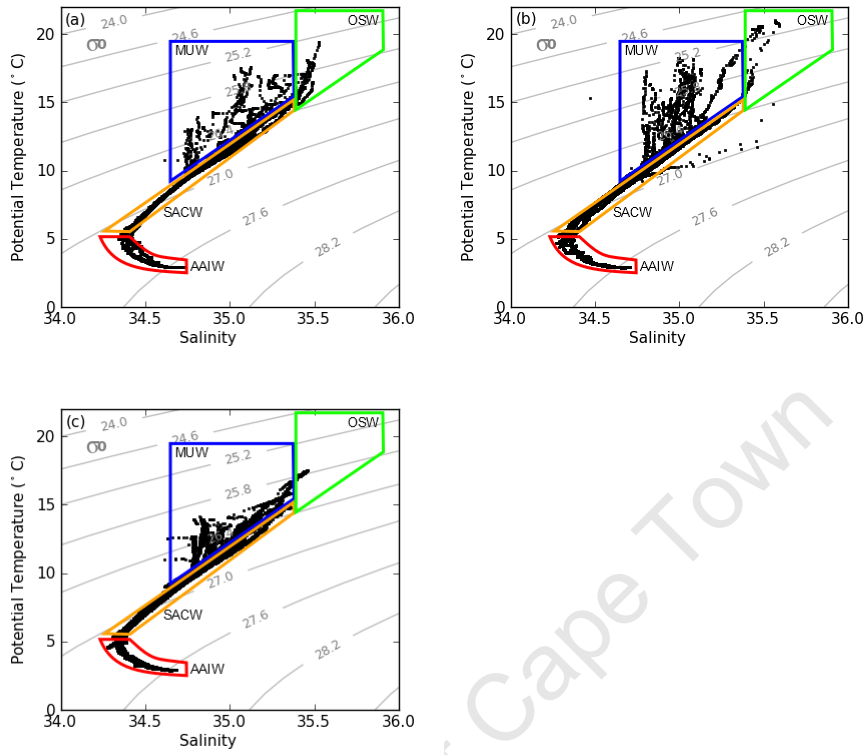

Figure 4.4: TS-diagrams for summer (a)*, autumn* (b) *and winter* (c)*. Blocks denote the following water masses: AAIW = Antarctic Intermediate Water; SACW = South Atlantic Central Water; MUW = Modified Upwelled Water; OSW = Oceanic Surface Water.*

However, Guastella (1992) points out that evaporation rates in upwelling systems are low, thus salinity can be used as a quasi-tracer.

By the same token, temperature can be used as a short term (<15 days) measure of modification, with Guastella (1992) reporting a warming rate of 0.52 °C day^{-1}for the upper 10 m. During summer months upwelled water was present, but temperatures remained relatively low (13.0 °C) due to persistent upwelling. During autumn, upwelled water temperatures rose to 17.4 °C as longer quiescent periods allowed for warming due to greater stratification. Stations further offshore also showed extensive warming during autumn, with shoaling thermoclines (figure 4.5). Inshore stations showed far less variation in thermocline depth between seasons due to the retentive

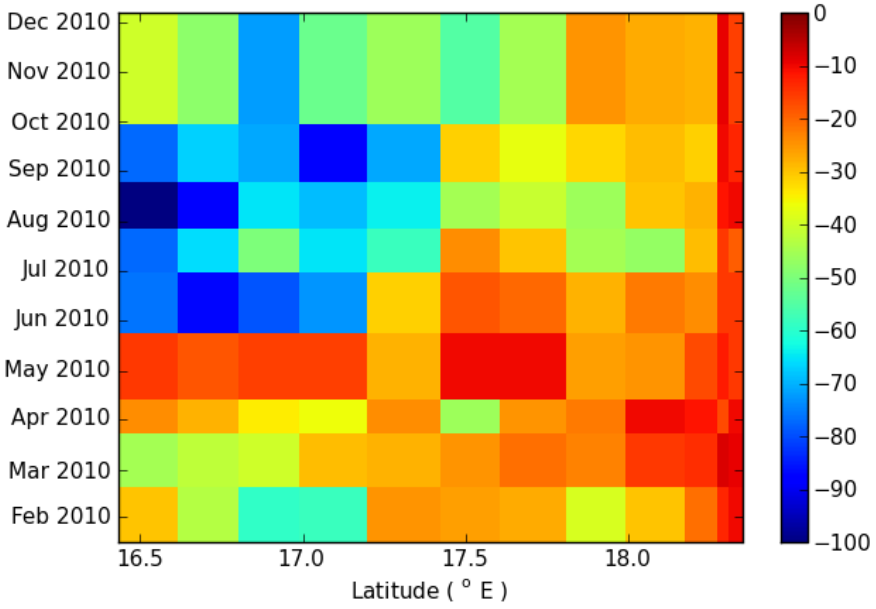

Figure 4.5: A plot showing the depths of the thermocline (m) for sampled months along the y-axis and longitude along the x-axis.

circulation of St. Helena Bay (Pitcher and Nelson, 2006). Winter presents a strong contrast to the other seasons with minimal modification of surface waters. Tight bunching in surface data indicates deep mixed layers where temperature is homogeneous. Few stations also showed freshening by precipitation or riverine input from the Berg River in the upper layer.

As mentioned earlier salinity is considered a conservative variable in the southern Benguela. It is thus useful to plot this physical tracer, against biogeochemical tracers to track biological changes relative to the physics. In figure 4.6 (a-c) salinity and nitrate are plotted against each other. Nitrate ranges (0.0 - 31.0 µmol kg^{-1}) were within those reported by Kearns and Carr (2003). There is a clear separation between the bottom and surface values, with the former being fresher than the source water salinity (34.8) and the latter more saline. The distribution of nitrate follows a similar pattern, with bottom samples having higher nitrate concentrations (10 to 30

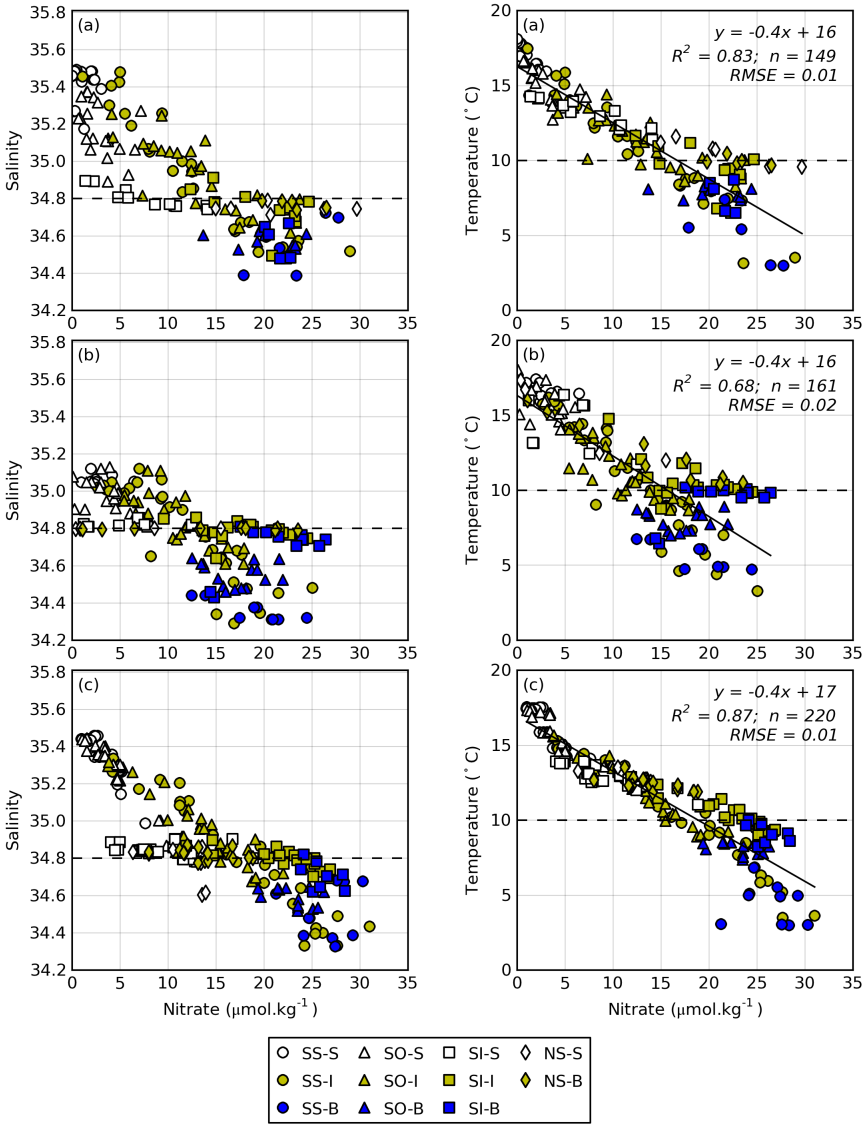

Figure 4.6: Plots of salinity vs. nitrate (a-c) *for each season: summer, autumn, winter respectively. The dashed line marks the upwelled waters' salinity (34.80). Plots of temperature vs. nitrate* (d-f) *for each season. The dashed line at 10° C represents the temperature of newly upwelled water. RMSE shows the root mean squared error.*
In reference to key: SS = shelf-slope, SO = outer-shelf, SI = inner-shelf and NS = near-shore

µmol kg^{-1}) and surface lower (0 to 15 µmol kg^{-1}) due to enrichment and depletion respectively. Surface salinity showed some variation throughout the seasons, as described above. The intermediate samples ranges' extend the full span of both salinity and nitrate. Near shore bottom samples formed distinct clusters along a salinity of ~34.8 for each of the seasons. These groupings are found at nitrate concentrations of 22, 18 and 12 µmol.kg^{-1} for summer, autumn and winter respectively.

These groupings are also visible in the temperature-nitrate plots (figures 4.6, d-f). Interestingly the winter grouping is not 10 °C or less, indicating that this water is in fact aged water. It is clear from this data that the relationship between nitrate and temperature in the southern Benguela is well correlated. This was also measured by Waldron and Probyn (1992), who used this relationship to determine productivity in the southern Benguela.

4.2 Marine Carbonate System

nDIC sections (figure 4.7, a-c) show average concentrations for each season in each zone, as defined in section 3.6. Concentrations were consistently lowest in the shelf-slope and outer-shelf surface waters (2053 to 2103 µmol kg^{-1}). The effects of benthic remineralisation were seen in the nearshore and inner-shelf bottom waters, which had high nDIC concentrations (2184 to 2287 µmol kg^{-1}). Nearshore surface nDIC concentrations had the greatest interseasonal range, decreasing from 2273 µmol kg^{-1}in summer to 2171 µmol kg^{-1} in winter. This large range was probably due the upwelling in summer *versus* the quiescent conditions of winter.

The mean nTA* for the SHBML data (2348 µmol kg^{-1}) is similar to that found by Monteiro (1996) for the Olifants River transect where upwelled water had a nTA* of 2361 µmol kg^{-1}. Compared to nDIC, the nTA range was far less, with the biggest difference being in autumn (2309 to 2420 µmol kg^{-1}). The low surface and high bottom values in autumn may have been due to calcification and anaerobic remineralisation respectively. In nTA was relatively con-

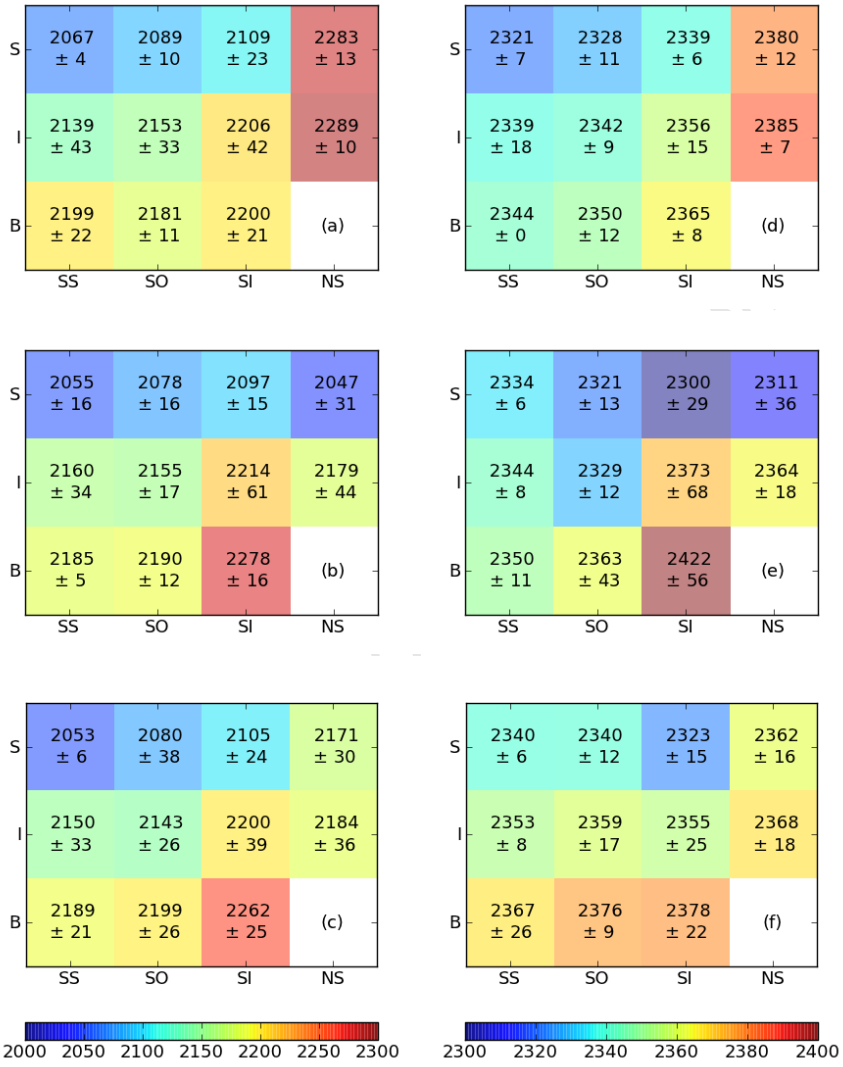

Figure 4.7: nDIC (a-c) and nTA (d-f) averages and standard deviations for each zone for summer (top), autumn (middle) and winter (bottom). Concentrations are in µmol kg^{-1}. SS = shelf-slope, SO = outer-shelf, SI = inner-shelf and NS = near-shore, S = Shallow, I = Intermediate and B = Bottom

stant throughout the year in the shelf-slope and outer-shelf regions (2332 to 2367 µmol kg^{-1}).

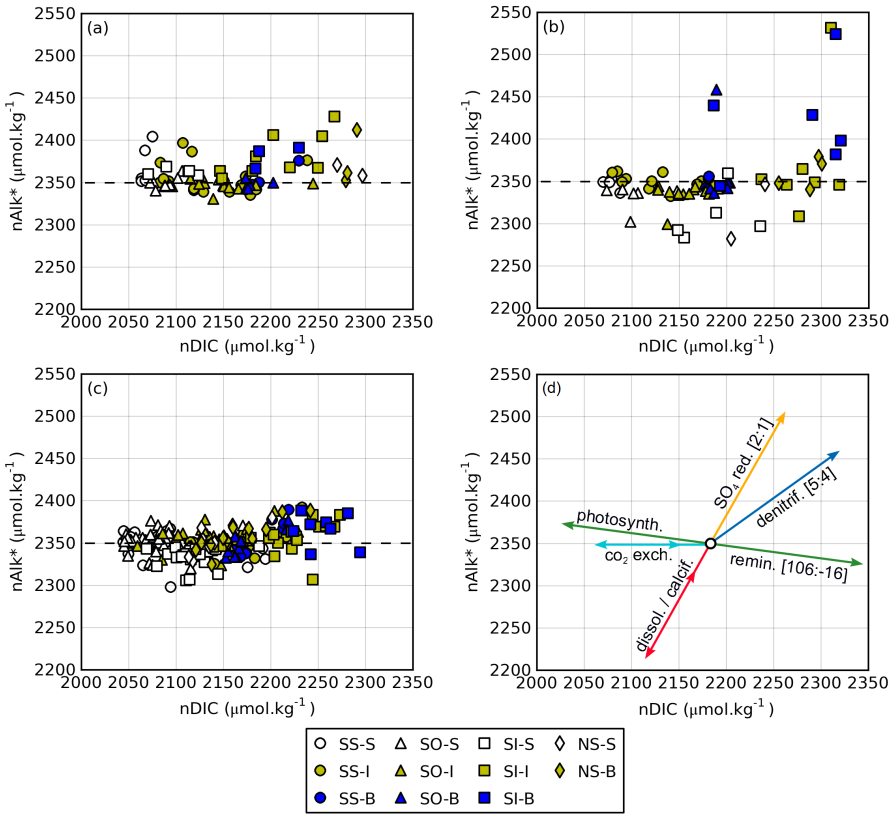

Figure 4.8: Three plots for summer (a)*, autumn* (b) *and winter* (c) *comparing nDIC and normalised total alkalinity nTA*. January, February, March and December were omitted due to unreliable data. A reference line of 2345 µmol kg^{-1} was drawn to highlight the source water concentration of nTA*. Colour vectors, in figure* (d) *show the various mechanisms of change to the marine carbonate system. SS = shelf-slope, SO = outer-shelf, SI = inner-shelf and NS = near-shore*

To gain greater insight about the changes observed in these two parameters, they were plotted against each other in figures 4.8 (a-c). Unreliable data in February, March and December means that summer and autumn have far fewer data points.

Bottom shelf-slope and outer-shelf samples were clustered around nDIC concentrations 2150 and 2200 µmol kg^{-1}. The median of this grouping of samples was ~2179 µmol kg^{-1}, which is a good approx-

imation for SACW. This is in agreement with data collected along a transect in the Olifants River region by Monteiro (1996), where a similar grouping of data had a nDIC concentration of 2194 µmol kg^{-1}. Monteiro (2009) reported greater values (2300 µmol kg^{-1}) for the inner-shelf region than was observed in this study. Though these high values did occur, they were infrequent. The median of nTA* for the same region arrived at a concentration of 2351 µmol kg^{-1}.

Changes in nDIC and nTA* (4.8, a-c) from the source water, SACW, can be attributed to a combination of the processes shown in figure 4.8 (d).To quantify these processes, stoichiometry of nutrients, DIC and TA need to be investigated.

4.2.1 Nutrients and Stoichiometry

Even though nitrate and phosphate are not part of the marine carbonate system, the relationship between these two variables (figures 4.9, a-c) is one that allows one to infer a great deal about the biogeochemical system. The ideal Redfield stoichiometery for N:P is 16:1. However, this is far from what was observed. The stoichiometric ratios for summer and winter were 12.29 and 12.43 respectively. In autumn the ratio is almost half of what the Redfield ratio predicts at 8.81. The absolute values of phosphate were greatest in autumn, indicating remineralisation. But the comparatively low nitrate values may suggest denitrification, which is further supported by the data which is significantly different to the Redfield ratio data ($P \ll 0.05$ for all plots). In all seasons, nitrate was clearly the limiting nutrient with values intersecting the x-axis before the y-axis.

The relationship between NO_3^- and nDIC is shown in figures 4.9 (d-f). January and February were excluded as these months had unreliable DIC values (section 3.2.3). There is a positive pattern in the data (6.4 to 8.0) similar to the Redfield ratio (6.6:1 for C:N, Redfield et al., 1963). Surface samples have the lower concentrations, increasing toward the shore. Bottom samples are found in the upper limb of the data, but there is far greater scatter amongst these points than surface samples. In addition, this scatter is found

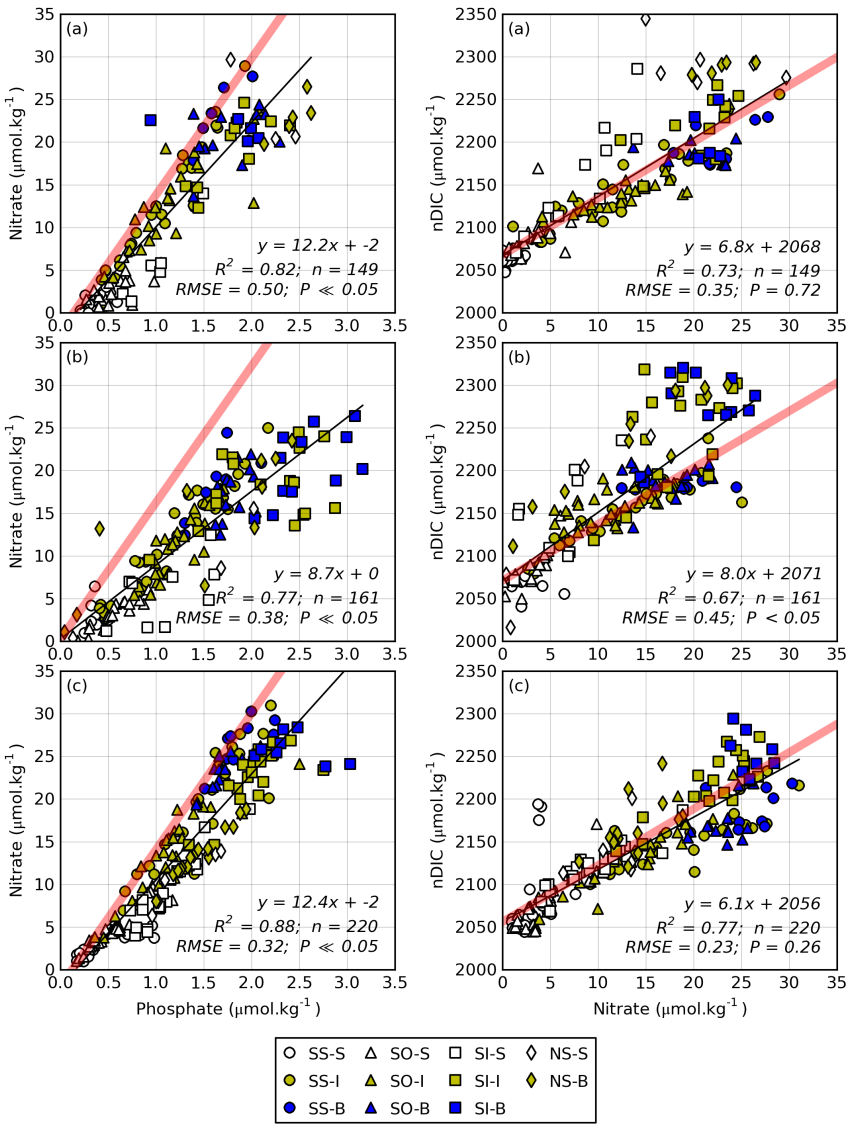

Figure 4.9: Scatter plots of nitrate vs. phosphate (a-c) *for summer, autumn and winter respectively. The red line represents the expected Redfield ratio of 16:1. Scatter plots of nDIC vs. nitrate* (d-f) *throughout the year for summer, autumn and winter respectively. Note that January and February were excluded due to failing quality control. The red line represents the Redfield ratio of 6.6:1. SS = shelf-slope, SO = outer-shelf, SI = inner-shelf and NS = near-shore. RMSE shows the root-mean-squared error of the best fit line. P shows the P-value for an independant t-test comparing the expected Redfield values to the observed values, where the null hypothesis is that the data fits the best-fit line.*

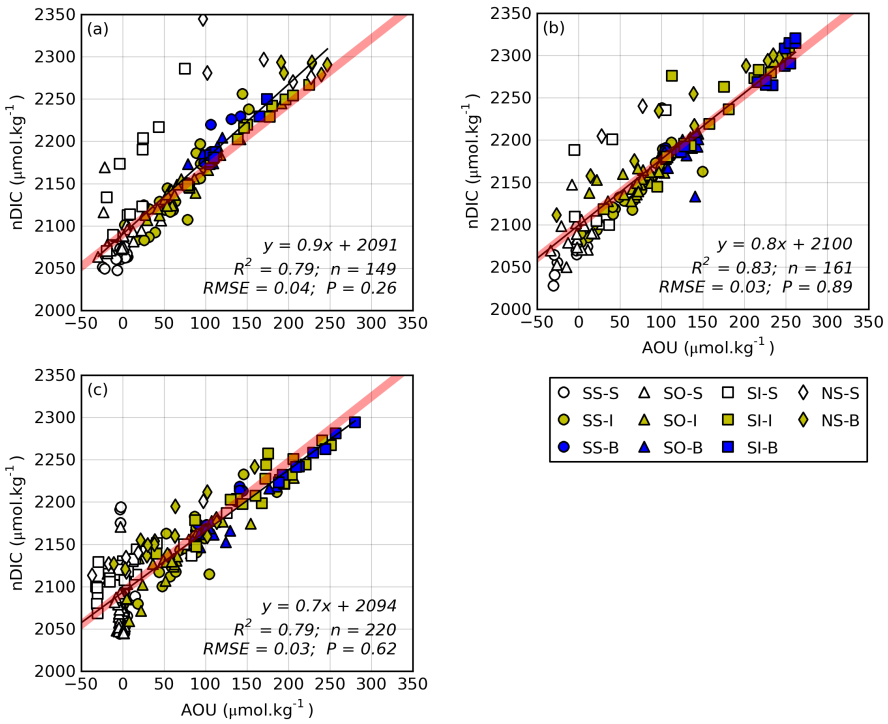

Figure 4.10: Normalised DIC (34.8) plotted against apparent oxygen utilisation (AOU). January and February were omitted due to bad quality data. The red line is the expected ratio according to Redfield stoichiometery (C:O = 0.77). RMSE shows the root-mean-squared error of the best fit line. P shows the P-value for an independant t-test comparing the expected Redfield values to the observed values, where the null hypothesis is that the data fits the best-fit line. SS = shelf-slope, SO = outer-shelf, SI = inner-shelf and NS = near-shore

mainly above the best-fit line. This may improve the case for denitrification changing stoichiometry, as was found by Tyrrell and Lucas (2002).

Figure 4.10 shows plots for normalised DIC against apparent oxygen utilisation (AOU), where the latter is the difference between the theoretical saturation of dissolved oxygen and the measured dissolved oxygen (DO). The relationship between DIC and AOU is dictated by the respiration and flux of both variables. A study by Hedges et al. (2002) estimates a ratio between C:O of 106:138. This equates to 0.77, which is in the range found in this study (0.74 - 0.89). Surface samples, with the exception of the near-shore sta-

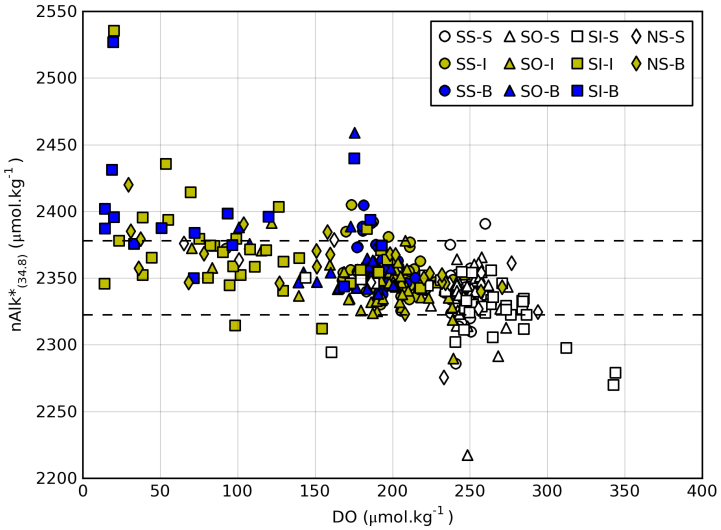

Figure 4.11: Plot of normalised alkalinity and dissolved oxygen (DO) for all months excluding February, March and December. The dashed lines are one standard deviation from the mean (2348.21±25.92). SS = shelf-slope, SO = outer-shelf, SI = inner-shelf and NS = near-shore

tions, are grouped near an AOU of 0. Shelf-slope and outer-shelf bottom samples, or source water, were relatively homogeneous with respect to AOU (∼100 µmol kg^{-1}). Bottom near-shore and inner-shelf samples were constrained closer to the trend-line than the DIC vs. NO_3^- plots (figures 4.9, d-f). In autumn there was a particularly high abundance of samples from this region concentrated at high DIC and AOU values. Several inner-shelf surface samples in summer and autumn lie well above the trend-line indicating higher DIC than expected. Oxygen has a far lower solubility than CO_2 in seawater, resulting in faster equilibration than DIC.

4.2.2 Alkalinity

The relationship between nTA* and DO can provide one with insight into changes in alkalinity. There are few mechanisms which alter alkalinity, of which denitrification and sulphate reduction are important in the southern Benguela (Tyrrell and Lucas, 2002). Figure 4.11 allows one to investigate this relationship thoroughly. Sev-

eral of the low DO values had high nTA* values, and the converse for high DO values. In order to calculate the average net gain or loss of alkalinity throughout the year, upper and lower limits of expected alkalinity were set. Expected alkalinity boundaries were determined by the sum or difference between the mean alkalinity (2348.21 µmol.kg^{-1}) and the standard deviation (25.92 µmol.kg^{-1}). Net gain or loss of alkalinity was calculated by finding the monthly change in alkalinity if values exceeded the set limits.

4.2.3 pH

Figures 4.12 (a-c) shows temperature plotted against pH. Here temperature is used as a tracer of the age of water, where water warmer than 10°C is upwelled and has been modified. Throughout the year, pH ranged from 7.60 to 8.25, both lower and higher than the global average for surface waters (8.1) as reported by Orr et al. (2001). Though average pH in autumn was more than 0.1 lower than average pH for winter. Note that this may be due to lack of data in autumn, as April was the only month with reliable data. The lower pH ranges are similar to those found by Feely et al. (2008a) along the Californian coast. A distinct pattern emerges in figures 4.12 (a-c), where the bottom waters in all the seasons had a similar decreasing trend in pH, shown by the red line. This is due to increased DIC by remineralisation.

pH trends in surface waters were not consistent throughout the year. In summer, the difference in pH between the nearshore and inner-shelf samples was about 0.2. Where the nearshore surface samples had low pH values (∼7.80). This difference shows the strong carbonate gradient which productive diatoms drive in summer. Nearshore surface pH values were similar to summer in autumn, but the inner-shelf samples had lower pH values than observed in summer. These high values were due to calcification in the surface waters. This in contrast to winter, when nearshore samples had pH values greater than 8.00, due to the changes in upwelling and productivity.

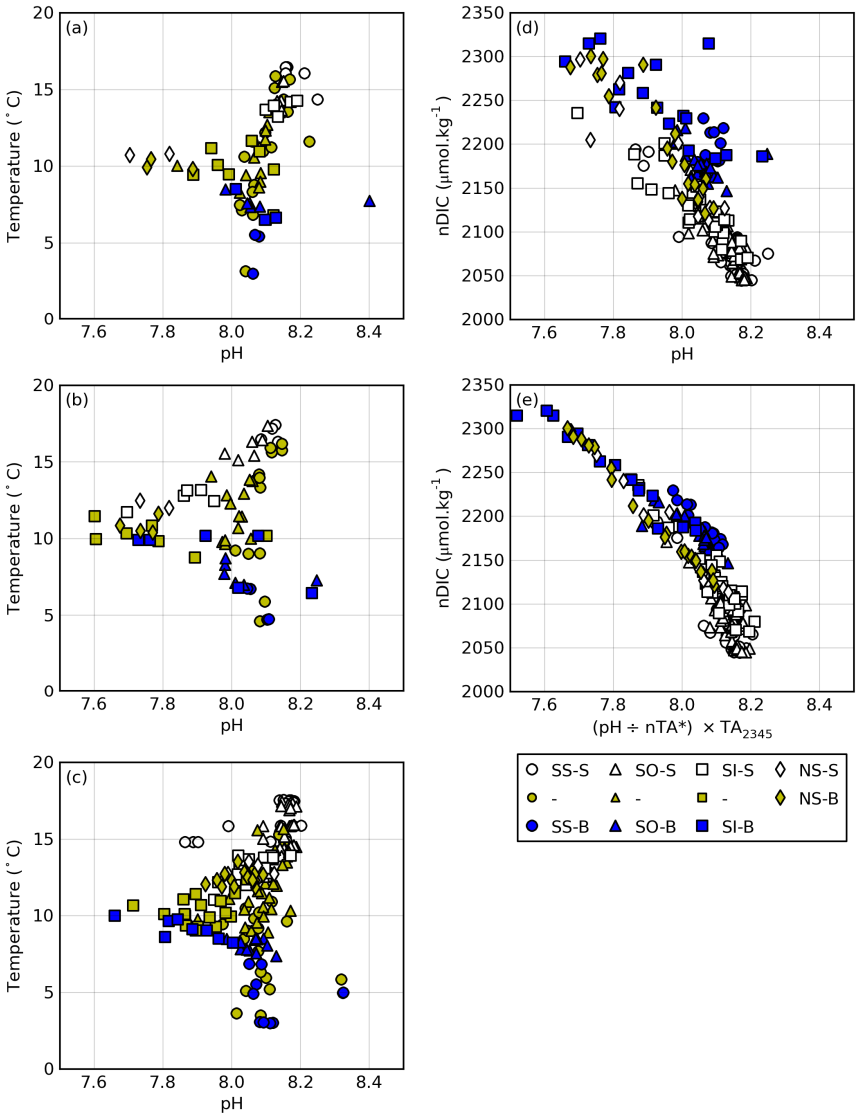

Figure 4.12: Temperature plotted against pH. The dotted lines are average pH for each season, summer (a)*, autumn* (b) *and winter* (c)*.*
Two plots of nDIC vs. pH (d) *and nDIC vs. pH normalised to a TA value of 2345 µmol kg^{-1}* (e)*. SS = shelf-slope, SO = outer-shelf, SI = inner-shelf and NS = near-shore*

Figures 4.12 (d and e) shows the relationship between the state variables (DIC and TA) and pH. The plot of DIC against standard pH shows a great deal of scatter compared to the plot of DIC against pH normalised to a TA value of 2345 µmol kg^{-1} by using the equation shown below:

$$pH_{2345} = \frac{pH_{obs}}{TA_{obs}} \cdot 2345 \tag{4.1}$$

Intermediate samples were omitted from this plot as they create unrealistic trends due to mixing. This value was chosen as it is the source water TA concentration used in this study. The scatter arises due to the contribution of alkalinity to pH. What emerges, is that several bottom values have higher pH values, than when pH is normalised. Conversely, several surface samples have lower pH values with the alkalinity contribution. Two trends develop from the pH normalisation. This may be due to a nitrate deficit in the offshore waters, which lead to changes in TA.

4.3 CO_2 Flux

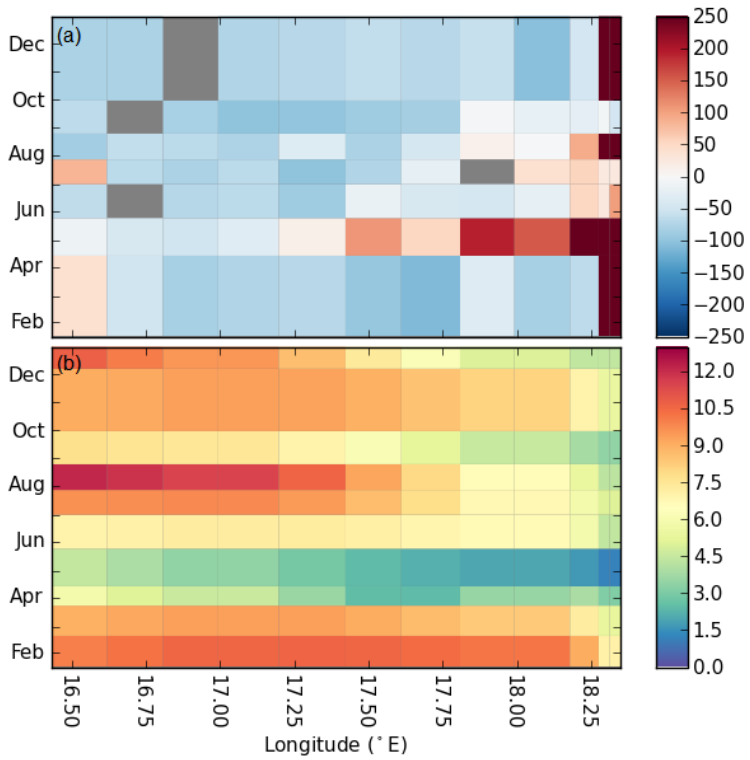

Figure 4.13: Hovmöller diagrams of ΔpCO_2 (a) *and wind speed* (b) *for January to December 2010. ΔpCO_2 (µatm) in the upper plot is calculated by $pCO_{2\ (sea)}$-$pCO_{2\ (air)}$. A positive value (red) is a carbon source. The lower plot, wind speed (m s^{-1}), is plotted from the CCMP product by Atlas et al. (2011).*

Figure 4.13 (a) shows ΔpCO_2 where negative values represent an air-sea flux. Atmospheric pCO_2 from Cape Point was used to calculate the difference (Globalview-CO2, 2011). The majority of the St. Helena Bay system was a weak sink of atmospheric CO_2. The near-shore pCO_2 was high for four out of seven months. April was anomalous as the majority of stations along the line were a source due to a combination of low nTA and high nDIC.

Wind speed, in figure 4.13 (b), ranges between 1.2 and 12.2 m s^{-1} on sampling dates. There was a general drop-off in wind from the offshore to the inshore region. Wind speeds in March and April

had lower ranges. Wind speeds were greatest in August over the shelf-slope and outer-shelf region.

Figure 4.14 shows CO_2 flux for months with good data. Data was interpolated along the x-axis in order to correct for spatial bias in calculating the average flux. All months except April were CO_2 sinks of magnitude -5.0 mmol m^{-2} d^{-1} or greater. January and August were the strongest sinks. April was only a weak source with a CO_2 flux of only $\sim$0.7 mmol m^{-2} d^{-1}. There was a persistent near-shore source region that weakened during the winter months, but covered a larger area. Chen and Borges (2009) reported a spring and winter flux of -11 and -5.5 mmol m^{-2} d^{-1} respectively, which is in accordance with this study. Their study does not report any autumn flux estimates for the southern Benguela.

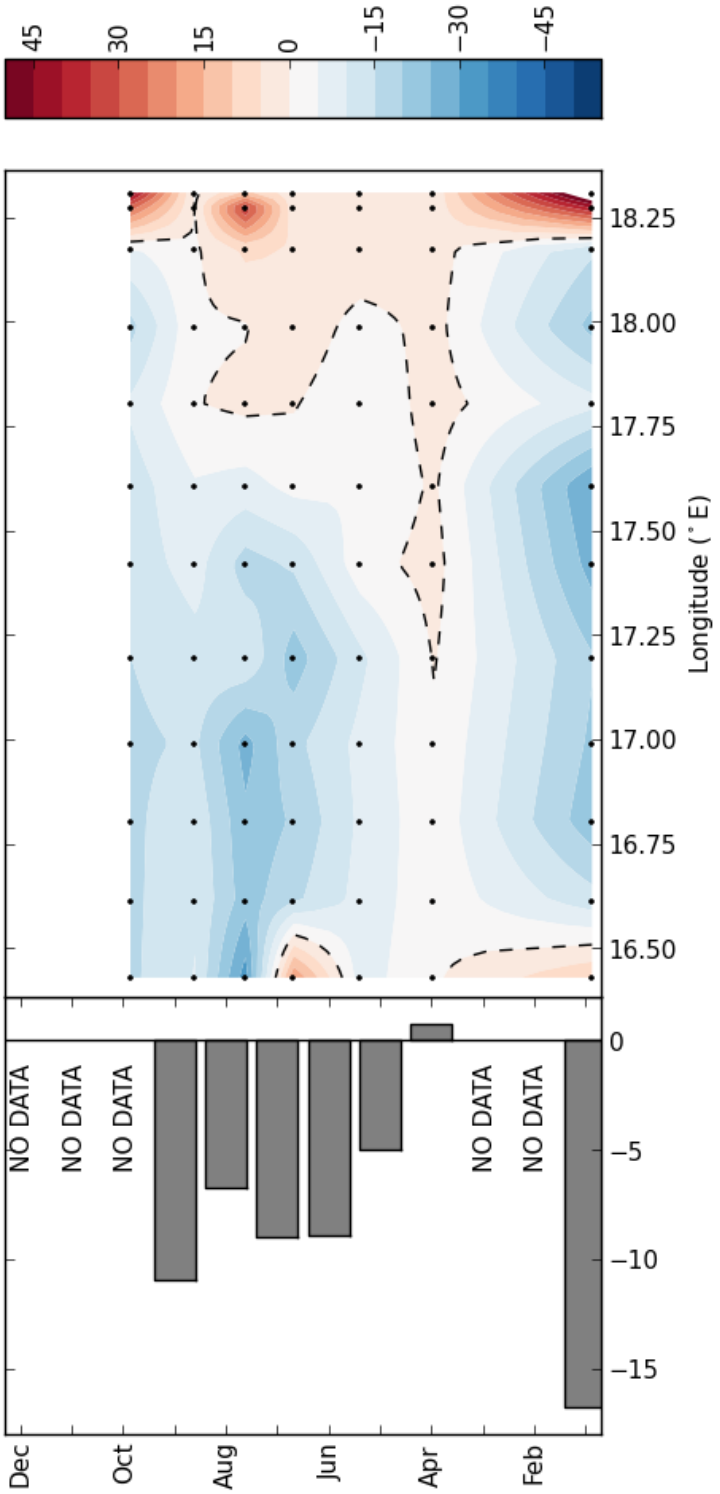

Figure 4.14: On the right, a plot of CO_2 flux (mmol $m^{-2} d^{-1}$) for all months with valid CO_2 data. The dashed line is where flux is zero. On the left is a plot of the flux averaged for the section.

5 Discussion

In this discussion, questions posed in section 2.9 will be investigated. In short, these are:

- What controls the stoichiometric ratios of nutrients?
- What is the alkalinity production of the southern Benguela?
- What is the seasonal air-sea flux of the southern Benguela?

The southern Benguela is a wind driven upwelling system, resulting in a tight coupling between the biology and physics. In order to understand the biogeochemistry, the physical milieu must first be set.

5.1 Physics

Of the three subsystems in the Benguela, the southern sector is the only seasonal upwelling system. This seasonality is caused by the meridional migration of the South Atlantic Anticyclone (SAAC) (Tyson and Preston-Whyte, 2000). The north-south migration of this system results in fluctuations of upwelling favourable winds. This is seen in figure 4.2, where the Bakun upwelling index has been used as a proxy for divergence. Tyson and Preston-Whyte (2000) suggest that the anticyclone reaches its northern most extent in late autumn. This compares well with the wind and upwelling data (figures 4.2, 4.3 and 4.1).

This seasonality was also seen in the temperature-salinity plots (figure 4.4). Summer showed the strongest and most persistent upwelling, with South Atlantic Central Water (SACW - 34.80 psu and 10 °C) being upwelled but not warming extensively, indicating resurgence of upwelling. Winter showed similar unmodified surface water, but lack of upwelling conditions implies that this is a consequence of reduced solar radiation and atmospheric temperatures. Using surface warming rates by Guastella (1992), it was found that these surface waters were a maximum of six days old. This is far less compared to the 14 day old modified upwelled water in autumn.

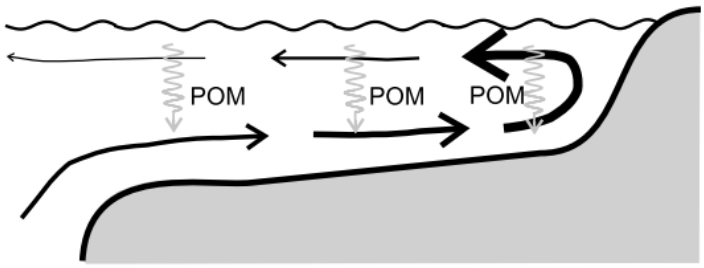

Figure 5.1: The nutrient trapping mechanism as described by Tyrrell and Lucas (2002). Water is circulated up onto the shelf along the bottom and off the shelf at the surface. This drives recycling of particulate organic matter on the shelf.

Circulation

Circulation undoubtedly plays an important role in regulating the biogeochemical mechanisms. However, circulation data was not collected during the sampling cruises. A basic cross-shore circulation was thus assumed. This circulation follows that shown in figure 5.1. Water flows from the deep ocean onto the shelf. This is driven by upwelling, which brings the water to the surface in the nearshore region. This water is then advected offshore. Using Estrade et al.'s (2008) formula for the active Ekman divergence area, it was found that the width of the upwelling region for the SHBML would theoretically be ∼10 km (equation A.1). This region is inclusive of the two nearshore stations.

Monteiro's (1996) gate hypothesis suggests that alongshore circulation in the Benguela is divided into three zones. The Cape Columbine upwelling cell falls within the southern zone. He suggested that water is upwelled onto the continental shelf at Olifants River in the southern Benguela. This water is advected southward along the shelf. This means that during upwelling periods, fresh SACW is fed into the St. Helena Bay region.

Table 5.1: Table showing the stoichiometric ratios for the SHBML. Surface stoichiometry are split from the intermediate and bottom samples. The ideal Redfield ratios are shown in the furthest right column.

	Summer	Autumn	Winter	Redfield
	N:P			
Surface	10.9	5.7	8.9	16
Subsurface	10.3	7.6	11.2	16
	DIC:N			
Surface	10.6	12.9	7.5	6.6
Subsurface	6.7	7.3	5.8	6.6
	DIC:P			
Surface	104	111.3	83.4	106
Subsurface	93.4	92.6	74.1	106

5.2 What controls stoichiometry?

As stated earlier, this question aims to investigate changes to the stoichiometry which is vital to the accuracy of biogeochemical models. A strong focus will be placed on carbon stoichiometry and processes that control the marine carbonate system. These processes will be investigated to see how they alter the chemistry and how they are affected by the seasonality of the southern Benguela.

The original study on nutrient stoichiometry in the ocean by Redfield et al. (1963), reported a C_{org}:N:P ratio of 106:16:1 in the deep oceans. Anderson and Sarmiento (1994) produced another result with similar ratios of 117:16:1. These, as Arrigo (2005) pointed out, are thus average uptake rates of phytoplankton for the entire ocean. Boehme et al. (1998) reassured that these ratios are equally valid for the coastal oceans. Pérez et al. (2000) found this to be true for uptake rates during upwelling periods in the Iberian upwelling system. But the authors reported that regeneration of organic to inorganic matter occurred at rates very different to the aforementioned stoichiometries. It must be stated that the ratios measured in this study are bulk ratios, *i.e.* extracellular nutrient and carbonate concentrations. They do not reflect the subtleties in short term changes due to phytoplankton uptake, rather they represent the long term averages.

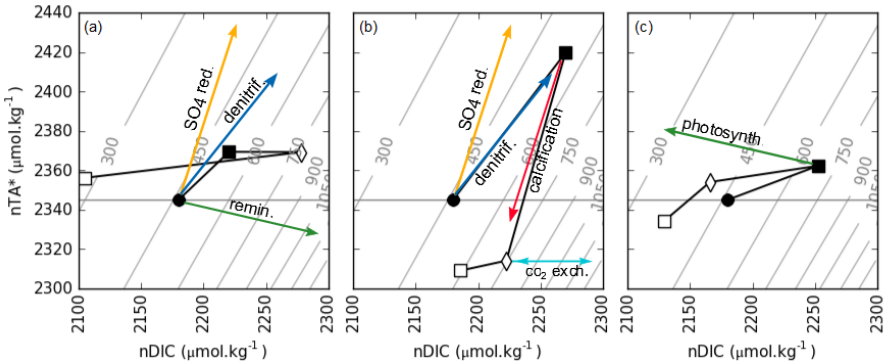

Figure 5.2: Trajectory plots of average nDIC and nTA for summer, autumn and winter (*a, b *and* c *respectively). Black circle (●) represents SACW; ■ is bottom inner-shelf water; ◊ shows near-shore surface water; and □ is inner-shelf surface water. Contours show pCO_2 at 10°C and salinity of 34.8. Plotted points represent SACW, followed by inner-shelf bottom, nearshore surface and inner-shelf surface. Coloured arrows show several of the dominant processes that are discussed throughout this chapter.*

Figures 4.9 and 4.10 show nutrients plotted against each other, but these plots include the surface and subsurface samples. It is useful to separate the surface and subsurface stoichiometric ratios to distinguish the respective processes. In the surface, CO_2 exchange, photosynthesis and calcification, and in subsurface, remineralisation and anaerobic remineralisation will be considered. To fully understand the system we will follow a water parcel as it moves its way across the continental shelf, as shown in figure 5.1. Figure 5.2 shows the average nDIC and nTA* values from figure 4.7 plotted against each other. The vectors of these points may agree with certain processes, but this does not necessarily mean that no other processes are involved in a trajectory. These processes will be explained and quantified in the sections that follow.

5.2.1 Remineralisation

Water moving onto the continental shelf in the Cape Columbine upwelling cell will be, as Monteiro (1996) called it, virgin SACW. As this water moves along the shelf it will constantly be enriched by organic matter remineralising to inorganic carbon and nutrients. This

is seen in figures 4.6 (a-c) where bottom and intermediate waters (< 34.8) had higher nitrate concentrations (> 20 µmol kg^{-1}) than that of SACW (14 - 18 µmol kg^{-1}). Remineralisation was particularly strong in the bottom and intermediate waters in the inner-shelf region.

Assuming Redfield ratios, one would expect N:P remineralisation to occur at a rate of 16:1. However, these values ranged between 7.6 and 11.2. Regarding remineralisation stoichiometry, oxygen is required by bacteria to oxidise organic matter, and thus liberate energy. Anoxic remineralisation subsequent to oxygen depletion by aerobic oxidation is the reason for the low N:P ratios. One would thus expect oxygen depletion to occur in summer, when productivity is greatest (Pitcher et al., 1992). However, the circulation of St. Helena Bay is such that during periods of upwelling (summer) circulation along the coast is northwards. Conversely during periods of relaxation (autumn) organic matter is advected southwards into the retention zone (Monteiro et al., 2005; Pitcher and Nelson, 2006). This collection of organic matter leads to intense remineralisation, which leads to depletion of oxygen (section 5.2.2). High nitrate, phosphate silicate concentrations and low DO shows that remineralisation was particularly intense in bottom and intermediate waters along the inner-shelf region, which corresponds to the retention area.

To get an idea of what the natural state of the system was, one can refer to a period when oxygen was not depleted. Bottom waters in the summer period were the most oxygen replete (figure 4.10). This would mean that nutrient ratios during this period could be representative of the aerobic remineralisation rates and thus the uptake rates of the SHBML. This is also supported by the C:N ratio in summer which was closest to the Redfield ratio. Deviations from these ratios cannot be described by simple remineralisation and requires that remineralisation during oxygen depletion is considered.

Table 5.2: Stoichiometric ratios for processes discussed in chapter5.2.

Mechanism	ΔDIC	ΔTA	ΔNO_3	ΔPO_4	ΔDO
Photosynth. $\Longleftrightarrow$ Remin.	-106	16	-16	-1	> 138
Denitrification	5	4	-4	-	-
Sulfate Reduction	1	2	-	-	-
Calcif. $\Longleftrightarrow$Dissol.	-1	-2	-	-	-
CO_2 Exchange	1	-	-	-	-

5.2.2 Anaerobic remineralisation

The St. Helena Bay region develops a seasonal oxygen minimum zone (OMZ) from summer through to autumn. This is due to the combination of the stratification of the water column, retention of organic matter and areobic remineralisation thereof (Seitzinger et al., 2006; Monteiro et al., 2006; Pitcher and Nelson, 2006). The seasonality of the OMZ is controlled by this build-up and oxidation of organic material and the "re-oxygenation" of these bottom waters in the winter. This will be discussed in more detail in section 5.3.2.

Denitrification

Denitrification is a remineralisation process that uses nitrate as an oxygen source for oxidation of organic matter, rather than oxygen. Seitzinger and Giblin (1996) reported that denitrification occurs in suboxic waters, that is, where oxygen is $< \sim 8$ µmol kg^{-1}. The result of this process is a permanent loss of nitrate from the system as it is reduced, stepwise, to N_2. This means that NO_2^- often accumulates in the surrounding water when denitrification is present (Capone et al., 2010). The net effect of this process is that for every four nitrate units reduced, five DIC units are produced. This should thus create a change in the overall stoichiometry of a system. A summary of all the changes to the marine carbonate system is shown in table 5.2.

Oxygen data shows that very few samples met the denitrification criteria (figure A.1). This may seem to contradict other aspects of the data, which suggest that there was nitrogen loss. Tyrrell and Lucas (2002) reported on denitrification in the central Benguela and found it to be a common process in the sediments. Diffusion of this

pore water into the water column would result in result in relatively high carbon, low nitrate water to be released into bottom water. This process could be accelerated by mixing or stirring of these sediments.

Figures 4.9 (d-f) and 4.10 show the relationship with nDIC vs. nitrate and nDIC vs. apparent oxygen utilisation respectively. Both figures show strong evidence for denitrification in autumn. A higher than expected C:N ratio indicates that nitrate was lost to denitrification. Similarly, a higher than expected C:O ratio indicates that more nDIC was produced by remineralisation than expected. The stoichiometry in summer was close to the ideal Redfield ratio, suggesting that only nitrification took place. Though, there appears to be evidence for denitrification in the nearshore samples. This is not surprising as the nearshore region falls within the active Ekman divergence zone. In summer, high productivity in this nearshore region would also lead to senescence of phytoplankton. The C:N ratio in winter was lower than that predicted by the Redfield ratio. The data indicates that winter shelf-slope and outer-slope bottom samples had higher nitrate concentrations than in summer and autumn. It may be that the water on the outer-shelf during this period was a different water mass, however, salinity did not substantiate this.

It is possible to calculate the contribution of denitrification using the N:P ratio, as the process only results in concentration changes in nitrate and carbonate, but not phosphate (table 5.2). However, in anoxic conditions, bacteria may facilitate the burial of phosphate as apatite, an inorganic mineral (Goldhammer et al., 2010). This may result in a net loss of usable phosphate from the system. Another indicator of denitrification, is an increase in alkalinity in the OMZ. More on the relationship between denitrification and alkalinity will be discussed in section 5.3.2.

Sulphate reduction

Methane oxidation by sulphate reduction is another form of anaerobic remineralisation that occurs in the Benguela system. But denitrification is energetically favorable, allowing denitrifying bacte-

ria to out-compete the sulphate reducing bacteria in anoxic conditions(Tyrrell and Lucas, 2002). This would suggest that typical remineralisation follows the order: aerobic remineralisation, denitrification and sulphate reduction. However, the relative abundances of the oxidative components of these processes changes this idealistic succession: oxygen $<$ 200 µmol kg^{-1}, nitrate $<$ 25 µmol kg^{-1}, and sulphate ≈28 000 µmol kg^{-1} (Tyrrell and Lucas, 2002). It is hardly surprising that sulphate reduction is the more common of the two anaerobic remineralisation processes. The overall effect of this process is a conversion of methane to bicarbonate (also leading to an increase in alkalinity). This may increase the C:N and C:O ratios more than predicted by denitrification.

Given the parameters collected, it was not possible to account for the sulphate reduction which may have occurred.

5.2.3 Photosynthesis

Water that has passed through the OMZ carries the biogeochemical signature of this zone: high DIC, nitrate and phosphate along with low oxygen. As this water is upwelled into the euphotic zone, phytoplankton make use of the high nutrient concentrations. In such high nutrient concentrations, fast growing species use nitrate as well as reduced (i.e. NH_4) nitrogen to satisfy their high N requirements. Phytoplankton production based primarily on nitrate uptake is termed *new production*. As water ages and moves offshore, nutrients are depleted by phytoplankton. In such an environment, production is driven largely by regenerated nutrients, hailing the name *regenerated production*. These two types of production will be considered individually as their influence on Redfield ratios may differ greatly.

New production

During upwelling phases, this upwelling region would be a well mixed-zone of high nutrients. This, according to Margalef (1978), is an environment that is suited to diatoms. This is supported by field studies in the southern Benguela that have assessed commu-

nity structure (Probyn, 1985; Armstrong et al., 1987; Pitcher et al., 1992). Evidence for the presence of this taxon can be seen by the rapid decrease in silicate concentrations in the nearshore and inner-shelf regions. A large decrease in DIC was also seen between the nearshore and inner-shelf surface regions, especially in summer. Arrigo et al. (1999) found that the N:P uptake ratio of diatoms in the Southern Ocean was far lower than that of *Phaeocystis antarctica* (9.7 vs. 19.2 respectively). This may suggest that diatoms have a relative preference for phosphate over nitrate. In other words, diatoms may contribute to the low N:P ratios seen in nearshore and inner-shelf surface waters. Another reason for these low N:P ratios, may be the atypically small contribution of new production to the total production in the southern Benguela Probyn (1992). The most likely reason for these N:P ratios is the expression of the subsurface N:P ratios in the nearshore region, which skews the expected uptake ratios.

Regenerated production

Upwelled water moving offshore has now been depleted of nutrients, beyond the uptake capacity of the r-selected species. Depletion of nutrients drives a community shift from a diatom dominated system to a slower growing phytoflagellate dominated system. This slow growing taxa are able to satisfy their N requirements on regenerated, reduced nitrogen (i.e. NH_4, urea) that has been excreted by zooplankton.

This was observed by Pitcher et al. (1992) who found that small flagellates were dominant in nutrient limiting, stratified waters. Figures 4.9 (a-c) show that in summer and autumn, nitrate was the limiting nutrient. Along with this, the N:P ratios in the surface offshore and outer-shelf regions were very low (6.1, 5.9 and 7.7 for summer, autumn and winter respectively). These two factors indicate the strong reliance of phytoplankton on regenerated nutrients, particularly in autumn. This is also supported by the high C:N ratios of 7.8, 8.0 and 8.5 successively.

The lower and higher N:P and C:N ratios in summer and winter respectively, are explained by seasonal changes in the f-ratio reported by Probyn (1992). His study found that f-ratios were 0.2 and 0.3 for summer and winter respectively. This is internally consistent given that nitrate was limiting in summer and autumn, but not winter. Low, but not limiting nutrients in winter suggest that phytoplankton may have been limited by physics rather than nutrients. This is supported by the deepening and weakening thermocline during winter (figure 4.5). Increased turbidity due to mixing and a deeper mixed layer depths mean that phytoplankton spent less time in a photosynthetically optimal light zone.

5.2.4 Air-sea CO_2 Flux

Air-sea CO_2 flux is the only physical mechanism that drives changes to the stoichiometry. Compared to other gas fluxes air-sea CO_2 exchange is unique due to buffering of marine carbonate chemistry, which reduces the flux rate considerably. This means that flux contributions are often small compared to the biological contribution. The strong biological CO_2 drawdown in the southern Benguela's nearshore zone is effectively fueled by upwelled CO_2 rather than atmospheric CO_2. Vital to the drawdown of upwelled CO_2 is the concomittant upwelling of nutrients, which further suggests that decoupling of C:N needs to occur for C-fixation to occur. This decoupling is observed in the offshore region where primary production is dominated by regenerated production.

Previous studies have estimated air-sea CO_2 flux in the southern Benguela to 1.62 mol m^{-2} yr^{-1} (Santana-Casiano et al., 2009), which translates to 4.4 mmol m^{-2} day^{-1}. Below is the method used to calculate air-sea CO_2 flux in figure 5.3:

- Calculate flux rate (FCO_2) from state parameters (DIC and TA) using wind speed measured on sampling date.
- Volume was calculated from surface area. It was assumed that pCO_2 is homogenous in the MLD.

- Find the total flux of upwelled water parcel by using the water age ($\boldsymbol{\alpha}$) derived from temperature (Guastella, 1992).
- $CO_2\ flux = \frac{FCO_2}{MLD} \cdot \alpha$

Note that this method has many limitations, such as its dependance on warming rates of surface water, which are only given for summer.

5.2.5 Calcification

The last process to consider is calcification and subsequent dissolution of calcium carbonate ($CaCO_3$) in the bottom waters. Past studies have found that calcification by coccolithophores typically occurs during late autumn in the southern Benguela (Mitchell-Innes and Winter, 1987; Weeks et al., 2011). Giraudeau and Bailey (1995) reported these phytoplankton had been neglected in prior studies due to their small size and occasional appearance, despite their dominant contribution of biogenic sediments in the southern Benguela.

Calcification along the SHBML was observed only in autumn, apparent by the decrease in TA (figure 4.8). The decrease in TA due to calcification is concomitant with a decrease in DIC. But this was not observed. It is clear that the bulk nutrient ratios of the subsurface processes expressed themselves in the surface waters as bottom waters were upwelled into the euphotic zone.

Dissolution of $CaCO_3$ occurs when the saturation state of the particular mineral phase (calcite or aragonite) is below 1, though calcite is thought to only dissolve at a saturation state (Ω_{Ca}) of 0.8 Milliman et al. (1999). The lowest Ω_{Ca} measured along the SHBML in 2010 was 1.3. This is far greater than the saturation state, implying that $CaCO_3$ dissolution did not occur. However, low pH in the sediments may have resulted in calcite dissolution. This raises one of the issues with biogeochemical measurements: the period of sampling represents one instantaneous moment from which one tries to infer long term changes. In such cases it is more convenient to use bulk flux methods as these capture the long term trends of a system.

Table 5.3: The conceptual methodology to arrive at the contributions of each process discussed in section 5.2. Note that the contribution by some processes cannot be found due to insufficient data. These were grouped together as "other" in figure 5.3.

Subsurface Processes		$\Delta DIC = Rm + Dn + Cd + Sr$
Aerobic Oxidation	Rm	$\Delta PO_4^- \times C:P$
Denitrification	Dn	$Rm - (\Delta NO_3^- \times N:C)$
Calcite dissolution	Cd	if $\Omega_{Ca} > 1 \ \therefore NA$
Sulphate Reduction	Sr	$\Delta DIC - (Rm + Dn + Cd)$

Surface Processes		$\Delta DIC = Ps + Cl + Fl$
Photosynthesis	Ps	$\Delta PO_4^- \times C:P$
Calcification	Cl	$-\Delta nTA * \div 2$
Carbon Flux	Fl	$FCO_2 \div MLD \times \alpha$ (see section 5.2.4)

However, the Ω_{Ca} may well have reached dissolution point in the sediment layer as was found by Suykens et al. (2011). Evidence for this is poor, due to the large biogenic $CaCO_3$ component in southern Benguela sediments.

5.2.6 Contributions to the Marine Carbonate System

Using the nutrient ratios obtained from this study, the contribution of these processes to the marine carbonate system were calculated. The aim was to explain the variations of the two state parameters, nTA* and nDIC. In order to make the "contribution calculations" several assumptions were made:

- Cross-shelf circulation followed the proposed nutrient trapping mechanism (figure 5.1). This includes the assumption that virgin SACW is upwelled.
- Averages in the various zones (figure 3.5 and 4.7), were representative of the season.
- Nutrient concentrations are correct. Due to the large factor by which phosphate is multiplied any inaccuracies will be multiplied by ~70.

- Summer stoichiometry was most representative of an oxygen replete system. C:N (6.73:1), N:P (10.88) and therefore C:P (73.27).
- Change in nitrate concentrations can be used to determine aerobic remineralisation and photosynthetic contributions. Recycled production was not included in this estimate.
- Phosphate concentrations do not change in anaerobic remineralisation processes (denitrification and sulfate reduction) - after Tyrrell and Lucas (2002). The denitrification contribution can thus be found in the difference between the stoichiometrically calculated DIC concentrations from nitrate and phosphate.
- Only calcification lowers alkalinity in the surface water. Dilution by precipitation or changes due to river influx were ignored.
- CO_2 air-sea flux is uniform throughout the MLD

Figure 5.3 shows the results from the stoichiometric contribution calculation (see table A.1 for values). One must keep in mind that these results show the calculated differences in DIC between zones, rather than processes that occurred in that particular zone.

Remineralisation was present in the inner-shelf bottom zone throughout all seasons. Denitrification was dominant in autumn, but this may be an overestimation of denitrification. This overestimation can be seen by the large negative "other" contribution in figure 5.3. The cause of this may be that phosphate may have changed due to apatite formation. Goldhammer et al. (2010) reported that apatite formation in the Benguela was greatest under anoxic conditions, thus resulting in a phosphate loss. The magnitude calculated calcification in autumn in the nearshore region is possibly an overestimate or an underestimate of productivity and is explained by:

- the difference in nTA* between this zone and the the inner-shelf bottom waters and;
- the assumption that this bottom water upwells in the nearshore surface region.

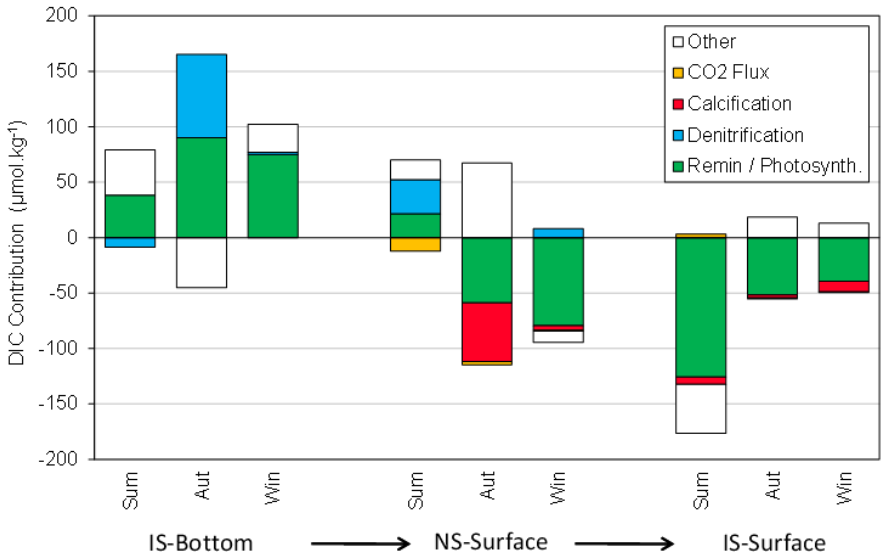

Figure 5.3: Plot of the contributions by various processes to the marine carbonate system. Note that positive black bars represent aerobic oxidation (or remineralisation) and negative black bars are the photosynthetic contribution to carbon. 'Other' represents the difference between the actual and the calculated nDIC. Age of the water using warming rates (Guastella, 1992) for the nearshore is 1.9 and 4.3 days for summer, autumn. For the inner-shelf the water age is 5.5 and 5.4 days old respectively. For more information see table A.1.

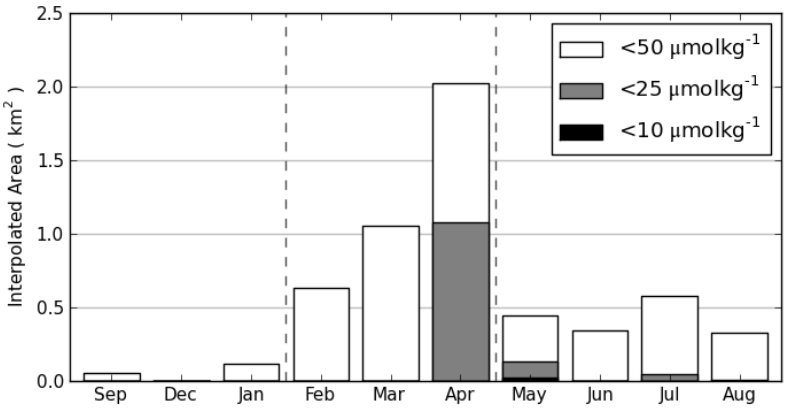

Figure 5.4: Bar graph showing the interpolated area for dissolved oxygen throughout 2010. Note that months on the x-axis are not plotted chronologically, but rather by season.

- regenerated productivity not taken into account.

The photosynthetic contribution was largest in the inner-shelf surface region. This is due to the high nDIC from the previous location (IS-Surface). Calcification was present in this region, but resulted in minimal CO_2 draw-down.

In their paper Tyrrell and Lucas (2002) stated that upwelled water in the Benguela system may be "supercharged" with DIC, relative to other nutrients. They make this statement on the basis that denitrification and sulphate reduction lead to higher than expected DIC (200 µmol kg^{-1}). This may be an overestimation for the southern Benguela, where the phosphate increase is not as high (1.2 mol kg^{-1}) as suggested by Tyrrell and Lucas. This implies that, whilst it is still important, anaerobic remineralisation is not as prevalent in the southern Benguela as in the central and northern sectors. This may be due to the persistent OMZ found in the these latter sectors, whereas the OMZ in the southern Benguela is a seasonal feature (figure 5.4). The influx of oxygenated water in winter and summer clears the "legacy of denitrification" that would otherwise persist. It is due to this seasonality that large fluctuations in nutrient ratios were observed (table 5.1).

5.2.7 Oxygen Ventilation in the OMZ

The loss and replenishment of the oxygen in the bottom shelf waters has been identified as a key driver of biogeochemistry in the southern Benguela. Figure 5.4 shows that oxygen ventilation in the OMZ (i.e. bottom inner-shelf) was not gradual throughout winter, but rather an event driven mechanism (Monteiro et al., 2011). This coincides with winds with a strong northerly component (mid-latitude cyclones) preceding sampling, as in the months of May and September (figure 4.2). These events only occured in winter, despite similar wind speeds in summer. This is due to the reduction in solar radiation in winter, which reduced stratification and allowed deep mixing to occur.

DO concentrations in the bottom samples of stations four and five, show that ventilation of oxygen was not by the same mechanism. The DO concentrations for station five fluctuated far more than those of station four (figure 5.5 b). This was inversely matched by salinity (figure 5.5 c). This proves that oxygen ventilation occurred when deeper, less saline water replaced the more saline, low oxygen water. So what drives oxygen replenishment in these two adjacent stations?

Bathymetry may hold the answer. Figure 5.5 (a) shows that station four is situated on a slight plateau in the lee of Cape Columbine. Whereas station five is located adjacent to the Cape Canyon. This explains the consistent replacement of water by more saline water, which may flow up the Cape Canyon and into the region surrounding station five. This is most likely driven by upwelling events as shown by the upwelling index in figure 4.2. An alternative could be the baratropic Cape Jet, which could replace the low oxygen water with more ventilated shelf water.

The plateau on which station four situated acts as a barrier from the Cape Jet or water upwelled via the Cape Canyon. This bottom water was replaced during the two storm events originally proposed as mixing events. However the fresher salinity that accompanied the oxygen replenishment events suggests that these events were not

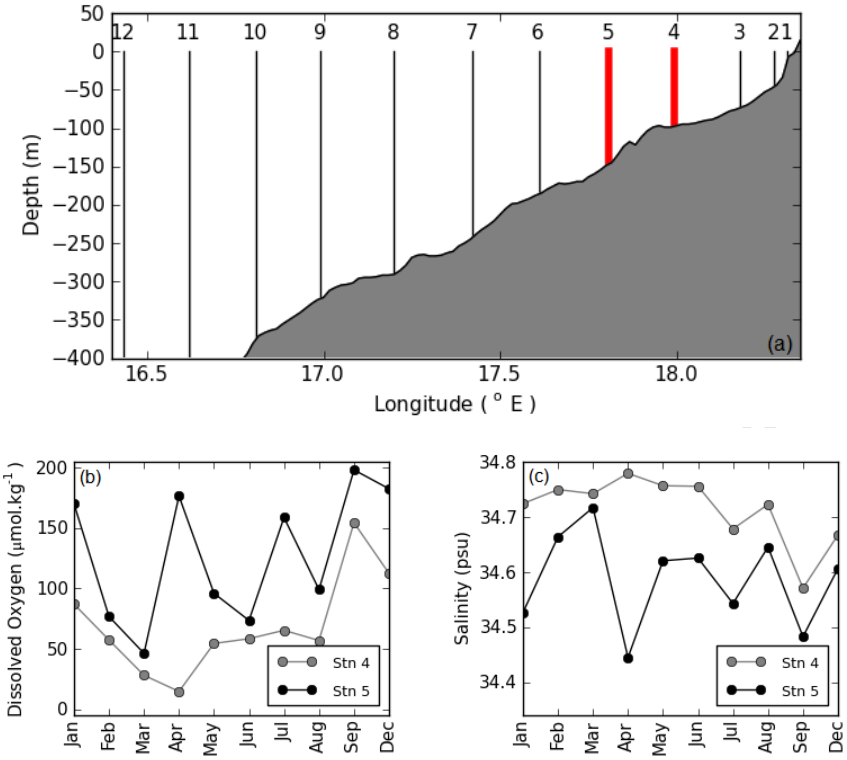

Figure 5.5: A map showing the positions of stations 4 and 5 relative to stoichiometry (a). *Two line plots showing the dissolved oxygen* (b) *and salinity* (c) *of bottom samples of stations four and five. Correlation between the two parameters for stations four and five was -0.86 and -0.93 respectively.*

only driven by vertical mixing, but also by advection of a fresher, more oxygenated watermass.

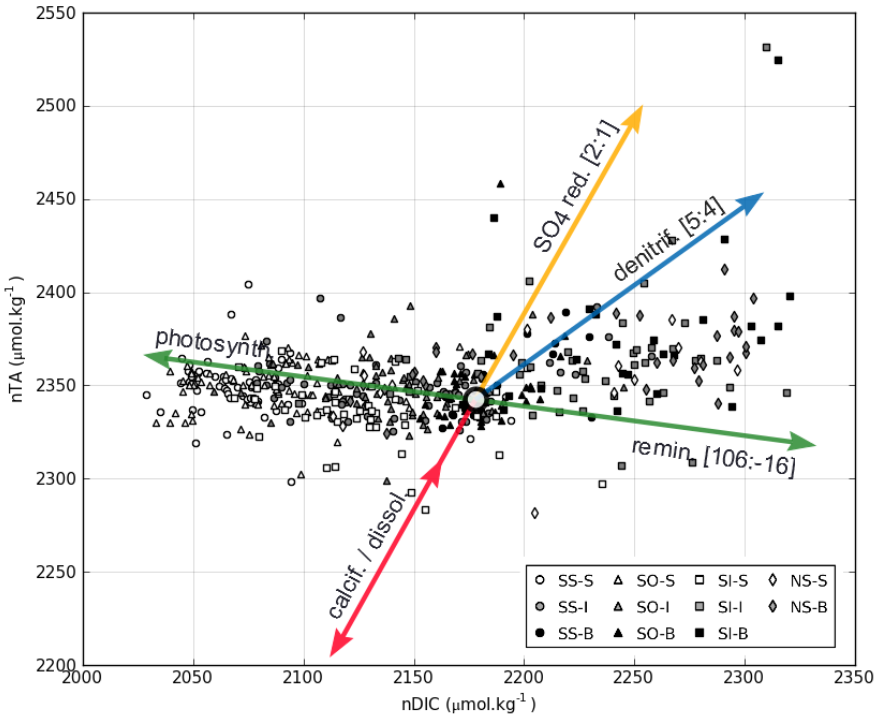

Figure 5.6: A scatter plot showing nTA and nDIC plotted against each other. Note that nTA is not corrected for nitrate. The vectors indicate the various processes that alter nTA.

5.3 Coastal Alkalinity Production

In recent years the production of alkalinity has gained attention due to its role as the ocean's acidification "buffer" (Hu and Cai, 2011). In this chapter, the production of alkalinity on the southern Benguela shelf will be quantified and placed into a global perspective. The role of alkalinity as a pH buffer will also be assessed. There are several processes which result in alkalinity changes, i.e. photosynthesis by new production, calcification, denitrification and sulphate reduction. But, according to Hu and Cai (2011), only the latter two are responsible for a permanent gain in alkalinity. Each of these will be discussed.

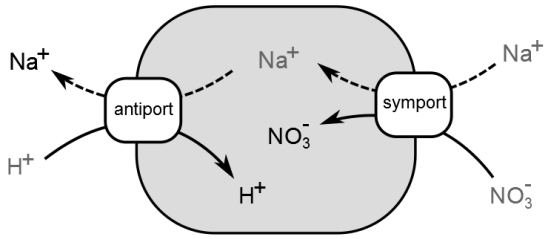

Figure 5.7: Diagram showing the uptake of nitrate (NO_3^-) as explained by Wolf-Gladrow et al. (2007). In order to maintain ionic charge, a cell has to co-transport a NO_3^- ion with a sodium ion (Na^+) via a sodium-dependant symport. To avoid a buildup of Na^+, it is exchanged with a H^+ ion via an antiport. A decrease in H^+ leads to an increase in alkalinity.

5.3.1 Biogeochemistry of shelf alkalinity

New production, remineralisation and nitrification

The uptake of nitrate by phytoplankton results in an increase in surface alkalinity (figure 5.7). Correcting alkalinity for nitrate uptake (nTA*) removes this effect. Figure 5.6 shows nDIC plotted against nTA, which has not been corrected for nitrate uptake. This effect of nitrate is seen in the surface waters, indicating that photosynthesis by new production resulted in increased TA. However the subsurface samples did not follow this trend. This does not mean that remineralisation by nitrification did not take place, but it does mean that other processes were important in driving changes in the nTA.

Denitrification

Hu and Cai (2011) accredited denitrification for being one of the two mechanisms for TA production on continental shelves. Note that anammox and denitrification cannot be distinguished as the result in the same changes in stoichiometry as denitrification (Hu and Cai, 2011). Denitrification has already been discussed in section 5.2.2 with regard to changes to DIC and it was found to be a significant contributer. The contribution to nTA by denitrification (relative to SACW) can be calculated by applying stoichiometry to the DIC calculations: summer = 21 µmol kg^{-1}, autumn = 59 µmol kg^{-1} and 20 µmol kg^{-1}. Though it must be stated that there was

suspicion that the denitrification contribution was an overestimate due to phosphate loss by apatite formation during anoxic conditions (Goldhammer et al., 2010). Also take note that these are average values for the inner-shelf bottom region.

Sulphate Reduction

Sulphate reduction is the other mechanism whereby shelf TA is produced. Tyrrell and Lucas (2002) found that this process may be more important than denitrification in the central Benguela due to the abundance of sulphate in the sediment. This process could not be quantified in this study due to the lack of sulphate data.

Calcification and dissolution

The presence of coccolithophores was strongest in the nearshore waters in late autumn, as was found by Weeks et al. (2011). Calcification in this nearshore region accounted for a nTA reduction of 105.5 μmol kg^{-1}. Previous studies have found that the abundance of coccolithophores in the southern Benguela increases from March to June (Mitchell-Innes and Winter, 1987; Giraudeau and Bailey, 1995; Weeks et al., 2011). One theory that explains the presence of coccolithophores in the late upwelling season is: energy balance of producing coccoliths in lower pH waters. In low pH water, coccoliths have to be productive enough to overcome the energetic cost of maintaining an internal pH as high as 8.3 (Barcelos e Ramos et al., 2010). This means that during periods where pCO_2 decreases and calcite saturation state increases, it becomes energetically viable for coccolithophores to achieve the cell counts seen in autumn in the southern Benguela.

The high pCO_2 values observed in autumn contradict the afore mentioned theory, but can be explained by the fact that these samples were taken at the end of the bloom event. The formation of $CaCO_3$ led to a decrease in TA and resulted in high pCO_2. This in effect is a self mitigating effect for the transport of TA from the surface ocean into the sediment (Zondervan et al., 2001).

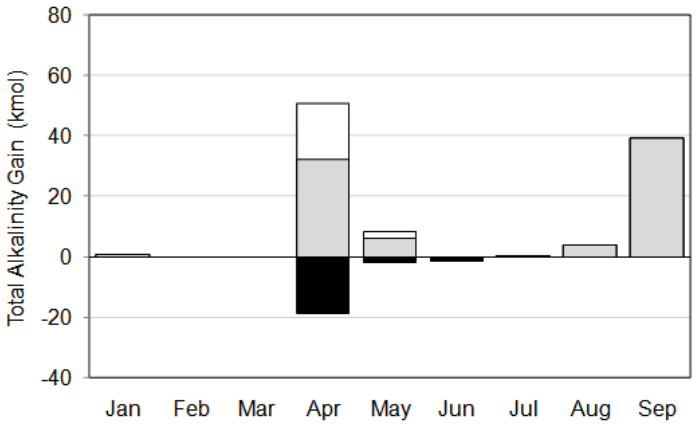

Figure 5.8: Bar chart showing the loss or gain of TA during 2010 where positive (gray) is net gain, negative (black) is loss. Where there is a simultaneous loss and gain of TA, a white bar represents the total gain for that month. February, March and December were omitted due to bad data. See table A.2 for more info.

5.3.2 Alkalinity Production

Figure 4.11 shows nTA* plotted against dissolved oxygen. The majority of samples which showed alkalinity gains had low oxygen concentrations, though not exclusively. In order to calculate the changes to alkalinity in the southern Benguela, thresholds for losses and gains were set to the average (2348 µmol kg^{-1}) minus or plus one standard deviation (2322 and 2374 µmol kg^{-1} respectively).

Alkalinity production was calculated by interpolating the data linearly in both the horizontal (longitude) and vertical (depth). The result (figure 5.8) is surprising. It would be expected that April, the period with the strongest OMZ to be the greatest alkalinity producer due to denitrification. The net production however was lower than that measured in September. The source of this high TA watermass may have one of two origins:

- A spate of north westerly winds prior to September sampling may have resulted in a strong southerly flow of shelf water. Monteiro (1996) found that upwelled TA in the Olifants River region, north of the SHBML, had a mean TA of 2378 µmol kg^{-1}. Further north, in the Namaqua upwelling cell, he found

that upwelled TA had concentration of 2409 µmol kg^{-1}. This is in the range of what was observed in September. However, according to Monteiro's gate hypothesis, water from the central Benguela sector is advected offshore at the Olifants river, with virgin SACW upwelling onto the shelf. Monteiro does mention that during certain circumstances that shelf water from the central segment may be advected into the southern Benguela. Cessation of upwelling favourable winds during winter may result in "opening" of the Olifants River gate between the central and southern sectors.

- Tyrrell and Lucas (2002) stated that denitrification and sulphate reduction in suboxic sediments play an important part in the central Benguela system. This could mean that the source of high TA was pore water due to mixing and stirring of the sediments, after an intense north westerly storm. A lens of warmer surface water caused the watermass to form a subsurface tongue.

Though both scenarios are plausible, the latter is more likely. The unstratified waters after winter allow mixing and turbulence to penetrate down to the bottom layer. This would also explain why the strong downwelling event in May (figure 4.2) did not result in the same suspension of pore water.

No previous estimates of TA production in the southern Benguela have been calculated. A rough estimate for the central Benguela system could be calculated using Tyrrell and Lucas' (2002) nitrate loss estimate. They found that up to 40 µmol kg^{-1} of nitrate was lost due to denitrification. This would equate to an equivalent gain in TA, but the lack of geographical context given with their estimate makes it difficult to compare to this study.

5.3.3 Global Relevance

Given the calculated alkalinity production along the SHBML for 2010 was only ~80.67 kmol yr^{-1} (equivalent to 1.2 mmol m^{-2} d^{-1}).

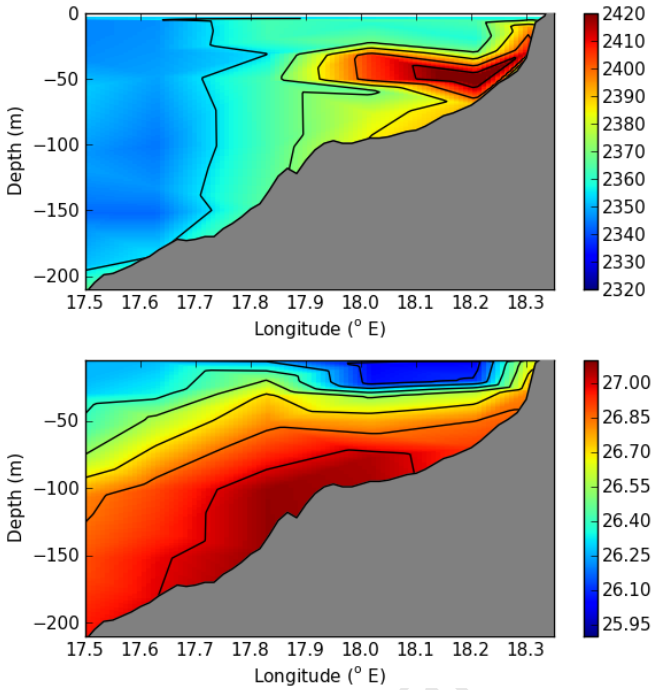

Figure 5.9: Sections of interpolated TA ($\mu mol.kg^{-1}$) on top and potential density (σ = $kg.L^{-1}$ - 1000) on the bottom. Notice how the strong density gradient coincides with the top of the TA tongue.

Dollar et al. (1991) found that TA production in Tomales Bay in California , a shallow system, was 7 mmol m^{-2} d^{-1}. This comparison shows that the southern Benguela is by no means an effective TA producer. So how does the southern Benguela TA production compare to global production?

If constant alkalinity production along the entire southern Benguela shelf (∼585 km) is assumed then TA production of the southern Benguela would be ∼473 Gmol yr^{-1}. At best this means that the southern Benguela produces 1.2% of global shelf produced alkalinity, using an estimate of 4 Tmol yr^{-1} (Hu and Cai, 2011). This is most likely an overestimation, despite extensive anoxic sediments along the southern Benguela coast. St. Helena Bay is a unique area in the southern Benguela due to its retentive nature (Pitcher and Nelson, 2006), resulting in greater oxygen loss and thus more production of alkalinity.

An alternative extrapolation would be to use the upwelling cells as SHBML equivalents. This would include the rest of the Cape Columbine cell and the Cape Point upwelling cell. If one assumes that each cell has a width of half a degree (∼55 km) then each upwelling cell would have a TA production of ∼4.5 Gmol yr^{-1}. The total production of TA for the southern Benguela using this method would then be 9.0 Gmol yr^{-1} equating to 0.1% of global shelf produced alkalinity. This would suggest that the southern Benguela, is an insignificant global producer of TA.

5.3.4 Contribution to pH

In section 2.5, the ocean's CO_2 buffering capacity, the Revelle factor, was discussed. In this section, alkalinity's contribution to the buffering capacity of seawater will be investigated.

pH in the southern Benguela showed strong variation between seasons (figures 4.12, a-c) in the surface waters. These differences arise from the age of the upwelled water, where biological uptake of CO_2 is key. The persistent and strong upwelling in summer, resulted in the low pH (7.7 - 7.9) ranges in the nearshore surface samples. The older inner-shelf samples had higher pH values (8.1 - 8.2) due to biological uptake. Compared to winter, when upwelling was minimal, the same nearshore samples had higher pH (8.0 - 8.1). The pH in autumn in the nearshore and inner-shelf surface samples was low (7.7 - 8.0), owing to calcification by coccolithophores.

The plot nDIC and pH (figure 4.12 d) has a fair amount of scatter. The majority of this scatter can be removed by normalising pH to nTA* (figure 4.12 e). Normalising pH also yields two slightly different trends. These trends are due to differences in the Revelle factor in the surface and bottom waters (figure 5.10 a).

Subtracting pH from the normalised pH (ΔpH_{2345}), shows the contribution of nTA* to pH (figure 5.10 b). The greatest contribution that alkalinity made to pH was just under 0.4 units. Conversely the greatest loss due to calcification was -0.25. Figure 5.10 (b) also shows that where ΔpH_{2345} was largest, the Ω_{Ca} was low. Meaning,

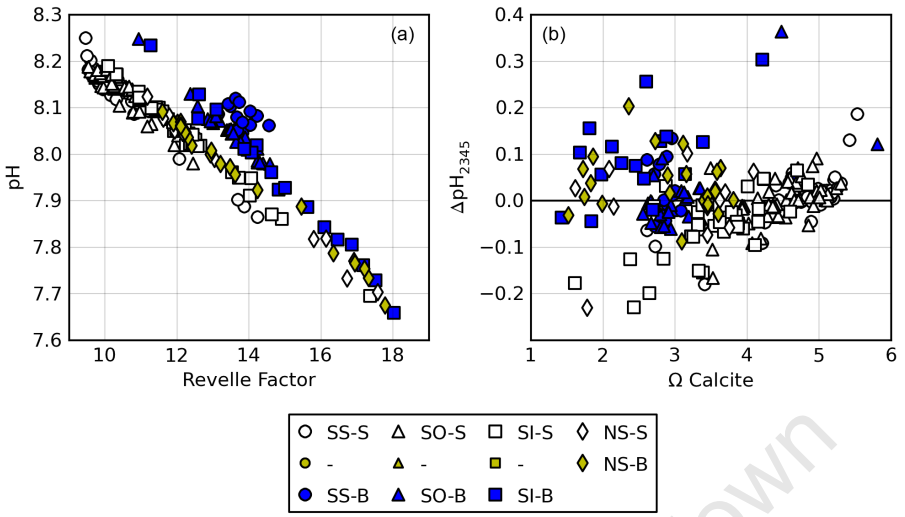

Figure 5.10: Scatter plot showing the Revelle factor vs. pH (a). *There is a clear distinction between the surface and bottom waters due to differences in the Revelle factor.*
Plot of Ω_{Ca} against ΔpH_{2345} (b). *The latter is the difference between pH and pH normalised to a TA of 2345 µmol kg^{-1},* i.e. *the contribution of nTA* to pH.*

that if there had been no TA contribution, these values would been considerably lower. This could have thus led to the dissolution of calcite, which would in turn lead to increased TA and thus increased Ω_{Ca}. This mechanism is thus a negative feedback to increasing pH.

A study of acidification along the Californian coast by Feely et al. (2008a) showed that aragonite saturation had shoaled in several regions along the coast. The authors attributed anthropogenic CO_2 to contributing to this shoaling. The low TA along the North America west coast would also play a large role. The width of the shelf in their study region is far narrower than the shelf in the St. Helena Bay region. This wider shelf allows for the development of an OMZ, which leads to TA production by anaerobic remineralisation. Lower productivity and a narrower shelf in the California region do not favour the development of an OMZ and thus TA cannot be produced. This again highlights the biogeochemical importance of St. Helena Bay's retentive circulation.

5.3.5 High CO_2 World

A simple backward calculation, shows that a parcel of upwelled water in the southern Benguela, with a pH of ∼7.80 has a pCO_2 of ∼750 µatm. This could make the southern Benguela a useful analogue for a "high CO_2 world". As discussed in section 2.5, the most likely regions to be affected by increased CO_2 concentrations are the high latitude oceans (Orr et al., 2005). Similarly to the southern Benguela, these high latitude regions have high DIC, but low TA, which makes these regions susceptible to acidification due to high Revelle factors. Upwelling and frontal regions in the Southern Ocean, where iron is not limited, may be reasonable analogues for the southern Benguela. High latitude oceans in the northern hemisphere experience large scale spring diatom blooms (Siegel et al., 2002). These blooms could be considered analogous to blooms during upwelling periods in the southern Benguela in summer. However, there will always be limits to the extent that an analogue can be drawn. Most blatant difference in the analogue drawn above may be the difference between temperature increases in high latitudes. The IPCC (2007) found that temperatures in the high latitudes of the northern hemisphere are amongst the fastest increasing. Pörtner and Farrell (2008) reported that temperature plays a large role in determining ecological dominance of one species over another. Such large temperature changes in the northern high latitude oceans could thus be more important than ocean acidification for non-calcifying species.

What then could the future of these high latitude oceans be? The most likely phytoplankton assemblage in a high CO_2 world would be that found in the nearshore region, where pCO_2 is highest. The southern Benguela nearshore phytoplankton community, is dominated by diatoms and, in quiescent conditions, dinoflagellates (Smayda and Trainer, 2010). A study by Giraudeau et al. (1993) may provide a possible outcome for future planktonic caclifiers in the northern high latitude oceans. The authors found that coccolithophores in the northern Benguela had malformed coccoliths. This

is also supported by lab studies, which found that coccoliths started deforming in an environment where pCO_2 was 780 - 850 ppmv. However, Iglesias-Rodriguez et al. (2008) found that net productivity of certain coccolithophore species increased in an environment with the same pCO_2. The complexity of the situation was expounded by Burkhardt et al. (1999), who reported that the effects of increased pCO_2 on phytoplankton C:N:P ratios was variable from one species to another. It is thus difficult to speculate the fate of these high latitude oceans, given all the uncertainties from the literature.

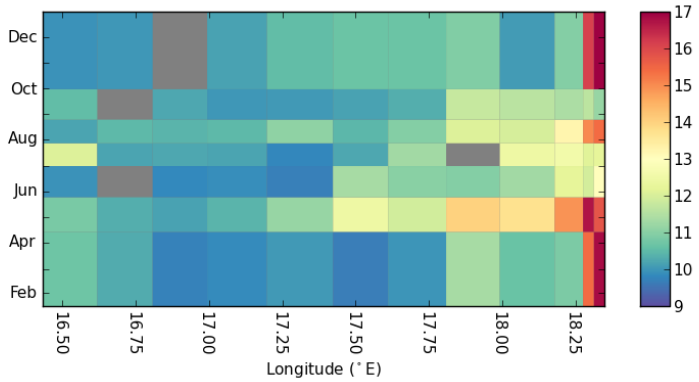

Figure 5.11: A Hovmöller plot of the Revelle factor for the southern Benguela throughout 2010.

5.4 CO_2 Flux

Sections 5.2 and 5.3 dealt with the state parameters of the marine carbonate system. In this chapter, I will discuss carbon flux, which is essentially the combined effect of the biogeochemistry and the physics.

5.4.1 Revelle Factor

Sabine et al. (2004) described the Revelle factor as an indicator of the ocean's capacity to take up anthropogenic CO_2. Where a low Revelle factor indicates a high uptake capacity, and *vice-versa*. This is also useful in assessing the vulnerability of a region. Regions with a high Revelle factor, *e.g.* high latitude oceans, are susceptible to small changes in pCO_2.

The Revelle factor of the southern Benguela in 2010 had a large range, from *circa* 9.7 in the outer-shelf and shelf-slope region, to 17.6 in the nearshore region (Figure 5.11). This indicates that the prior mentioned regions were effective sink regions, resulting in small pCO_2 changes for CO_2 taken up. Conversely the nearshore region, would have been weak sink if atmospheric pCO_2 was high enough to result in seaward flux of CO_2, as in the Antarctic. However, this was not the case, as the nearshore region was a source. This means that

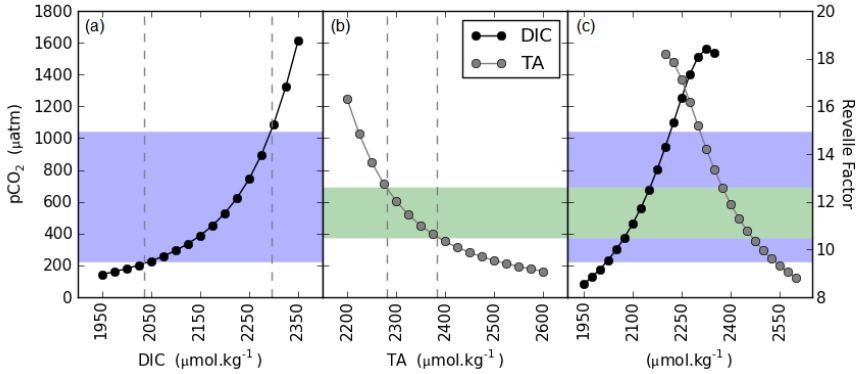

Figure 5.12: Three plots showing the influence of the state parameters on the Revelle factor (c). *pCO_2 is plotted against DIC* (a) *and TA* (b). *The vertical dashed lines represent the surface ranges of DIC and TA in the southern Benguela. The coloured areas demarcate the corresponding pCO_2 and Revelle factor ranges expected in the southern Benguela. The Revelle factor is plotted with DIC and TA on the same x-axis. In each data-set, non-changing parameters were set to SACW values.*

for every unit of DIC that was lost to the atmosphere, the pCO_2 would have decreased quickly.

TA is important in determining the Revelle factor, but analysis shows that DIC was the dominant role player. Given the TA range of surface water, the maximum potential for change to the Revelle factor is 3.5, compared to 8.1 of DIC (figure 5.12). The figure also shows how out-gassing of DIC, at a high Revelle factor, results in a rapid decrease in pCO_2. With the potential of increasing atmospheric pCO_2, one could expect the blue region in figures 5.12 (a, c) to increase. Unless this leads to changes in alkalinity gains or losses, the green bar would remain the same. But it must be remembered that these two factors can operate in unison, their effects potentially being cumulative.

5.4.2 Wind and ΔpCO_2: Components of flux

CO_2 flux is a combined result between ΔpCO_2 and wind speed. ΔpCO_2 is arguably the more important of the two as it determines the direction of flux, i.e. sink or source. Wind plays the important role of determining the rate of the flux. That is to say, the

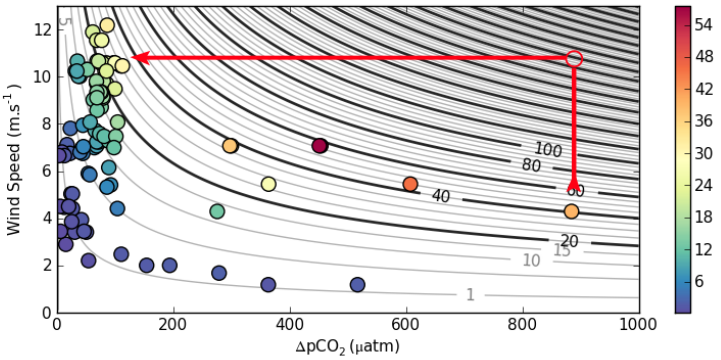

Figure 5.13: Scatter plot of wind speed (m s^{-1}) against $|\Delta pCO_{2\ (sea-air)}|$ (µatm). Contours represent the CO_2 flux (mmol $m^{-2}d^{-1}$), where black and gray lines have 20 and 5 mmol intervals respectively. However, the first gray line is plotted at 1 mmol $m^{-2}d^{-1}$. The color axis is absolute flux (mmol $m^{-2}d^{-1}$). The red arrow shows a hypothetical increase of wind speed and consequent out-gassing.

magnitude of the sink or source. The relationship between these two parameters is thus an interesting one, especially in the southern Benguela. Figures 4.13 (a, b) show surface plots for these two parameters for all surface samples.

The majority of the SHBML was a weak sink in the offshore region. This is due to filaments which advect shelf water into the open ocean and longstanding phytoplankton stock that survive in the low nutrient environment of the shelf-slope and outer shelf regions (Pitcher et al., 1992). These low nutrients limit the amount of carbon that they take up, explaining why this reason was only a weak sink. April was an exception to the trend, where the majority of the SHBML was a source. This is due to calcification in the surface waters (as explained in section 5.3.2). A loss in alkalinity, coupled with an increase in CO_2 results in an overall increase in pCO_2. The nearshore region was almost consistently a source. Discussion from previous sections suggest that this was due to upwelling of SACW, which was enriched by aerobic and anaerobic remineralisation of organic matter resulting in higher DIC. If constant wind speeds throughout the year were assumed, the flux would mirror ΔpCO_2, but changes in the wind speed produce a different result.

Table 5.4: Table summarising the results from the CO_2 flux calculations. Note that season fluxes are given in mmol m^{-2} d^{-1} and that yearly is given in mol m^{-2} yr^{-1}. Yearly estimates given in this study are those from different wind configurations. Ingassing is negative and outgassing is positive. See text for more details.

(mmol m^{-2} d^{-1})	Spr. / Sum.	Autumn	Winter	Yearly
Sample winds	-13.84	0.8	-7.2	-2.90
Daily winds	-8.31	4.13	-5.15	-1.53
Average winds	-6.41	5.62	-2.66	-0.80
Chen and Borges, 2009	-11	-	-5.5	-1.62
Monteiro (1996)	-	-	-	-1.36

Wind speeds for sampling days show that summer wind speeds were on average moderately high. This resulted in the moderate fluxes shown in figure 4.14. In April, wind speeds were very low. This combined with the high ΔpCO_2 resulted in only a weak outward flux. To investigate this relationship between ΔpCO_2, wind speed and carbon flux these parameters were plotted on one set of axes (figure 5.13). An interesting trend in the data is that samples with low negative ΔpCO_2 had relatively high wind speeds. And samples with high positive ΔpCO_2 did not have very high wind speeds. Though it must be mentioned that this is only for sampling days only.

If one considers the samples with high ΔpCO_2 and low wind speeds, the flux was considerably low. However, if wind speed increased by only a a few m s^{-1}, then flux would increase drastically. While this does not increase the amount of CO_2 that is exchanged with the atmosphere, increased wind speed and a high Revelle factor would lead to a rapid decrease in CO_2.

5.4.3 Flux quantified

Table 5.4 shows the average flux measurements from this study and those from Chen and Borges (2009), which incorporates the study by Santana-Casiano et al. (2009). This study confirms the southern Benguela as a sink for CO_2.

Three different flux estimates were calculated from the data shown in figure 4.14. For each of these it was assumed that the system returns to the starting state, January 16th 2010. The higher flux estimate was calculated simply by interpolating the instantaneous flux rates from sampling days. The second was calculated by interpolating each individual parameter for the flux calculation, and then using winds for each day of the year. This yielded a lower flux, as the high ΔpCO_2 in April was interpolated, rather than the low FCO_2. This meant that high winds combined with high ΔpCO_2 resulted in a greater source region. The third method used average parameters, averaged for each month, and resulted in the lowest estimate. This is due to strong winds in April when ΔpCO_2 was high, making this flux estimate unlikely. Conversely, the instantaneous flux method may be an overestimation due to favorable winds on sampling dates. However, all the methods may be misrepresenting flux for the large hiatus from February to March, where flux was interpolated over this entire period. Moreover, this period represents the most uncertain period in the flux changes. Thus, the intermediate flux estimate was very close to the flux estimation found by Santana-Casiano et al. (2009) and Monteiro (1996).

With three yearly estimates from different studies, based on different methodologies, in such close range, it can be stated that the carbon air-sea flux in the southern Benguela is between -1.36 and -1.62 molC m^{-2} yr^{-1}. This may seem low considering the magnitude of ingassing and outgassing fluxes observed in figure 5.14, but these opposing fluxes cancel each other out, resulting in a low net flux.

To place this study in global perspective, the SHBML needs to extrapolated over the entire southern Benguela region. But how representative is the SHBML of the southern Benguela? The study by Santana-Casiano et al. (2009) can provide insight on this question, as their study investigated CO_2 flux meridionally along the Benguela. FCO_2 in the southern Benguela during 2005 and 2006 (figure 5.15) was fairly homogeneous in the southern Benguela, similarly so for summer. These values were also in close agreement

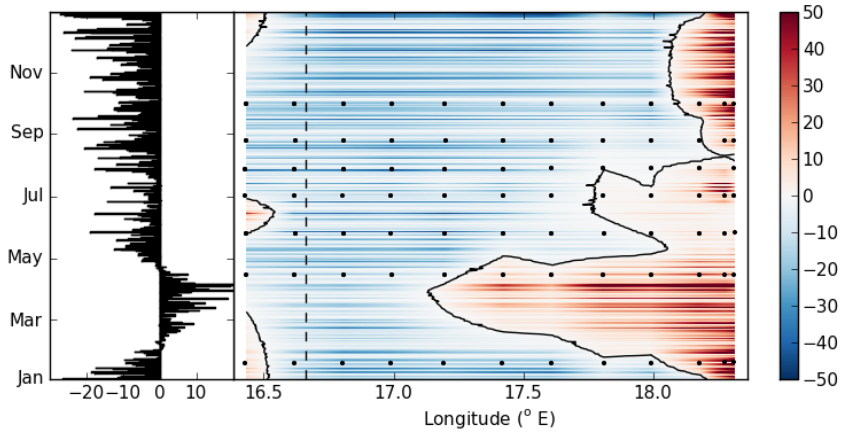

Figure 5.14: A plot showing the FCO_2 (mmol m^{-2} d^{-1}) for the SHBML. The Hovmöller diagram on the right shows daily CO_2 flux using daily winds and ΔpCO_2 calculated from interpolated parameters. The solid black line is where flux is zero and black dots are actual samples. The dotted line is the end of the shelf, and samples beyond this line were not included in flux calculations. On the left is the integrated CO_2 flux (mmol m^{-2} d^{-1}) for each day of the year.

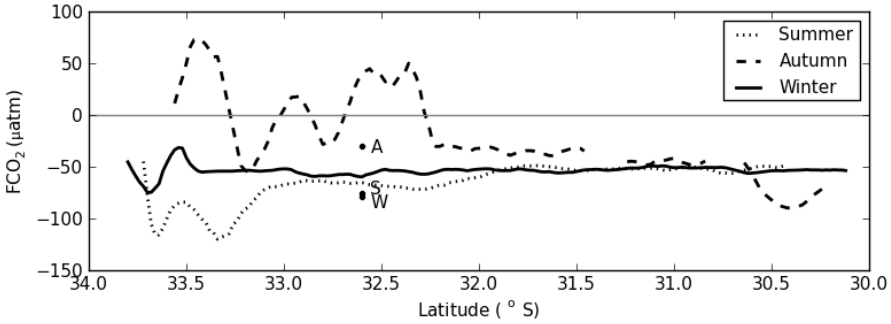

Figure 5.15: FCO_2 data from the QUIMA-VOS line for 2005 and 2006 (after Santana-Casiano et al., 2009). The markers show pCO_2 (summer, autumn and winter) for where the SHBML intersects the QUIMA line. Data accessed via the SOCAT library Pfeil et al. (2011). A constant atmospheric CO_2 concentration of 390 µatm was assumed.

with data from the SHBML at the intersection of the QUIMA and SHBML lines. Autumn FCO_2 was higher and more variable. From this figure it can be induced that the SHBML represents the southern Benguela fairly well with regard to carbon flux. There may be some inaccuracy for the lower latitudes for autumn extrapolation, but summer and winter are in good agreement. On this premise the SHBML flux rate can be extrapolated over the entire southern Benguela region.

Using the daily winds estimate and the area of the southern Benguela (104 000 km^2 after Brown et al., 1991) results in an annual flux of -1.91 TgC yr^{-1}. This equates to 0.53% of coastal fluxes based on a global shelf export of -0.36 PgC yr^{-1}(Chen and Borges, 2009) and 0.095% of the global CO_2 flux of -2.0Pg C yr^{-1} (Sweeney et al., 2009). It may be useful for South Africa, the 13^{th} largest carbon emitter, to know the magnitude of its coastal sinks. In 2008 the national CO_2 emissions were 0.12 PgC, which was 1.3% of global emissions (Boden et al., 2009). This means that only 1.0% of South African emissions are taken up by the southern Benguela. This finds the southern Benguela as a relatively unimportant regional and global sink.

6 Conclusion

This study aimed to examine the seasonality of the marine carbonate system of the southern Benguela. Three major questions were asked with regard to the bulk stoichiometric ratios, shelf production of alkalinity and air-sea CO_2 fluxes. In this section these questions will be addressed directly and in brief.

6.1 Seasonality of the stoichiometry

Does the seasonal nature of upwelling in the southern Benguela express itself on the bulk C:N stoichiometery?

The results from this study show that there is definite interseasonal variability of stoichiometry in the southern Benguela. Monteiro (1996) stated that Redfield stoichiometry should not be used for the Benguela due to the highly variable ratios. This study confirms this view and finds that a seasonality should also be taken into account when performing stoichiometric carbon flux calculations. The C:N stoichiometry was closest to the Redfield ratio in summer in the bottom water.

Is C:N stoichiometry driven predominantly by remineralisation?

There was a very clear distinction between the nutrient ratios in the surface waters and the subsurface waters. This a very strong feature in the C:N ratios, where the difference between the surface and bottom stoichiometries are greater than the interseasonal differences. These large differences were attributed to anaerobic remineralisation of organic matter by denitrification and sulphate reduction. The former being particularly effective due to an increase in DIC and a decrease in nitrate.

How do these processes contribute to changes in DIC?

These processes were quantified to gain an understanding of the drivers of the marine carbonate system. Figure 6.1 shows these seasonal contributions of all quantifiable mechanisms. Photosynthesis

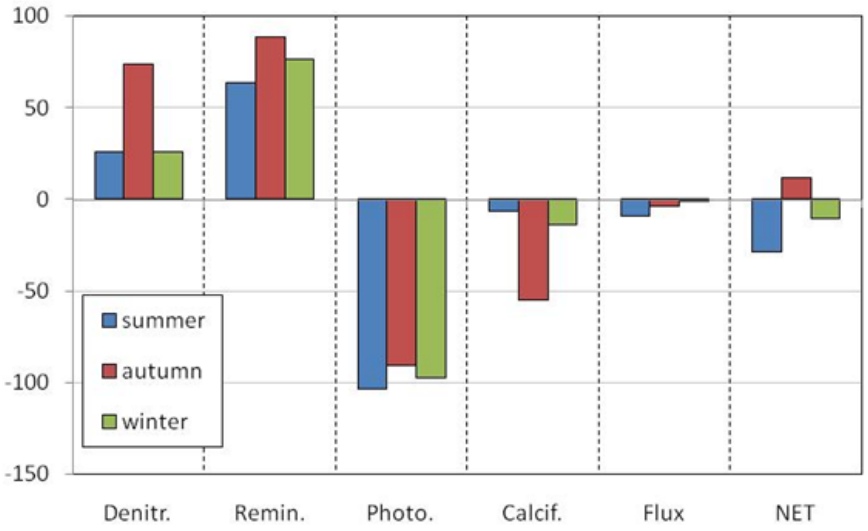

Figure 6.1: Bar graph summarising each mechanism responsible for DIC changes. The last column, 'NET', shows the sum of all the other processes. This indicates that there is a net export flux of carbon, i.e. *the sum of photosynthesis calcification and flux is greater than the remineralisation processes.*

was the largest contributor to DIC, accounting for 39% of absolute DIC flux for 2010. Note that this process typically abides to the Redfield ratio (Boehme et al., 1998). The same goes for the second most abundant process, oxic remineralisation, which accounted for 31% of absolute DIC flux. Denitrification was a large contributor (17%), especially in autumn when low oxygen water in the St. Helena Bay retention zone was at its most extensive. This is important as this mechanism results in changes in the C:N stoichiometry.

It could thus be inferred that stoichiometry of the southern Benguela is defined by the intensity and area of the OMZ. It was found that this feature was strongest in autumn due to stratification and retentive circulation in the St. Helena Bay region. Ventilation of the OMZ occurred by two processes:

- Adjacent to the Cape Canyon, deep waters replenished oxygen during upwelling favourable winds.
- In the lee of Cape Columbine, winter mixing allowed by weakened stratification occurred due to strong mid-latitude cyclones.

This process was confined to winter due to the northward migration of the SAAC, which allows these mid-latitude cyclones to propagate further north.

6.2 Alkalinity: Sink or Source

Is the southern Benguela an alkalinity sink or source?

The development of the OMZ during the summer and autumn facilitated anaerobic remineralisation by denitrification and sulphate reduction. These processes resulted in the southern Benguela being a net TA source in 2010. An upper and lower estimate of TA production were calculated by interpolation.

	TA (Gmol yr^{-1})	% Global shelf TA
Upper estimate	47.23	1.2%
Lower estimate	8.96	0.1%

The upper estimate is probably an overestimation as the St. Helena Bay region may not be representative of southern Benguela TA production. This is due to the retention of the system.

Does calcification play an important role?

Monteiro (1996) stated that based on DIC/TA stoichiometry, calcification was not important to controlling DIC in the Benguela system. However, this study shows that calcification may play an important role in offsetting the amount of TA produced. The greatest gross alkalinity production was in autumn, but simultaneous calcification reduced TA by an appreciable quantity. This suggests that calcification does in fact play a potentially significant role in TA fluxes in the southern Benguela.

Is there seasonal "carry-over"?

Much of the TA produced originates from the sediments and pore water. Accumulation and respiration of organic material in the sediment layer suggests that there is a seasonal carry-over or fingerprint (Tyrrell and Lucas, 2002). However, the TA sinal was only realised

after mixing transported sedimentary pore water into the water column. This occurred in September when apparent TA "production" was greatest, but DO was clearly not low enough to produce TA.

A study of sediment and pore water processes may be useful in determining more accurately the production of TA.

Is the buffering effect of alkalinity important to the southern Benguela?

TA production typically intensifies in the southern Benguela in the retention zone of the St. Helena Bay region during stratified conditions. Typically these conditions would result in very low pH due to increased DIC. But TA production results in a lower Revelle factor and thus a higher pH. Data showed that pH was buffered by nearly as much as 0.4 pH units. This is important during the upwelling season when high DIC water is exposed to the atmosphere, where a lower Revelle factor would result in lower pCO_2 and thus less out-gassing. However, low TA values due to calcification in surface waters resulted in decreased pH by 0.25 units.

6.3 Seasonal air-sea pCO_2 Flux

What is the seasonal air-sea CO_2 flux in the southern Benguela?

This study found that annual air-sea CO_2 flux was -1.53 molC m^{-2} yr^{-1}. This is in agreement with previous studies which found flux to be between -1.36 and -1.62 molC m^{-2} yr^{-1} (Monteiro, 1996; Santana-Casiano et al., 2009). Seasonal CO_2 fluxes were as follows for summer, autumn and winter respectively: -8.31, 4.13 and -5.15mmol m^{-2} day^{-1}.

These estimates suggest that the southern Benguela is a small atmospheric CO_2 sink. The annual flux found in this study equates to only 0.095% of global CO_2 uptake. Per metre squared the southern Benguela air-sea CO_2 flux is three times greater than the global air-sea flux. This is lower than one would expect based on productivity measurements for the Benguela (Carr, 2002). The reason for this weak sink is large opposing photosynthetic and respiration fluxes as shown in figure 6.1.

The small role of the southern Benguela as a carbon sink, nationally and globally, does not support further study to resolve air-sea CO_2 fluxes in the region. However, further multidisciplinary studies on responses of coupled ecological-biogeochemical responses are necessary to further our understanding of the changing environment.

What are the key constituents in determining air-sea CO_2 fluxes?

González-Dávila et al. (2009) reported that biology is more important than temperature in determining the magnitude of ΔpCO_2 in the southern Benguela. This study found that wind speed played a greater role in determining the magnitude of flux in all but the nearshore zone, where ΔpCO_2 was large. The Revelle factor was also important in determining the rate at which surface water equilibrated with the atmosphere.

References

Amante, C. and Eakins, B. W. (2009). ETOPO1 1 Arc-Minute Global Relief Model: Procedures, Data Sources and Analysis. *NOAA Technical Memorandum NESDIS NGDC-24*, page 19.

Anderson, L. A. and Sarmiento, J. L. (1994). Redfield ratios of remineralization determined by nutrient data analysis. *Global Biogeochemical Cycles*, 8(1):65–80.

Andrews, W. and Hutchings, L. (1980). Upwelling in the Southern Benguela Current. *Progress In Oceanography*, 9(1):1–81.

Armstrong, D., Mitchell-Innes, B., Verheye-Dua, F., Waldron, H., and Hutchings, L. (1987). Physical and biological features across an upwelling front in the southern Benguela. *Afr. J. Marine Sci.*, 5(1):171–190.

Arrhenius, S. (1896). On the influence of carbonic acid in the air upon the temperature of the ground. *Philosophical Magazine and Journal of Science Series*, 5(41):237–276.

Arrhenius, S. (1908). *Worlds in the Making: the Evolution of the Universe*. Harper & Brothers Publishers, London, h. borns t edition.

Arrigo, K. R. (2005). Marine microorganisms and global nutrient cycles. *Nature*, 437:349–356.

Arrigo, K. R., Robinson, D. H., Worthen, D. L., Dunbar, R. B., DiTullio, G. R., VanWoert, M., and Lizotte, M. P. (1999). Phytoplankton Community Structure and the Drawdown of Nutrients and CO2 in the Southern Ocean. *Science*, 283(5400):365–367.

Atlas, R., Hoffman, R. N., Ardizzone, J., Leidner, S. M., Jusem, J. C., Smith, D. K., and Gombos, D. (2011). A Cross-calibrated, Multiplatform Ocean Surface Wind Velocity Product for Meteorological and Oceanographic Applications. *Bulletin of the American Meteorological Society*, 92(2):157–174.

Bakun, A. (1973). Coastal upwelling indices, west coast of North America, 1946 to 1971. *NOAA Tech. Rep. NMFS SSFR-671*, page 103.

Barcelos e Ramos, J., Müller, M. N., and Riebesell, U. (2010). Short-term response of the coccolithophore Emiliania huxleyi to an abrupt change in seawater carbon dioxide concentrations. *Biogeosciences*, 7(1):177–186.

Berelson, W. M., Balch, W. M., Najjar, R., Feely, R. A., Sabine, C. L., and Lee, K. (2007). Relating estimates of CaCO 3 production, export, and dissolution in the water column to measurements of CaCO 3 rain into sediment traps and dissolution on the sea floor: A revised global carbonate budget. *Global Biogeochemical Cycles*, 21(1):1–15.

Boden, T., Marland, G., and Andres, R. J. (2009). Global, Regional, and National Fossil-Fuel CO2 Emissions. *Carbon Dioxide Information Analysis Center, Oak Ridge National Laboratory*, pages U.S. Department of Energy, Oak Ridge, Tennessee.

Boehme, S., Sabine, C. L., and Reimers, C. E. (1998). CO2 fluxes from a coastal transect: a time-series approach. *Marine Chemistry*, 63(1-2):49–67.

Borges, A. V. (2011). *Oceans and the Atmospheric Carbon Content*. Springer Netherlands, Dordrecht.

Borges, A. V., Delille, B., and Frankignoulle, M. (2005). Budgeting sinks and sources of CO2 in the coastal ocean: Diversity of ecosystems counts. *Geophysical Research Letters*, 32(14):1–6.

Borges, A. V. and Frankignoulle, M. (2001). Short-term variations of the partial pressure of CO2 in surface waters of the Galician upwelling system. *Progress In Oceanography*, 51(2-4):283–302.

Broecker, W. S. and Peng, T. (1974). Gas exchange rates between air and sea. *Tellus*, XXVI:21–35.

Brown, P., Painting, S., and Cochrane, K. (1991). Estimates of Phytoplankton and bacterial biomass and production in the nothern and southern Benguela ecosystems. *South African Journal of Marine Science*, 11:537–564.

Brzezinski, M. (1985). The Si:C:N ratios of marine diatoms: interspecific variability and the effect of some environmental variables. *Journal of Phycology*, 21:347–357.

Burkhardt, S., Zondervan, I., and Riebesell, U. (1999). Effect of CO 2 concentration on C: N: P ratio in marine phytoplankton: A species comparison. *Limnology and oceanography*, 44(3):683–690.

Cai, W.-J., Dai, M., and Wang, Y. (2006). Air-sea exchange of carbon dioxide in ocean margins: A province-based synthesis. *Geophysical Research Letters*, 33(12):1–4.

Callendar, G. (1938). The artificial production of carbon dioxide and its influence on temperature. *Quarterly Journal of the Royal Meteorological Society*, 64(275):223–240.

Capone, D. G., Bronk, D. A., Mulholland, M. R., and Carpenter, E. J. (2010). *Nitrogen in the Marine Environment*. Elsevier, second edi edition.

Carr, M.-E. (2002). Estimation of potential productivity in Eastern Boundary Currents using remote sensing. *Deep Sea Research Part II: Topical Studies in Oceanography*, 49:59–80.

Chelton, D. B., Schlax, M. G., Freilich, M. H., and Milliff, R. F. (2004). Satellite measurements reveal persistent small-scale features in ocean winds. *Science (New York, N.Y.)*, 303(5660):978–83.

Chen, C.-t. A. (2002). Shelf-vs . dissolution-generated alkalinity above the chemical lysocline. *Deep-Sea Research*, 49:5365–5375.

Chen, C.-t. A. and Borges, A. V. (2009). Reconciling opposing views on carbon cycling in the coastal ocean: Continental shelves as sinks and near-shore ecosystems as sources of atmospheric CO2. *Deep Sea Research Part II: Topical Studies in Oceanography*, 56(8-10):578–590.

Cockcroft, A., van Zyl, D., and Hutchings, L. (2008). Large-scale changes in the spatial distribution of South African West Coast rock lobsters: an overview. In *Afr. J. Marine Sci.*, volume 30, pages 149–159.

Danckwerts, P. V. (1951). Significance of liquid-film coefficient in gas absorber. *Ind and Eng Chemistry*, 43(6):1460–1466.

Dickson, A. G. (1981). An exact definition of total alkalinity and a procedure for the estimation of alkalinity and total inorganic carbon from titration data. *Deep Sea Research Part A Oceanographic Research Papers*, 28(6):609–623.

DOE (2004). *Handbook of methods for the analysis of the various parameters of the carbon dioxide system in sea water*. ORNL/CDIAC, third edition.

Dollar, S., Smith, S., Vink, S., Obrebski, S., and Hollibaugh, J. (1991). Annual cycle of benthic nutrient fluxes in Tomales Bay, California, and contribution of the benthos to total ecosystem metabolism. *Marine Ecology Progress Series*, 79:115–125.

Doney, S. C., Fabry, V. J., Feely, R. A., and Kleypas, J. (2009). Ocean Acidification: The Other CO 2 Problem. *Annual Review of Marine Science*, 1(1):169–192.

Dugdale, R. C. and Goering, J. J. (1967). Uptake of new and regenerated forms of nitrogen in primary productivity. *Limnology and Oceanography*, 12:196–206.

Eppley, R. W. and Peterson, B. J. (1979). Particulate organic matter flux and planktonic new production in the deep ocean. *Nature*, 282:677–680.

Estrade, P., Marchesiello, P., A, C. D. V., and Roy, C. (2008). Cross-shelf structure of coastal upwelling: a two - dimensional extension of Ekman's theory and a mechanism for inner shelf upwelling shut down. 66(September):589–616.

Falkowski, P. G., Scholes, R. J., Boyle, E. A., Canadell, J. G., Canfield, D., Elser, J., Gruber, N., Hibbard, K., Hogberg, P., Linder, S., Mackenzie, F. T., Moore, B., Pederson, T., Rosenthal, Y., Seitzinger, S., Smetacek, V., and Steffen, W. (2000). The Global Carbon Cycle: A Test of Our Knowledge of Earth as a System. *Science*, 290(5490):291–296.

Feely, R. A., Sabine, C. L., Hernandez-Ayon, J., Ianson, D., and Hales, B. (2008a). Evidence for upwelling of corrosive" acidified" water onto the continental shelf. *science*, 320(5882):1490.

Feely, R. a., Sabine, C. L., Hernandez-Ayon, J. M., Ianson, D., and Hales, B. (2008b). Evidence for upwelling of corrosive "acidified" water onto the continental shelf. *Science (New York, N.Y.)*, 320(5882):1490–2.

Fiedler, P. C. (2010). Comparison of objective descriptions of the thermocline. *Limnology and Oceanography: Methods*, 8:313–325.

Field, C. B., Behrenfeld, M. J., Randerson, J. T., and Falkowski, P. G. (1998). Primary production of the biosphere: integrating terrestrial and oceanic components. *Science*, 281(5374):237–240.

Field, J. G. and Shillington, F. (2006). Variability of the Benguela Current System. In Robinson, A. and Brink, K., editors, *The Sea: Ideas and observations on progress in the study of*, chapter Volume 14,, pages 835–864. Harvard University Press.

Friederich, G. E., Walz, P., Burczynski, M., and Chavez, F. (2002). Inorganic carbon in the central California upwelling system during the 1997-1999 El Niño-La Niña event. *Progress in oceanography*, 54(1-4):185–203.

Friis, K., Körtzinger, A., and Wallace, D. W. R. (2003). The salinity normalization of marine inorganic carbon chemistry data. *Geophysical research letters*, 30(2):1085.

Gattuso, J.-P., Frankignoulle, M., and Wollast, R. (1998). Carbon and Carbonate Metabolism in Coastal Aquatic Ecosystems. *Annual review of Ecology and Systematics*, 29:405–434.

Giraudeau, J. (1992). Distribution of Recent Nannofossils beneath the Benguela System - Southwest African Continental-Margin. *Marine Geology*, 108(2):219–237.

Giraudeau, J. and Bailey, G. (1995). Spatial dynamics of coccolithophore communities during an upwelling event in the Southern Benguela system. *Continental Shelf Research*, 15(14):1825–1852.

Giraudeau, J., Monteiro, P. M. S., and Nikodemus, K. (1993). Distribution and malformation of living coccolithophores in the northern Benguela upwelling system off Namibia. *Marine Micropaleontology*, 22(1-2):93–110.

Globalview-CO2 (2011). Cooperative Atmospheric Data Integration Project - Carbon Dioxide.

Goldhammer, T., Brüchert, V., Ferdelman, T. G., and Zabel, M. (2010). Microbial sequestration of phosphorus in anoxic upwelling sediments. *Nature Geoscience*, 3(8):557–561.

González-Dávila, M., Santana-Casiano, J. M., and Ucha, I. R. (2009). Progress in Oceanography Seasonal variability of fCO 2 in the Angola-Benguela region. *Progress in Oceanography*, 83(1-4):124–133.

Goyet, C. and Poisson, A. (1989). New determination of carbonic acid dissociation constants in seawater as a function of temperature and salinity. *Deep Sea Research Part A Oceanographic Research Papers*, 36(11):1635–1654.

Grasshoff, K., Ehrhardt, M., Kremling, K., and Anderson, L. G. (1999). *Methods of seawater analysis*. Vch Verlagsgesellschaft Mbh.

Guastella, L. A. (1992). Sea surface heat exchange at St Helena Bay and implications for the southern Benguela upwelling system. *South African Journal of Marine Science*, 12:61–70.

Hales, B., Takahashi, T., and Bandstra, L. (2005). Atmospheric CO 2 uptake by a coastal upwelling system. *Global Biogeochemical Cycles*, 19:1–11.

Hansson, I. (1973). new set of acidity constants for carbonic acid and boric acid in sea water. *Deep-Sea Research*, 20:461–478.

Hauck, J., Hoppema, M., Bellerby, R. G. J., Völker, C., and Wolf-Gladrow, D. (2010). Data-based estimation of anthropogenic carbon and acidification in the Weddell Sea on a decadal timescale. *Journal of Geophysical Research*, 115(C3):1–14.

Hedges, J. I., Baldock, J. A., Gelinas, Y., Lee, C., Peterson, M. L., and Wakeham, S. G. (2002). The biochemical and elemental compositions of marine plankton: A NMR perspective. *Marine Chemistry*, 78(1):47–63.

Ho, D. T., Law, C. S., Smith, M. J., Schlosser, P., Harvey, M., and Hill, P. (2006). Measurements of air-sea gas exchange at high wind speeds in the Southern Ocean: Implications for global parameterizations. *Geophysical Research Letters*, 33(16):1–6.

Hu, X. and Cai, W.-J. (2011). An assessment of ocean margin anaerobic processes on oceanic alkalinity budget. *Global Biogeochemical Cycles*, 25:11.

Huertas, I. E., Navarro, G., Rodríguez-Gálvez, S., and Lubián, L. M. (2006). Temporal patterns of carbon dioxide in relation to hydrological conditions and primary production in the northeastern shelf of the Gulf of Cadiz (SW Spain). *Deep Sea Research Part II: Topical Studies in Oceanography*, 53(11-13):1344–1362.

Hutchings, L., Pitcher, G., Probyn, T. A., and Bailey, G. (1994). The Chemical and Biological Consequences of Coastal Upwelling. In Summerhayes, C., Emeis, K.-C., Angel, M., Smith, R., and Zeitzschel, B., editors, *Upwelling in the Ocean Modern Processes and Ancient Records*, chapter Three, pages 65–82. John Wiley & Sons.

Hutchings, L., van Der Lingen, C. D., Shannon, L., Crawford, R. J. M., Verheye, H. M., Bartholomae, C. H., Van der Plas, A. K., Louw, D., Kreiner, A., Ostrowski, M., Fidel, Q., Barlow, R., Lamont, T., Coetzee, J., Shillington, F., Veitch, J., Currie, J., and Monteiro, P. M. S. (2009). The Benguela Current: An ecosystem of four components. *Progress in Oceanography*, 83(1-4):15–32.

Ianson, D., Feely, R. A., Sabine, C. L., and Juranek, L. W. (2009). Features of coastal upwelling regions that determine net air-sea CO 2 flux. *Journal of oceanography*, 65:677–687.

Iglesias-Rodriguez, M., Halloran, P. R., Rickaby, R., Hall, I., Colmenero-Hidalgo, E., Gittins, J., Green, D., Tyrrell, T., Gibbs, S., Von Dassow, P., Rehm, E., Armbrust, E. V., and Boessenkool, K. P. (2008). Phytoplankton calcification in a high-CO2 world. *Science*, 320(5874):336.

IOC (2010). IAPSO, 2010: The international thermodynamic equation of seawater - 2010: Calculation and use of thermodynamic properties.

IPCC (2007). Contribution of Working Groups I, II and III to the Fourth Assessment Report of the Intergovernmental Panel on Climate Change. In Core Writing Team, Pachauri, R., and Reisinger, A., editors, *IPCC Fourth Assessment Report*, number November, page 104. Geneva, Switzerland.

IPCC (2011). History of the IPCC.

JGOFS (1990). Joint Global Ocean Flux Study - Science Plan. Technical report.

Jouzel, J., Genthon, C., Lorius, C., Petit, J., and Barkov, N. (1987). Vostok ice core-A continuous isotope temperature record over the last climatic cycle (160,000 years). *Nature*, 329:403–408.

Kearns, E. J. and Carr, M.-e. (2003). Seasonal climatologies of nutrients and hydrographic properties on quasi-neutral surfaces for four coastal upwelling systems. *Deep-Sea Research*, 50:3171–3197.

Keeling, C. D. (1960). The concentration and isotopic abundances of carbon dioxide in the atmosphere. *Tellus*, 12(2):200–203.

Klausmeier, C. A., Litchman, E., Daufresne, T., and Levin, S. A. (2004). Optimal nitrogen-to-phosphorus stoichiometry of phytoplankton. *Nature*, 429:171–174.

Kudela, R., Pitcher, G., Probyn, T. A., Figueiras, F. G., Moita, T., and Trainer, V. (2005). Harmful algal blooms in coastal upwelling systems. *Oceanography*, 18(2):184–197.

Kuypers, M. M. M., Lavik, G., Woebken, D., Schmid, M., Fuchs, B. M., Amann, R., Jø rgensen, B. B., and Jetten, M. S. M. (2005). Massive nitrogen loss from the Benguela upwelling system through anaerobic ammonium oxidation. *PNAS*, 102(18):6478–6483.

Laruelle, G. G., Dürr, H. H., Slomp, C. P., and Borges, A. V. (2010). Evaluation of sinks and sources of CO 2 in the global coastal ocean using a spatially-explicit typology of estuaries and continental shelves. *Geophysical Research Letters*, 37(15).

Le Treut, H., Somerville, R., Cubasch, U., Ding, Y., Mauritzen, C., Mokssit, A., Peterson, T. C., and Prather, M. (2007). Historical Overview of Climate Change. In Solomon, S., Qin, D., Manning, M., Chen, Z., Marquis, M., Averyt, K., Tignor, M., and Miller, H., editors, *Climate Change 2007: The Physical Science Basis.*

Contribution of Working Group I to the Fourth Assessment Report of the Intergovernmental Panel on Climate Change. Cambridge University Press, Cambridge, United Kingdom and New York, NY, USA.

Lee, K., Millero, F. J., and Campbell, D. M. (1996). The reliability of the thermodynamic constants for the dissociation of carbonic acid in seawater. *Marine Chemistry*, 55:233–245.

Lewis, E. and Wallace, D. W. R. (1998). Program developed for CO2 system calculations. Technical report.

Liss, P. S. and Merlivat, L. (1986). Air-Sea Gas Exchange Rates: Introduction and Synthesis. In Buat-Menard, P., editor, *The Role of AirSea Exchange in Geochemical Cycling*, volume C 185, pages 113–127. D. Reidel Publishing Company.

Liss, P. S. and Slater, P. G. (1974). Flux of Gases across the Air-Sea Interface. *Nature*, 247:181–184.

Liu, K. K., Atkinson, L., Chen, C.-t. A., Gao, S., Hall, J., Macdonald, R. W., McManus, L. T., and Quiñones, R. (2000). Exploring Continental Margin Carbon Fluxes on a Global Scale. *Eos Trans. AGU*, 81(52):641–652.

LOICZ (2005). Science Plan and Implementation Strategy. Technical report, Land-Ocean Interactions in the Coastal Zone, Stockholm, Sweden.

Margalef, R. (1978). Life-forms of phytoplankton as survival alternatives in an unstable environment. *Oceanologica Acta*, 1(4):493–509.

McCready, M. J. and Hanratty, T. J. (1984). Concentration fluctuations close to a gas-liquid interface. *AIChE Journal*, 30(5):816–817.

Mcneil, B. I. and Matear, R. J. (2008). Southern Ocean acidification : A tipping point at 450-ppm atmospheric CO 2. *PNAS*, 105(48):18860–18864.

Mehrbach, C., Culberson, C. H., Hawley, J. E., and Pytkowcz, R. M. (1973). Measurement of the apparent dissociation constants of carbonic acid in seawater at atmospheric pressure. *Limnology and Oceanography*, 18:897–907.

Millero, F. J., Graham, T. B., Huang, F., Bustos-Serrano, H., and Pierrot, D. (2006). Dissociation constants of carbonic acid in seawater as a function of salinity and temperature. *Marine Chemistry*, 100(1-2):80–94.

Milliman, J. D. and Droxler, A. W. (1996). Neritic and pelagic carbonate sedimentation in the marine environment: ignorance is not bliss. *Geologische Rundschau*, 85(3):496–504.

Milliman, J. D., Troy, P. J., Balch, W. M., Adams, A. K., Li, Y., and Mackenzie, F. T. (1999). Biologically mediated dissolution of calcium carbonate above the chemical lysocline ? *Deep-Sea Research*, 46:1653–1669.

Mintrop, L. (2010). VINDTA: Manual for Versions 3S and 3C. Technical report, Marianda, Kiel, Germany.

Mitchell-Innes, B. and Winter, A. (1987). Coccolithophores: a major phytoplankton component in mature upwelled waters off the Cape Peninsula, South Africa in March, 1983. *Marine Biology*, 30:25–30.

Mojica-Prieto, F. and Millero, F. J. (2002). The values of pK1 + pK2 for the dissociation of carbonic acid in seawater. *Geochimica et Cosmochimica Acta*, 66(14):2529–2540.

Monteiro, P. M. S. (1996). *The Oceanography, the Biogeochemistry and the Fluxes of Carbon Dioxide in the Benguela Upwelling System*. Phd, University of Cape Town.

Monteiro, P. M. S. (2009). Eastern Boundary Current Systems. In Liu, K.-K., Atkinson, L., Quiñones, R., and Talaue-McManus, L., editors, *Carbon and Nutrient Fluxes in Continental Margins: A Global Synthesis*, chapter 2.4, pages 64–77. Springer, 1 edition.

Monteiro, P. M. S., Dewitte, B., Scranton, M. I., Aurélien Paulmier, and Van der Plas, A. K. (2011). The role of open ocean boundary forcing on seasonal to decadal-scale variability and long-term change of natural shelf hypoxia. *Environ. Res. Lett.*, 025002(6):18.

Monteiro, P. M. S., Nelson, G., Vanderplas, A., Mabille, E., Bailey, G., and Klingelhoeffer, E. (2005). Internal tide - shelf topography interactions as a forcing factor governing the large-scale distribution and burial fluxes of particulate organic matter (POM) in the Benguela upwelling system. *Continental Shelf Research*, 25(15):1864–1876.

Monteiro, P. M. S. and Van der Plas, A. K. (2006). Low Oxygen Water (LOW) variability in the Benguela System: Key processes and forcing scales relevant to forecasting. In Shannon, V., Hempel, G., Malanotte-Tizzoli, P., Moloney, C., and Woods, J., editors, *Bengulea: Predicting a Large Marine Ecosystem*, volume 14, pages 71–90. Elsevier, Amsterdam.

Monteiro, P. M. S., Van der Plas, A. K., Mohrholz, V., Mabille, E., Pascall, a., and Joubert, W. (2006). Variability of natural hypoxia and methane in a coastal upwelling system: Oceanic physics or shelf biology? *Geophysical Research Letters*, 33(16):1–5.

Monteiro, P. M. S., Vanderplas, A., Melice, J., and Florenchie, P. (2008). Interannual hypoxia variability in a coastal upwelling system: Ocean-shelf exchange, climate and ecosystem-state implications. *Deep Sea Research Part I: Oceanographic Research Papers*, 55(4):435–450.

Nightingale, P. D. (2009). Air-Sea Gas Exchange. In Le Quéré, C. and Saltzman, E. S., editors, *Surface-Ocean Lower Atmosphere Processes*, pages 69–97. AGU.

Nightingale, P. D., Malin, G., Law, C. S., Watson, A., Liss, P. S., Liddicoat, M., Boutin, J., and Upstill-Goddard, R. C. (2000). In situ evaluation of air-sea gas exchange parameterizations using novel conservative and volatile tracers. *Global Biogeochemical Cycles*, 12(1):373–387.

Orr, J. C., Fabry, V. J., Aumont, O., Bopp, L., Doney, S. C., Feely, R. A., Gnanadesikan, A., Gruber, N., Ishida, A., Joos, F., Key, R. M., Lindsay, K., Maier-Reimer, E., Matear, R., Monfray, P., Mouchet, A., Najjar, R. G., Plattner, G.-K., Rodgers, K. B., Sabine, C. L., Sarmiento, J. L., Schlitzer, R., Slater, R. D., Totterdell, I. J., Weirig, M.-F., Yamanaka, Y., and Yool, A. (2005). Anthropogenic ocean acidification over the twenty-first century and its impact on calcifying organisms. *Nature*, 437(7059):681–686.

Orr, J. C., Maier-Reimer, E., Mikolajewicz, U., Monfray, P., Sarmiento, J. L., Toggweiler, J., Taylor, N., Palmer, J., Gruber, N., Sabine, C. L., Le Quéré, C., Key, R. M., and Boutin, J. (2001). Estimates of anthropogenic carbon uptake from four three-dimensional global ocean models. *Global Biogeochemical Cycles*, 15(1):43–60.

Paillard, D. and Parrenin, F. (2004). The Antarctic ice sheet and the triggering of deglaciations. *Earth and Planetary Science Letters*, 227:263 – 271.

Peng, T.-H. and Broecker, W. S. (1987). C/P ratios in marine detritus. *Global Biogeochemical Cycles*, 1:155–161.

Pérez, F., Alvarez-Salgado, X. A., and Rosón, G. (2000). Stoichiometry of the net ecosystem metabolism in a coastal inlet affected by upwelling. The Ría de Arousa (NW Spain). *Marine Chemistry*, 69(3-4):217–236.

Peterson, T. C., Connolley, W. M., and Fleck, J. (2008). The Myth of the 1970s Global Cooling Scientific Consensus. *Bulletin of the American Meteorological Society*, 89(9):1325–1337.

Pfeil, B., Olsen, A., Bakker, D. C. E., and Others (2011). A uniform, quality controlled, Surface Ocean CO2 Atlas (SOCAT). *Earth System Science Data*, in prepara.

Pitcher, G., Brown, P., and Mitchell-Innes, B. (1992). Spatio-temporal variability of phytoplankton in the southern Benguela upwelling system. *South African Journal of Marine Science*, 12(1):439–456.

Pitcher, G. and Nelson, G. (2006). Characteristics of the surface boundary layer important to the development of red tide on the southern Namaqua shelf of the Benguela upwelling system Greville. *Limnology*, 51(6):2660–2674.

Pitcher, G., Walker, D., Mitchell-Innes, B., and Moloney, C. (1991). Short-term variability during an anchor station study in the southern Benguela upwelling system: Phytoplankton dynamics. *Progress In Oceanography*, 28(1-2):39–64.

Pörtner, H.-O. and Farrell, A. P. (2008). Physiology and climate change. *Science*, (October):690–692.

Probyn, T. A. (1985). Nitrogen uptake by size-fractionated phytoplankton populations in the southern Benguela upwelling system. *Marine ecology progress series*, 22(3):249–258.

Probyn, T. A. (1992). The inorganic nitrogen nutrition of phytoplankton in the southern Benguela: new production, phytoplankton size and implications for pelagic foodwebs. *South African Journal of Marine Science*, 12:411–420.

Redfield, A. C., Ketchum, B. H., and Richards, F. A. (1963). The influence of organisms on the compostion of seawater. In Hill, M. N., editor, *The Sea*, volume 2, pages 26–77. John Wiley and Sons.

Revelle, R. and Suess, H. (1957). Carbon dioxide exchange between atmosphere and ocean and the question of an increase of atmospheric CO2 during the past decades. *Tellus*, 9(1):18–27.

Reynolds, C. S. (1987). Community organization in the freshwater plankton. In Gee, J. H. R. and Giller, P. S., editors, *Organization of Communities Past and Present*, number 27, pages 297–325. Blackwell Scientific Publications.

Ribas-Ribas, M., Gómez-Parra, A., and Forja, J. M. (2011). Air-sea CO2 fluxes in the north-eastern shelf of the Gulf of Cádiz (southwest Iberian Peninsula). *Marine Chemistry*, 123(1-4):56–66.

Richards, F. A. (1965). Anoxic basins and fjords. In Riley, J. O. and Skirrow, D., editors, *Chemical Oceanography Vol 1*, pages 611–645. Academic Press, New York.

Riebesell, U., Schulz, K. G., Bellerby, R. G. J., Botros, M., Fritsche, P., Meyerhöfer, M., Neill, C., Nondal, G., Oschlies, a., Wohlers, J., and Zöllner, E. (2007). Enhanced biological carbon consumption in a high CO2 ocean. *Nature*, 450(7169):545–8.

Riebesell, U., Zondervan, I., Rost, B., Tortell, P. D., Zeebe, R. E., and Morel, F. M. (2000). Reduced calcification of marine plankton in response to increased atmospheric CO2. *Nature*, 407(6802):364–7.

Roy, R. N., Roy, L. N., Vogel, K. M., Porter-Moore, C., Pearson, T., Good, C. E., Millero, F. J., and Campbell, D. M. (1993). The dissociation constants of carbonic acid in seawater at salinities 5 to 45 and temperatures 0 to 45C. *Marine Chemistry*, 44:249–269.

Royal-Society (2005). Ocean acidification due to increasing atmospheric carbon dioxide. *London: The Royal Society*, page 223 pp.

Sabine, C. L., Feely, R. A., Gruber, N., Key, R. M., Lee, K., Bullister, J., Wanninkhof, R., Wong, C. S., Wallace, D. W. R., Tilbrook, B., Millero, F. J., Peng, T.-H., Kozyr, A., Ono, T., and Rios, A. F. (2004). The oceanic sink for anthropogenic CO 2. *Science*, 305:367–371.

Santana-Casiano, J. M. and González-Dávila, M. (2008). Air-sea carbon dioxide exchange along the oceanic fronts of the Angola-Benguela region. In *Atlantic*, pages 1–32.

Santana-Casiano, J. M., González-Dávila, M., and Ucha, I. R. (2009). Carbon dioxide fluxes in the Benguela upwelling system during winter and spring: A comparison between 2005 and 2006. *Deep Sea Research Part II: Topical Studies in Oceanography*, 56(8-10):533–541.

Sarmiento, J. L. and Bender, M. (1994). Carbon biogeochemistry and climate change. *Photosynthesis Research*, 39(3):209–234.

Sarmiento, J. L. and Gruber, N. (2006). *Ocean Biogeochemical Dynamics*. Princeton University Press, Princeton.

Schlitzer, R. (2002). Carbon export fluxes in the Southern Ocean: Results from inverse modeling and comparison with satellite-based estimates. *Deep Sea Research Part II*, 49(9-10):1623–1644.

Schlitzer, R. (2009). Ocean Data View. *http://odv.awi.de*.

Schwing, F. B., Farrell, M. O., Steger, J. M., and Baltz, K. (1996). Coastal Upwelling Indicies: West coast of North America, 1946-95. *NOAA Technical Memorandum NMFS*.

Seitzinger, S. and Giblin, A. (1996). Estimating denitrification in North Atlantic continental shelf sediments. *Biogeochemistry*, 35(1):235–260.

Seitzinger, S., Harrison, J. a., Böhlke, J. K., Bouwman, a. F., Lowrance, R., Peterson, B., Tobias, C., and Van Drecht, G. (2006). Denitrification across landscapes and waterscapes: a synthesis. *Ecological applications : a publication of the Ecological Society of America*, 16(6):2064–90.

Shannon, L. and Nelson, G. (1996). The Benguela: Large scale features and processes and system variability. In Wefer, F., Berger, A., Siedler, G., and Webb, D., editors, *The South Atlantic Past and Present Circulation*, pages 163–210. Springer Verlag, Berlin, Heidelberg.

Shillington, F., Reason, C., Duncombe Rae, C., Florenchie, P., and Penven, P. (2006). Large scale physical variability of the Benguela Current Large Marine Ecosystem (BCLME). *Large marine ecosystems*, 14:49–70.

Siegel, D., Doney, S. C., and Yoder, J. (2002). The North Atlantic spring phytoplankton bloom and Sverdrup's critical depth hypothesis. *Science*, 296(5568):730.

Sigman, D. M. and Boyle, E. A. (2000). Global/interglacial variations in atmospheric carbon dioxide. *Hemisphere*, 407(October):859–869.

Smayda, T. and Reynolds, C. S. (2001). Community assembly in marine phytoplankton : application of recent models to harmful dinoflagellate blooms. *Journal of Plankton Research*, 23(5):447–461.

Smayda, T. and Trainer, V. (2010). Dinoflagellate blooms in upwelling systems: Seeding, variability, and contrasts with diatom bloom behaviour. *Progress In Oceanography*, 85(1-2):92–107.

Smith, S. V. and Hollibaugh, J. T. (1993). Coastal metabolism and the oceanic organic carbon balance. *Reviews of Geophysics*, 31(1):75.

Solomon, S., Hegerl, G., Heimann, M., and Hewitson, B. (2007). Technical summary. *Perspective*.

Suykens, K., Schmidt, S., Delille, B., Harlay, J., Chou, L., De Bodt, C., Fagel, N., and a.V. Borges (2011). Benthic remineralization in the northwest European continental margin (northern Bay of Biscay). *Continental Shelf Research*, 31(6):644–658.

Sweeney, C., Feely, R. A., Chipman, D. W., Hales, B., Friederich, G. E., Chavez, F., Sabine, C. L., Watson, A., Bakker, D. C. E., Schuster, U., Metzl, N., Yoshikawa-Inoue, H., Ishii, M., Midorikawa, T., Nojiri, Y., Kortzinger, A., Steinhoff, T., Hoppema, M., Olafsson, J., Arnarson, T. S., Tilbrook, B., Johannessen, T., Olsen, A., Bellerby, R. G. J., Wong, C. S., Delille, B., Bates, N. R., and De Baar, H. J. W. (2009). Climatological mean and decadal change in surface ocean pCO2, and net sea-air CO2 flux over the global oceans. *Deep Sea Research Part II: Topical Studies in Oceanography*, 56(8-10):554–577.

Takahashi, T., Broecker, W. S., and Langer, G. (1985). No Title. *Journal of Geophysical Research1*, 90:6907–6924.

Takahashi, T., Feely, R. A., Weiss, R. F., Wanninkhof, R., Chipman, D. W., Sutherland, S. C., and Takahashi, T. T. (1997). Global air-sea flux of CO2: An estimate based on measurements of sea-air pCO2 difference. *Proceedings of the National Academy of Sciences*, 94(16):8292–8299.

Takahashi, T., Olafsson, J., Goddard, J. G., Chipman, D. W., and Sutherland, S. C. (1993). Seasonal variation of CO2 and nutrients in the high-latitude surface oceans: A comparative study. *Global Biogeochemical Cycles*, 7(4):843–878.

Takahashi, T., Sutherland, S. C., Sweeney, C., Poisson, A., Metzl, N., Tilbrook, B., Bates, N. R., Wanninkhof, R., Feely, R. A., Sabine, C. L., and Others (2002). Global sea-air CO2 flux based on climatological surface ocean pCO2, and seasonal biological and temperature effects. *Deep Sea Research Part II: Topical Studies in Oceanography*, 49(9-10):1601–1622.

Takahashi, T., Wanninkhof, R., Feely, R. A., Weiss, R. F., Chipman, D. W., Bates, N., Olafsson, J., Sabine, C. L., and Sutherland, S. C. (1999). Net sea-air CO2 flux over the global oceans: An improved estimate based on the sea-air pCO2 difference. In *Proceedings of the 2nd International Symposium CO2 in the Oceans*, volume 15. Tsukuba, Japan: National Institute for Environmental Studies.

Tans, P. and Keeling, C. D. (2011). Trends in Atmospheric Carbon Dioxide. *NOAA/ESRL and Scripps Institute of Oceanography*, page http://www.esrl.noaa.gov/gmd/ccgg/trends/.

Trenberth, K., Large, W., and Olson, J. (1990). The mean annual cycle in global ocean wind stress. *J. Phys. Oceanogr*, 20(11):1742–1760.

Tyndall, J. (1861). On the Absorption and Radiation of Heat by Gases and Vapours, and on the Physical Connexion of Radiation, Absorption, and Conduction. *Philosophical Transactions of the Royal Society*, 151(1861):1–36.

Tyrrell, T. and Lucas, M. (2002). Geochemical evidence of denitrification in the Benguela upwelling system. *Continental Shelf Research*, 22(17):2497–2511.

Tyson, P. D. and Preston-Whyte, R. A. (2000). *The Weather and Climate of Southern Africa*. OUP Southern Africa, second edi edition.

Veitch, J. (2009). *Equilibrium dynamics of the Benguela system: a numerical modelling approach*. Phd, University of Cape Town.

Volk, T. and Hoffert, M. (1985). Ocean carbon pumps-Analysis of relative strengths and efficiencies in ocean-driven atmospheric CO2 changes. In *The carbon cycle and atmospheric CO2: natural variations Archean to present*, volume 1, pages 99–110.

Waldron, H., Monteiro, P. M. S., and Swart, N. C. (2009). Carbon export and sequestration in the southern Benguela upwelling system : lower and upper estimates. *Ocean Science Discussions*, 6:1173–1192.

Waldron, H. and Probyn, T. A. (1992). Nitrate supply and potential new production in the Benguela upwelling system. *South African Journal of Marine Science*, 12:29–39.

Waldron, H., Probyn, T. A., and Brundrit, G. (1998). Carbon pathways and export associated with the southern Benguela upwelling system: a re-appraisal. *South African Journal Of Marine Science*, 19(1):113–118.

Wanninkhof, R. (1992). Relationship between wind speed and gas exchange over the ocean. *Journal of Geophysical Research*, 97(C5):7373–7382.

Wanninkhof, R., Asher, W. E., Ho, D. T., Sweeney, C., and McGillis, W. R. (2009). Advances in Quantifying Air-Sea Gas Exchange and Environmental Forcing*. *Annual Review of Marine Science*, 1(1):213–244.

Wanninkhof, R. and McGillis, W. R. (1999). A cubic relationship between air-sea CO2 exchange and wind speed. *Geophysical Research Letters*, 26(13):1889–1892.

Weeks, S., Pitcher, G., and Bernard, S. (2011). Satellite monitoring of the evolution of a coccolithophorid bloom in the southern Benguela upwelling system. *Oceanography*, 17(1):83–89.

Weiss, R. and Price, B. A. (1980). Nitrous oxide solubility in water and seawater. *Marine Chemistry*, 8(4):347–359.

Wolf-Gladrow, D., Zeebe, R. E., Klaas, C., Kortzinger, A., and Dickson, A. G. (2007). Total alkalinity: The explicit conservative expression and its application to biogeochemical processes. *Marine Chemistry*, 106(1-2):287–300.

Yool, A., Martin, A. P., Fernández, C., and Clark, D. R. (2007). The significance of nitrification for oceanic new production. *Nature*, 447(7147):999–1002.

Zachos, J. C., Dickens, G. R., and Zeebe, R. E. (2008). An early Cenozoic perspective on greenhouse warming and carbon-cycle dynamics. *Nature*, 451(7176):279–83.

Zachos, J. C., Röhl, U., Schellenberg, S. a., Sluijs, A., Hodell, D. a., Kelly, D. C., Thomas, E., Nicolo, M., Raffi, I., Lourens, L. J., McCarren, H., and Kroon, D. (2005). Rapid acidification of the ocean during the Paleocene-Eocene thermal maximum. *Science*, 308(5728):1611–5.

Zeebe, R. E. and Wolf-Gladrow, D. (2001). *CO2 in seawater: equilibrium, kinetics, isotopes*, volume 65. Elsevier Science Ltd.

Zhang, J., Gilbert, D., Gooday, a. J., Levin, L., Naqvi, S. W. a., Middelburg, J. J., Scranton, M., Ekau, W., Peña, A., Dewitte, B., Oguz, T., Monteiro, P. M. S., Urban, E., Rabalais, N. N., Ittekkot, V., Kemp, W. M., Ulloa, O., Elmgren, R., Escobar-Briones, E., and Van der Plas, A. K. (2010). Natural and human-induced hypoxia and consequences for coastal areas: synthesis and future development. *Biogeosciences*, 7(5):1443–1467.

Zondervan, I., Zeebe, R. E., Rost, B., and Riebesell, U. (2001). Decreasing marine biogenic calcification: a negative feedback on rising atmospheric pCO2. *Global Biogeochemical Cycles*, 15(2):507–516.

A Appendix: Supplementary Data

A.1 Active upwelling divergence zone

(Estrade et al., 2008)

$$L_U = \frac{0.75 \cdot D}{S} \tag{A.1}$$

Where D is the depth of the Ekman layer and S is the slope of the continental shelf.

- D was assumed to be a depth of 30 m, the same value used by Veitch (2009).
- $S = \frac{(190-50)}{(72\,840-11\,500)} = 0.00229$
- $$\begin{aligned} L_U &= \frac{0.75 \cdot 30}{0.00229} \\ &= 9858\,\text{m} \end{aligned}$$

A.2 Biogechemical Data

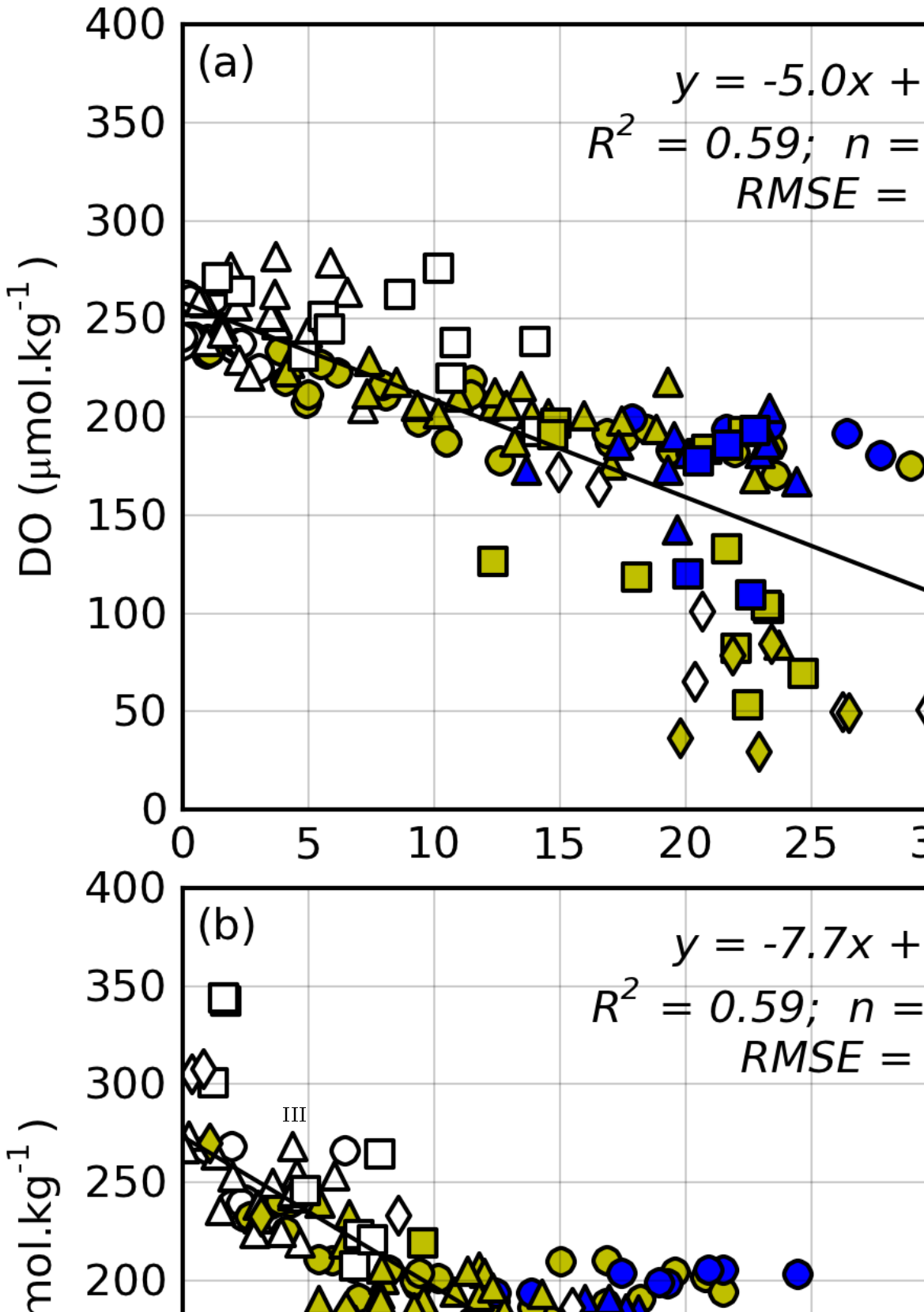

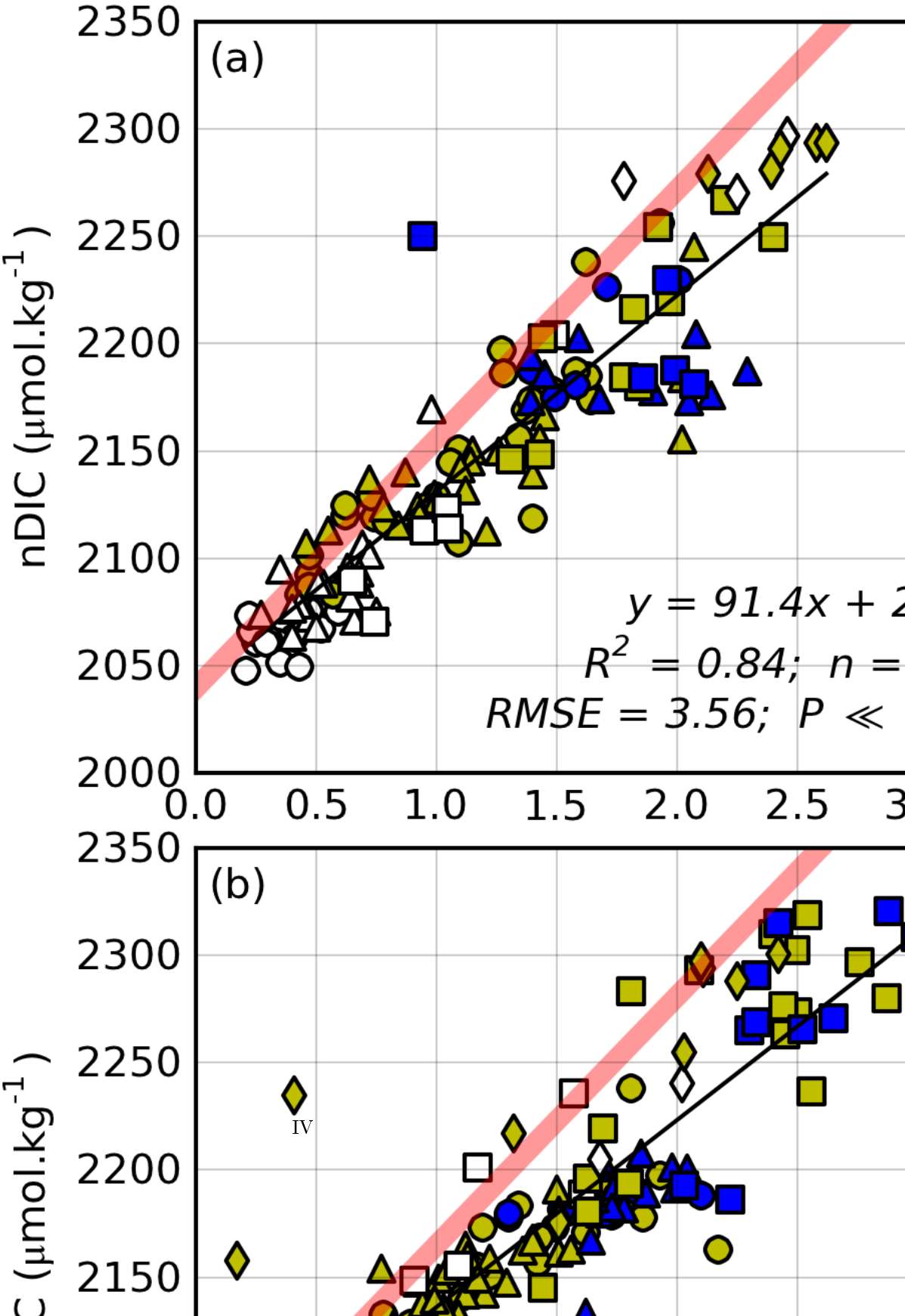
(a)
nDIC (µmol.kg-1)
2350
2300
2250
2200
2150
2100
2050
2000
0.0
0.5
1.0
1.5
2.0
2.5
y = 91.4x + 2
R2 = 0.84; n =
RMSE = 3.56; P ≪
(b)
IV
2350
2300
2250
2200
2150

A.3 Satellite Data

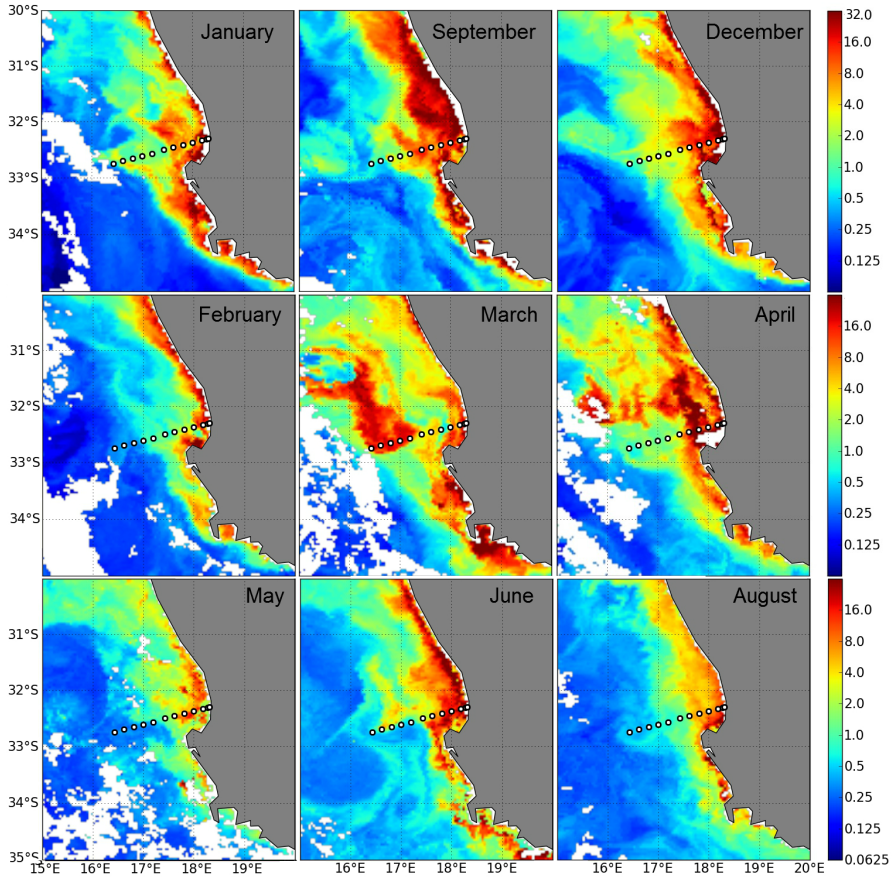

Figure A.3: An array of MODIS aqua chl-a (mg m^{-3}) images from ftp://podaac-ftp.jpl.nasa.gov. Nine of the ten sampled months are shown (July omitted). Images are a composite of four days prior to the sampling date. The white markers show the stations of the SHBML.

Table A.1: This table shows the contribution of various processes for three zones for all seasons. Three zones used were: inshore-bottom, bay-surface and inshore surface. The average of each zone was used for the measured variables (nTA, nDIC, NO_3^-, PO_4^-*). Age of surface water was calculated using the warming rate calculated by Guastella (1992). Contributions were calculated using stoichiometery from data trends (figures 4.9 a-f). See table 5.3 for derivation of marine carbonate system processes. The first line of each season (SRC) shows source water (SACW) concentrations.*

SUMMER

	Age	nTA	nDIC	NO_3^-	PO_4^-	Photosyn · Remin ·	Denitr.	Calcif.	Other	Flux
SACW	-	2350.00	2180.00	15.00	1.30	-	-	-	-	-
SI-B	-	2369.36	2220.54	22.00	1.93	46.16	-0.98	-4.64	0.00	-
NS-S	1.9	2369.22	2278.34	20.60	2.17	17.58	27.01	25.43	-0.07	-12.16
SI-S	5.5	2356.17	2105.05	4.10	0.76	-103.30	0.00	-66.73	-6.52	3.27

AUTUMN

	Age	nTA	nDIC	NO_3^-	PO_4^-	Photosyn · Remin ·	Denitr.	Calcif.	Other	Flux
SACW	-	2350.00	2180.00	15.00	1.30	-	-	-	-	-
SI-B	-	2419.63	2270.07	17.24	2.51	88.65	73.57	-72.15	0.00	-
NS-S	4.3	2314.16	2222.66	12.05	1.85	-48.36	0.00	56.70	-52.74	-3.02
SI-S	5.4	2309.09	2185.84	6.23	1.27	-42.49	0.00	9.30	-2.53	-1.09

WINTER

	Age	nTA	nDIC	NO_3^-	PO_4^-	Photosyn · Remin ·	Denitr.	Calcif.	Other	Flux
SACW	-	2350.00	2180.00	15.00	1.30	-	-	-	-	-
SI-B	-	2362.25	2252.29	25.88	2.34	76.20	2.93	-6.84	0.00	-
NS-S	6.3	2354.04	2165.88	12.82	1.45	-65.21	22.74	-39.15	-4.11	-0.69
SI-S	7.3	2334.36	2129.35	8.39	1.01	-32.24	0.00	6.04	-9.84	-0.49

Table A.2: Table showing the percentage area of good and bad linearly interpolated alkalinity data for a section from the coast to 17.5 °E. Percentage area of TA loss and gain are also shown. Section has a total area of ~89.29 km².

AREA	Jan		Apr	May	Jun	Jul	Aug	Sep
Good Data	99.4		88.8	99.7	100.0	100.0	81.0	100.0
Bad Data	0.6		11.2	0.3	0.0	0.0	19.0	0.0
TA Loss	0.0		12.3	3.5	2.6	0.0	0.0	0.0
TA Gain	2.0		15.0	20.0	0.0	1.5	7.9	23.7

B Appendix: Box and Whisker Plots

This section contains box and whisker plots of all the raw data before any quality control had been performed. The physical parameters (temperature, salinity, oxygen) did not need any corrections. Nutrients were also considered to be correct. These had already gone through quality control, as the Department of Environmental Affairs ran these samples. The DIC data appears to be suspect for only February when the data range was much larger than expected. Alkalinity data was suspect for Feb, Mar and Dec. This may be due to storage time for the Dec samples. General system inaccuracy may be to blame for Feb and Mar.

For all plots the red line shows the median of the sample set. The lower and upper bounds of the blue boxes show the lower (25%) and upper (75%) quartiles of the sample set respectively. The whiskers (blue dashed line) extend to the minimum and maximum of the sampleset unless values lie outside $^3/_2 \times (median \pm Q_n)$ which indicates outliers shown by plus symbols (+).

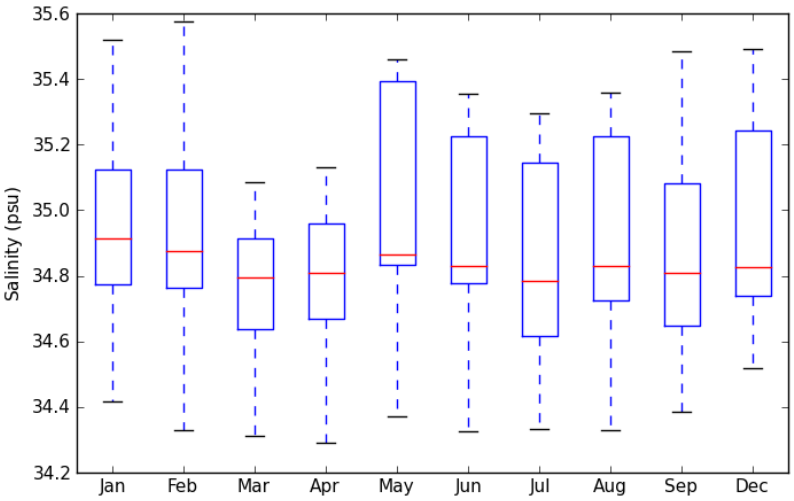

Figure B.1: Box and whisker plot of salinity data before quality control.

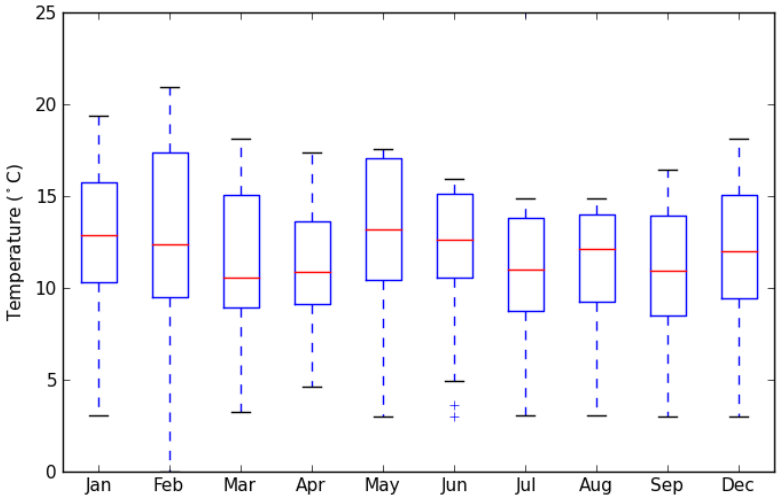

Figure B.2: Box and whisker plot of temperature data before quality control.

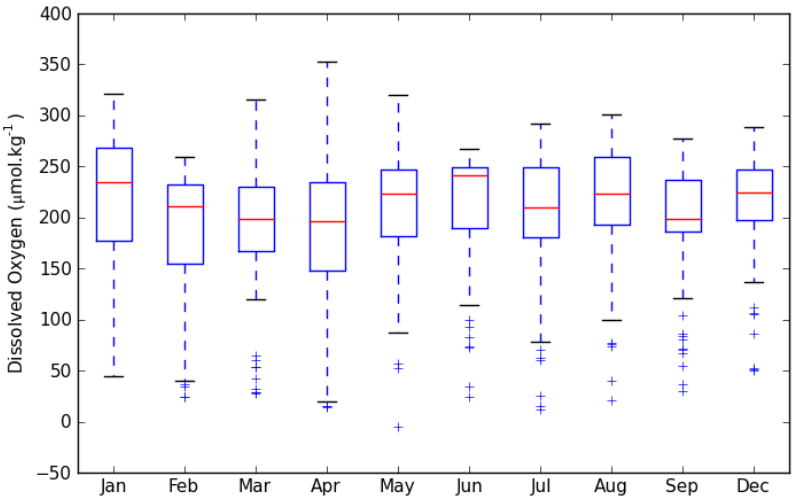

Figure B.3: Box and whisker plot of oxygen data before quality control.

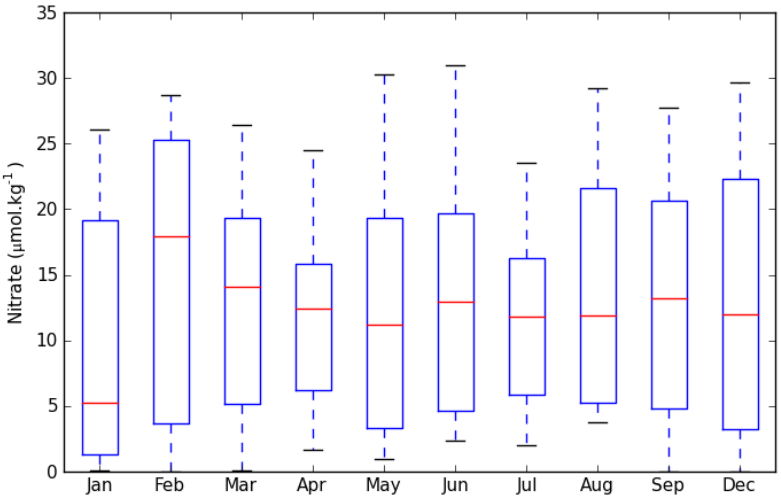

Figure B.4: Box and whisker plot of nitrate data before quality control.

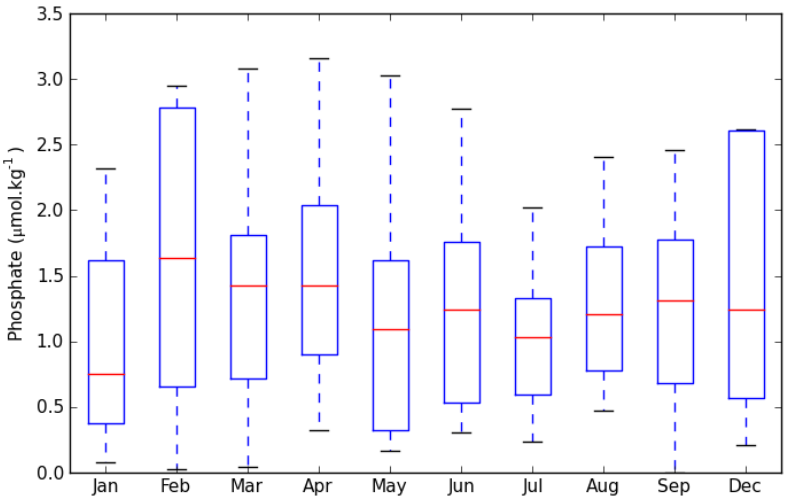

Figure B.5: Box and whisker plot of phosphate data before quality control.

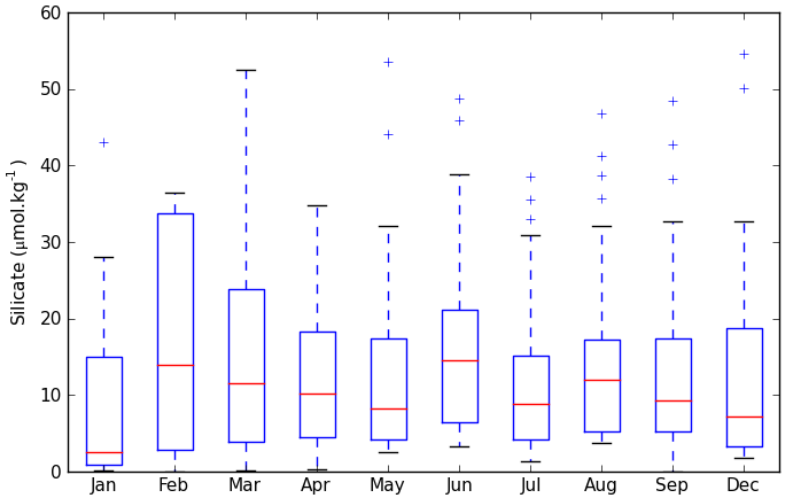

Figure B.6: Box and whisker plot of silicate data before quality control.

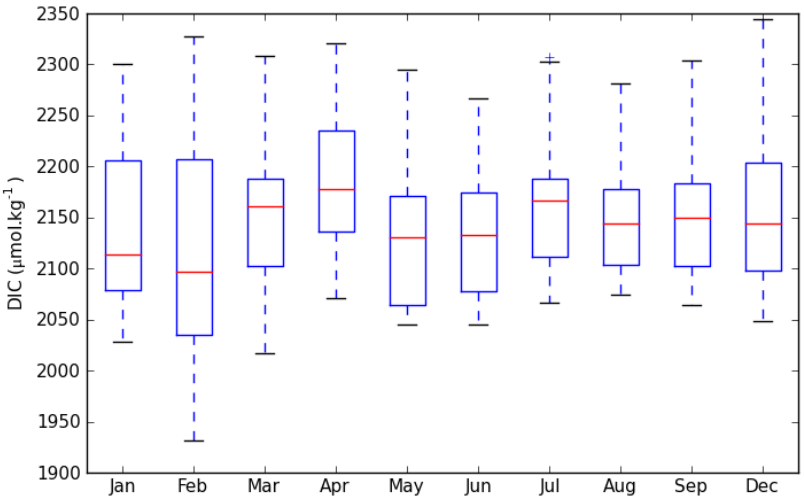

Figure B.7: Box and whisker plot of dissolved inorganic carbon data before quality control.

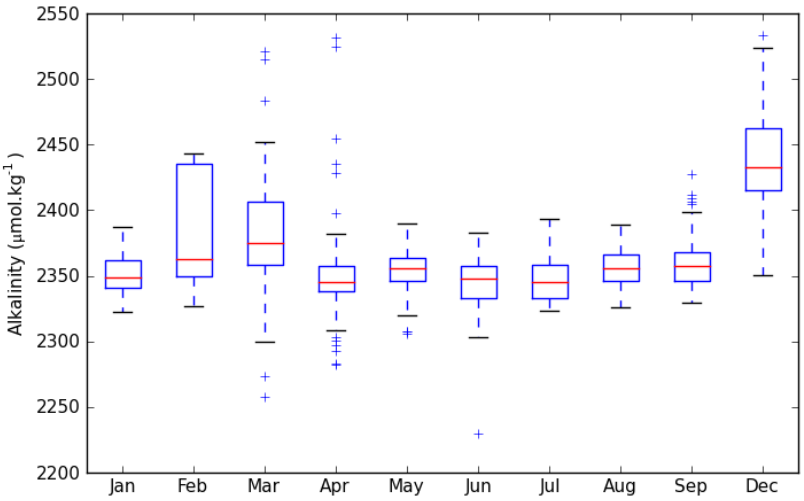

Figure B.8: Box and whisker plot of alkalinity data before quality control.

C Appendix: Recalculation Scripts

C.1 Script Downloads

All the scripts below are based on the source code given in the DOE (2004) manual

- MATLAB - The two scripts below were written for different releases of MATLAB where the *lsqnonlin* function has changed
  - r2008: http://ge.tt/9ZEmJj9/v/0
  - r2010: http://ge.tt/9ZEmJj9/v/1
- PYTHON
  - RecalcAlk.py: http://ge.tt/9ZEmJj9/v/4
  - RecalcAlk for VINDTA with GUI: http://ge.tt/9ZEmJj9/v/6

C.2 Code Listing

Below is the code listing for the python translation of "RecalcAlk.py" script. MATLAB versions are also available above.

```
#### RecalcAlk.py ###
####
#### IMPORTING ####
from numpy import array,log,log10,exp,sqrt
from scipy.optimize import leastsq

#### FUNCTIONS ####
def RecalcAlk_leastsq(
        sal,tempC,po4,si,
        samplevol,acidconcKG,aciddens,
        Vols,Emfs,pKconst):
    """
    This is the "master script" for the VINDTA_recalc_leastsq.py file.
    The script was orignally written by A.G. Dickson in 1993 and then
    coded into Python by Luke Gregor in 2011.
    Note
    INPUT:  The input has been adapted for VINDTA outputs [units].
        sal =         salinity [psu]
        tempC=        Temperature [degC]
        po4 =         Phosphate [umol/kg]
        si =          Silicate [umol/kg]
        samplevol =   Sample Volume [mL]
        acidconcKG =  Acid Concentration [mol/kg]
        aciddens =    Acid Density [kg/L]
        Vols =        array of acid volumes [mL]
```

```
        Emfs =        array of voltages [mV]
        pKconst =     1 to 12
    OUTPUT:
        Acid Concentration [mol/kg]
        Alkalinity [umol/kg]
    """
    pKstring = ['',
        'Roy et al, 1993',
        'Goyet and Poisson, 1989',
        'Hansson refit by Dickson and Millero, 1987',
        'Mehrbach refit by Dickson and Millero, 1987',
        'Hansson and Mehrbach refit BY Dickson and Millero, 1987',
        'Mehrbach et al, 1973',
        'Millero, 1979',
        'Cai and Wang, 1998',
        'Lueker et al, 2000',
        'Mojica Prieto and Millero, 2002',
        'Millero et al, 2002',
        'Millero, 2006',
        'Millero, 2010']

    S    = sal                 # psu
    T    = tempC               # degC
    PT   = po4*1e-6            # mol/kg from umol/kg
    SiT  = si *1e-6            # mol/kg from umol/kg
    V0   = samplevol           # mL or cm3
    C    = acidconcKG          # mol/kg
    DAcid = aciddens           # kg/L
    V    = array(Vols)         # mL
    E    = array(Emfs)*1e-3    # V form mV

    H, W, W0, Z, t, k, X0 = SetUp(
            S,T,PT,SiT,C,DAcid,V,V0,E,pKconst)

    X,covarience,info,mesg,ier = leastsq(
            FCN,X0,args=(H,W,W0,C,Z,t,k),
            full_output=1,xtol=0.0001,)

    residuals = FCN(X,H,W,W0,C,Z,t,k)

    F, AT,CT,K1 = X
    return C, AT*1e3, -log10(K1*1e-6),pKstring[pKconst],residuals

def SetUp(S,T,PT,SiT,C,DAcid,V,V0,E,pKconst):
    """Subroutine to set up calculation ready for optimisation

    Written by A.G. Dickson (from Fortran script)
    Transcribed by L. Gregor

    INPUT:  S  [psu]
```

```
        T  [degC]
        PT [mol/kg]
        SiT[mol/kg]
        V0 [cm3]
        DAcid [g/cm3]
        V  [cm3]
        E  [V]
    OUTPUT: H  []
        W  [g]
        t  [tot concts]
        k  [equ consts]
        X0 [initial estimates]
    """

    if S>5: # Seawater sample
        W0 = V0 * DensSW (S,T) # mass of sample titrated [g]
        # values for total concentrations (output global)
        t = ConcnsSW(S,PT,SiT)
        # values for equilibrium constants (output global)
        k = ConstsSW(S,T,t,pKconst)
        # pH conversion factor from free to total scale
        Z = 1. + t[-2]/k[-3]

    else: # A NaCl solution with conc S [mol/kg-soln]
        print "This sample cannot be analysed as it is not sea water."

    # Calculate Nernst Factor: E = E0 +/- (RT/F) ln[H]
    KNernst = 8.31451 * (273.15 + T) / 96485.309
    if E[0] > E[-1]: KNernst = -KNernst

    # mass of acid titrant at each titration point [g]
    W = V * DAcid

    # Estimate E0 using last two titration points (at low pH)
    # slightly different to Fortran script
    E0 = EstimE0(W0,W,E,C,KNernst)

    # Calculate [H] using this initial estimate of E0
    H = exp((E- E0)/KNernst)

    # Creating initial solution vector for the least-squares funcion
    X0 = [1.,2.,2.,1.]

    return H, W, W0, Z, t, k, X0

def FCN(X,H,W,W0,C,Z,t,k,**kwds):

    PT, SiT, BT, ST, FT = t
    K0, K1,K2, KB, K1P,K2P,K3P, KSi, KS, KF, KW = k
    F  = X[0]
```

```
    AT = X[1]*1e-3
    CT = X[2]*1e-3
    K1 = X[3]*1e-6

    Denom = (F*H)**2. + K1*F*H + K1*K2
    alkCT = CT * K1 * (F*H + 2.*K2) / Denom
    alkBT = BT / (1.+F*H/KB)
    alkPT = PT * ((K1P*K2P*F*H + 2.*K1P*K2P*K3P - (F*H)**3.)\
             / ((F*H)**3. + K1P*(F*H)**2.+K1P*K2P*F*H + K1P*K2P*K3P))
    alkSiT= SiT/ (1.+ F*H/KSi)
    alkST = ST / (1.+ KS*Z/(F*H))
    alkFT = FT / (1.+ KF/  (F*H))
    OH    = KW / (F*H)
    AcidAdd= (W0 + W)/W0 * (F*H/Z - OH) - (W/W0)*C

    Residual =  AT - alkCT - alkBT - alkPT - \
                alkSiT + alkST + alkFT + AcidAdd

    return Residual

## Subroutines to SetUp ##
def DensSW  (S,T):
    """Function to caclulate the density of sea water.
    Based on Millero and Poisson (1981) Deep-Sea Res. 28, 625.

    Written by A.G. Dickson (from Fortran script)
    Transcribed to Python by L. Gregor

    INPUT:  S [psu]
            T [degC]
    OUTPUT: DensSW
    """
    # Calculate seawater density (using sample's S titration
    # temperature (temperature is assumed constant during run)
    a0 =  999.842594
    a1 =  6.793952e-2
    a2 = -9.095290e-3
    a3 =  1.001685e-4
    a4 = -1.120083e-6
    a5 =  6.536332e-9

    b0 =  8.24493e-1
    b1 = -4.0899e-3
    b2 =  7.6438e-5
    b3 = -8.2467e-7
    b4 =  5.3875e-9

    c0 = -5.72466e-3
    c1 = +1.0227e-4
    c2 = -1.6546e-6
```

```
    d0 =  4.8314e-4

    DensSW  =   (a0 + (a1 + (a2 + (a3 + (a4 + a5*T) *T) *T) *T) *T) +\
                (b0 + (b1 + (b2 + (b3 + b4*T) *T) *T) *T) *S +\
                (c0 + (c1 + c2*T) *T) *S *sqrt(S) + d0*S **2
    DensSW=DensSW/1000.

    return DensSW

def ConcnsSW(S, PT, SiT):
    """Subroutine to calculate appropriate total concentrations,
    for seawater of salinity of, S.

    Written by A.G. Dickson (from Fortran script)
    Transcribed to Python by L. Gregor

    INPUT:  S [psu]
    OUTPUT: BT [mol/kg-soln]
          ST [mol/kg-soln]
          FT [mol/kg-soln]
    """
    # Uppstron (1974) Deep-Sea Res. 21, 161.
    BT = (0.000232/10.811) * (S/1.80655)

    # Morris and Riley (1966) Deep-Sea Res. 13, 699.
    ST = (0.1400/96.062) * (S/1.80655)

    # Riley (1965) Deep-Sea Res 12, 219.
    FT = (0.000067/18.998) * (S/1.80655)

    return (PT, SiT, BT, ST, FT)

def ConstsSW(S,T,t,pKconst):
    """Taken from the matlab script as it works
    need to rewrite this - also for option of other constants"""
    PT, SiT, BT, ST, FT = t

    IonS = 19.924 * S / (1000. - 1.005 * S)
    TK   = T + 273.15

    # Boric acid, DOEv3 compliant:
    lnKB = (-8966.9 - 2890.53 * (S**0.5) - 77.942 * S) / TK
    lnKB = lnKB + (1.728 * S**(3./2.) - 0.0996 * S**2.) / TK
    lnKB = lnKB + (148.0248 + 137.1942 * S ** 0.5 + 1.62142 * S)
    lnKB = lnKB + (-24.4344 - 25.085*S**0.5 - .2474 * S)*log(TK)
    lnKB = lnKB + (.053105 * S**0.5) * TK
    KB   = exp(lnKB)

    # Bisulfate ion, DOEv3 compliant:
```

```
lnKS = -4276.1 / TK + 141.328 - 23.093 * log(TK)
lnKS = lnKS + (-13856/TK + 324.57 - 47.986*log(TK))*(IonS)**0.5
lnKS = lnKS + (35474 / TK - 771.54 + 114.723 * log(TK)) * IonS
lnKS = lnKS - (2698/TK)*(IonS)**(3./2.) + (1776/TK)*IonS**2.
lnKS = lnKS + log(1. - .001005 * S)
KS   = exp(lnKS)

# ###################
# The DOEv3 method causes problems with X2-optimization under extremely
# high DIC levels (hydrothermal vents, etc.). Seems to be related to KF
# DOEv2's KF does a lot better, so i'm using that.
# For regular samples there's no big difference.
# ###################
#Hydrogen fluoride, DOEv3 compliant (as from Perez & Fraga, 1987):
# lnKF = 874 ./ TK - 9.68 + 0.111 .* S .** 0.5
# KF   = exp(lnKF)
# ###################
# Hydrogen fluoride, DOEv2 compliant (as from Dickson & Riley, 1979a):
IonS = 19.924 * S / (1000. - 1.005 * S)
lnKF = (1590.2/TK - 12.641 + 1.525 *\
        (IonS)**0.5) + log(1. - .001005 * S)
KF   = exp(lnKF) * (1. + ST / KS)   #convert from free to total pH scale
# ###################

# Water, DOEv3 compliant:
lnKW = 148.9652 - 13847.26 / TK - 23.6521 * log(TK)
lnKW = lnKW + (-5.977 + 118.67 / TK + 1.0495 * log(TK)) * S **0.5
lnKW = lnKW - .01615 * S
KW   = exp(lnKW)

# Phosporic acid K1, DOEv3 compliant
lnKP1 = -4576.752 / TK + 115.525 - 18.453 * log(TK)
lnKP1 = lnKP1 + (-106.736 / TK + .69171) * S **0.5
lnKP1 = lnKP1 + (-.65643 / TK - .01844) * S
K1P   = exp(lnKP1)

# Phosporic acid K2, DOEv3 compliant
lnKP2 = -8814.715 / TK + 172.0883 - 27.927 * log(TK)
lnKP2 = lnKP2 + (-160.34 / TK + 1.3566) * S **0.5
lnKP2 = lnKP2 + (.37335 / TK - .05778) * S
K2P   = exp(lnKP2)

# Phosporic acid K3, DOEv3 compliant
lnKP3 = -3070.75 / TK - 18.141
lnKP3 = lnKP3 + (17.27039 / TK + 2.81197) * S **0.5
lnKP3 = lnKP3 + (-44.99486 / TK - .09984) * S
K3P   = exp(lnKP3)

# Silicic acid, DOEv3 compliant:
lnKSi = -8904.2 / TK + 117.385 - 19.334 * log(TK)
```

```
    lnKSi = lnKSi + (-458.79 / TK + 3.5913) * (IonS) ** 0.5
    lnKSi = lnKSi + (188.74 / TK - 1.5998) * IonS
    lnKSi = lnKSi + (-12.1652 / TK + .07871) * IonS ** 2.
    lnKSi = lnKSi + log(1. - .001005 * S)
    KSi   = exp(lnKSi)

    lnK0 = -60.2409 + 93.4517*(100/TK) + 23.3585*log(TK/100)\
    + S*(0.023517 - 0.023656*(TK/100) + 0.0047036*(TK/100)**2.)
    K0   = exp(lnK0)

    SWStoTOT  = (1. + ST/KS)/(1. + ST/KS + FT/KF)
    K1,K2 = ConstsK1K2(S,TK,pKconst,SWStoTOT)

    return K0, K1,K2, KB, K1P,K2P,K3P, KSi, KS, KF, KW

def DesnNaCl(CNaCl, T):
    """Function to calculate the density of a sodium chloride solution.
    Based on equation by Lo Surdo et al.
      J. Chem. Thermodynamics 14, 649 (1982)

    Written by A.G. Dickson (from Fortran script)
    Transcribed to Python by L. Gregor

    INPUT:  CNaCl - conc of sodium chloride [mol/kg-soln]
          T [degC]
    OUTPUT: DensNaCl
    """
    mNaCl = CNaCl/ (1. - 0.058443*CNaCl) # molality

    # density of SMOW [kg/m3]
    DH2O = 999.842594 + 6.793952e-2 * T - 9.095290e-3 * T**2.\
    + 1.001685e-4 * T**3. - 1.120083e-6 * T**4. - 6.53633e-9 * T**5.

    # density of NaCl (kg/m3)
    DNaCl = DH2O + mNaCl * (46.5655 - 0.2341*T + 3.4128e-3 *T**2.\
    - 2.7030e-5 * T**3. + 1.4037e-7 * T**4)\
    + mNaCl**1.5 * (-1.8527 + 5.3956e-2 * T - 6.2635e-4 * T**2.)\
    + mNaCl**2. *  (-1.6368 - 9.5653e-4 * T + 5.2829e-5 * T**2.)\
    + 0.2274 * mNaCl**2.5

    DensNaCl = 1.e-3 * DNaCl

    return DensNaCl

def ConstsNaCl(CNaCl,T):
    """Subroutine to calculate values of dissociation constants,
    appropriateto a sodium chloride solution of concentration,
    CNaCl, and temperature, T.

    Written by A.G. Dickson (from Fortran script)
```

```
    Transcribed to Python by L. Gregor

    INPUT:  CNaCl - conc of sodium chloride [mol/kg-soln]
          T [degC]
    OUTPUT: K1,K2
          KW
    """
    global K1,K2,KW

    TK = 273.15 + T
    # Dyrssen and Hansson (1973) Mar. Chem. 1, 137.
    K1 = exp (-13.82)
    K2 = exp ( 21.97)
    KW = exp (-31.71)

    return (K1,K2,KW)

def EstimE0 (W0,W,E,C,KNernst):
    """This subroutine estimates an initial value of E0 using a Gran
    function an the last two titration points to estimate AT.
    [H] is calculated at those 2 points and an average E0 estimated.

    Written by A.G. Dickson (from Fortran script)
    Transcribed to Python by L. Gregor

    INPUT:  W0 [g]
          W  [g]
          E  [V]
          C  [mol/kg]
          KNernst [V]
    OUTPUT: E0 [V]
    """
    WA = W[-2]
    WB = W[-1]
    EA = E[-2]
    EB = E[-1]

    # Calculate gran function (W0+W) exp(E/K) and fit to y = a0 + a1*x
    #   A1 = (yB - yA) / (xB - xA)
    #   A0 = yA - A1*xA
    A1 = ((W0+WB)*exp(EB/KNernst) - (W0 + WA)*exp(EA/KNernst)) / (WB-WA)
    A0 = (W0+WA) *exp(EA/KNernst) - A1*WA

    # Estimate of TA
    AT = (-A1/A0) * C/W0
    # Calculate [H] at those 2 points and hence an average E0
    HA = (WA*C - W0*AT) / (W0 + WA)
    HB = (WB*C - W0*AT) / (W0 + WB)
    E0 = (EA - KNernst*log(HA) + EB - KNernst* log(HB))/2.
```

```
    return E0

def ConstsK1K2(S,TK,n,SWStoTOT):
    # These constants were taken from the CO2SYS_calc
    # script for MATLAB (van Heuven et al. 2011)
    # see their script for more details on dissociation constants
    # http://cdiac.ornl.gov/oceans/co2rprt.html

    if n==1:  # ROY et al, 1993
        # ROY et al, Marine Chemistry, 44:249-267, 1993
        lnK1 = 2.83655 - 2307.1266/TK - 1.5529413*log(TK) +\
          (-0.20760841 - 4.0484/TK)*sqrt(S) + 0.08468345*S -\
          0.00654208*sqrt(S)*S
        K1 = exp(lnK1)*(1 - 0.001005*S)/SWStoTOT # convert to SWS pH scale
        lnK2 = -9.226508 - 3351.6106/TK - 0.2005743*log(TK) +\
          (-0.106901773 - 23.9722/TK)*sqrt(S) + 0.1130822*S -\
          0.00846934*sqrt(S)*S
        K2 = exp(lnK2)*(1 - 0.001005*S)/SWStoTOT # convert to SWS pH scale

    if n==2:  # GOYET AND POISSON, 1989
        # GOYET AND POISSON, Deep-Sea Research, 36(11):1635-1654
        pK1 = 812.27/TK + 3.356 - 0.00171*S*log(TK)\
          + 0.000091*S**2
        K1 = 10**(-pK1) # this is on the SWS pH scale in mol/kg-SW
        pK2 = 1450.87/TK + 4.604 - 0.00385*S*log(TK)\
          + 0.000182*S**2
        K2 = 10**(-pK2) # this is on the SWS pH scale in mol/kg-SW

    if n==3:
        # HANSSON refit BY DICKSON AND MILLERO
        # Dickson and Millero, Deep-Sea Research,
        #       34(10):1733-1743, 1987
        pK1 = 851.4/TK + 3.237 - 0.0106*S + 0.000105*S**2
        K1 = 10**(-pK1) # this is on the SWS pH scale in mol/kg-SW
        pK2 = -3885.4/TK + 125.844 - 18.141*log(TK)\
          - 0.0192*S + 0.000132*S**2
        K2 = 10**(-pK2) # this is on the SWS pH scale in mol/kg-SW

    if n==4:  # MEHRBACH refit BY DICKSON AND MILLERO 1987
        # Dickson and Millero, Deep-Sea Research,
        #       34(10):1733-1743, 1987
        pK1 = 3670.7/TK - 62.008 + 9.7944*log(TK)\
              - 0.0118*S + 0.000116*S**2
        K1 = 10**(-pK1) # this is on the SWS pH scale in mol/kg-SW
        # This is in Table 4 on p. 1739.
        pK2 = 1394.7/TK + 4.777 - 0.0184*S + 0.000118*S**2
        K2 = 10**(-pK2) # this is on the SWS pH scale in mol/kg-SW

    if n==5:
        # HANSSON and MEHRBACH refit BY DICKSON AND MILLERO 1987
```

```
    # Dickson and Millero, Deep-Sea Research,
    #       34(10):1733-1743, 1987
    pK1 = 845/TK + 3.248 - 0.0098*S + 0.000087*S**2
    K1 = 10**(-pK1) # this is on the SWS pH scale in mol/kg-SW
    # This is in Table 5 on p. 1740.
    pK2 = 1377.3/TK + 4.824 - 0.0185*S + 0.000122*S**2
    K2 = 10**(-pK2) # this is on the SWS pH scale in mol/kg-SW

if n==6:
    # GEOSECS and Peng et al use K1, K2 from Mehrbach et al,
    # Limnology and Oceanography, 18(6):897-907, 1973.
    pK1 = - 13.7201 + 0.031334*TK + 3235.76/TK\
      + 1.3e-5*S*TK - 0.1032*S**0.5
    K1 = 10**(-pK1)/fH   # convert to SWS scale
    pK2 = 5371.9645 + 1.671221*TK + 0.22913*S + 18.3802*log10(S)\
           - 128375.28/TK - 2194.3055*log10(TK) - 8.0944e-4*S*TK\
           - 5617.11*log10(S)/TK + 2.136*S/TK
    # pK2 is not defined for S=0, since log10(0)=-inf
    K2 = 10**(-pK2)/fH  # convert to SWS scale

if n==7:
    # PURE WATER CASE
    # Millero, F. J., Geochemica et Cosmochemica Acta
    #       43:1651-1661, 1979:
    lnK1 = 290.9097 - 14554.21/TK - 45.0575*log(TK)
    K1 = exp(lnK1)
    lnK2 = 207.6548 - 11843.79/TK - 33.6485*log(TK)
    K2 = exp(lnK2)

if n==8:  # From Cai and Wang 1998
    # From Cai and Wang 1998, for estuarine use.
    fH = 1.29 - 0.00204*  TK + (0.00046 - 0.00000148*TK)*S*S
    F1 = 200.1/TK + 0.3220
    pK1 = 3404.71/TK + 0.032786*TK - 14.8435 -\
            0.071692*F1*S**0.5 + 0.0021487*S
    K1  =10**-pK1/fH  # convert to SWS scale
    F2 = -129.24/TK + 1.4381
    pK2 = 2902.39/TK + 0.02379*TK - 6.4980 -\
            0.3191*F2*S**0.5 + 0.0198*S
    K2  = 10**-pK2/fH # convert to SWS scale

if n==9:  # From Lueker, Dickson, Keeling, 2000
    # From Lueker, Dickson, Keeling, 2000
    pK1 = 3633.86/TK-61.2172+9.6777*log(TK)-\
            0.011555*S+0.0001152*S**2
    K1  = 10**-pK1/SWStoTOT   # convert to SWS pH scale
    pK2 = 471.78/TK+25.929 -3.16967*log(TK)-\
            0.01781 *S+0.0001122*S**2
    K2  = 10**-pK2/SWStoTOT   # convert to SWS pH scale
```

```
if n==10: # Mojica Prieto and Millero 2002
    # Mojica Prieto and Millero. 2002.
    # Geochim. et Cosmochim. Acta. 66(14) 2529-2540.
    pK1 =  -43.6977 - 0.0129037*S + 1.364e-4*S**2 +\
            2885.378/TK +  7.045159*log(TK)
    pK2 = -452.0940 + 13.142162*S - 8.101e-4*S**2 +\
            21263.61/TK + 68.483143*log(TK)\
          + (-581.4428*S + 0.259601*S**2)/TK - 1.967035*S*log(TK)
    K1 = 10**-pK1 # this is on the SWS pH scale in mol/kg-SW
    K2 = 10**-pK2 # this is on the SWS pH scale in mol/kg-SW

if n==11: # Millero et al., 2002
    # Millero et al., 2002. Deep-Sea Res. I (49) 1705-1723.
    pK1 =  6.359 - 0.00664*S - 0.01322*T + 4.989e-5*T**2
    pK2 =  9.867 - 0.01314*S - 0.01904*T + 2.448e-5*T**2
    K1 = 10**-pK1 # this is on the SWS pH scale in mol/kg-SW
    K2 = 10**-pK2 # this is on the SWS pH scale in mol/kg-SW

if n==12: # From Millero 2006
    # Millero, Graham, Huang, Bustos-Serrano, Pierrot.
    #      Mar.Chem. 100 (2006) 80-94
    pK1_0 = -126.34048 + 6320.813/TK + 19.568224*log(TK)
    A_1   = 13.4191*S**0.5 + 0.0331*S - 5.33e-5*S**2
    B_1   = -530.123*S**0.5 - 6.103*S
    C_1   = -2.06950*S**0.5
    pK1= A_1 + B_1/TK + C_1*log(TK) + pK1_0
    K1 = 10**-(pK1)
    pK2_0= -90.18333 + 5143.692/TK + 14.613358*log(TK)
    A_2   = 21.0894*S**0.5 + 0.1248*S - 3.687e-4*S**2
    B_2   = -772.483*S**0.5 - 20.051*S
    C_2   = -3.3336*S**0.5
    pK2= A_2 + B_2/TK + C_2*log(TK) + pK2_0
    K2 = 10**-(pK2)

if n==13: # From Millero, 2010
    # Marine and Freshwater Research, v. 61, p. 139-142.
    pK10 = -126.34048 + 6320.813/TK + 19.568224*log(TK)
    # This is from their table 2, page 140.
    A1 = 13.4038*S**0.5 + 0.03206*S - 5.242e-5*S**2
    B1 = -530.659*S**0.5 - 5.8210*S
    C1 = -2.0664*S**0.5
    pK1 = pK10 + A1 + B1/TK + C1*log(TK)
    K1 = 10**-pK1
    pK20 =  -90.18333 + 5143.692/TK + 14.613358*log(TK)
    A2 = 21.3728*S**0.5 + 0.1218*S - 3.688e-4*S**2
    B2 = -788.289*S**0.5 - 19.189*S
    C2 = -3.374*S**0.5
    pK2 = pK20 + A2 + B2/TK + C2*log(TK)
    K2 = 10**-pK2
```

```
    return K1,K2

## Run script to test with example data ##
if __name__ == '__main__':
  """For documentation on the input variables please see the
  comparison document (pdf) that comes with this package.
  As for pK constants, 13 options from CO2SYS
  """
  # TEST DATA
  V = array([
            0,0.1,0.2,0.3,0.4,0.5,0.6,0.7,0.8,
            0.9,1,1.1,1.2,1.3,1.4,1.5,1.6,1.7,
            1.72,1.74,1.76,1.78,1.8,1.82,1.84,
            1.86,1.88,1.9,2,2.1,2.2,2.3,2.4])
  E = 1000.*array([
            -0.03249,-0.0132,0.00049,0.01055,
            0.01866,0.02559,0.03179,0.03753,
            0.043,0.04831,0.0536,0.059,0.0646,
            0.0706,0.0772,0.08476,0.09393,
            0.10601,0.10879,0.11218,0.11574,
            0.11959,0.1239,0.12868,0.13389,
            0.13951,0.14524,0.15097,0.17332,
            0.18664,0.1956,0.20227,0.20755])
  S    = 34.80
  T    = 20.05
  PT   = 0.00
  SiT  = 0.00
  V0   = 165.391
  C    = 0.20455
  DAcid   = 1.02409
  pKconst = 13
  DIC = 2200

  C,A,K1,pKstr,resd = RecalcAlk_leastsq(S,T,PT,SiT,V0,C,DAcid,V,E,pKconst)

  print '    Lev-Mar Fortran:    %.2f  (Roy et al, 1993)'%2320.21
  print '   *Lev-Mar Python:     %.2f  (%s)\n'%(A,pKstr)
  print '        Acid Conc:      %.4f'%C
  print '        K1:             %.4f'%-log10(K1*1e-6)
  print '        R2:             %.4e'%sum(resd**2)
```